GUSTAVO JORGE RESENDE

A PROPOSAL OF TAIL AND CONTROL SURFACES DESIGN

UNIVERSIDADE FEDERAL DE UBERLÂNDIA
FACULDADE DE ENGENHARIA MECÂNICA
2019

GUSTAVO JORGE RESENDE

A PROPOSAL OF TAIL AND CONTROL SURFACES DESIGN

Projeto de Conclusão de Curso apresentado ao Curso de Graduação em Engenharia Aeronáutica da Universidade Federal de Uberlândia, como parte dos requisitos para a obtenção do título de **BACHAREL em ENGENHARIA AERONÁUTICA.**

Área de concentração: Projeto Aeronáutico, Mecânica do Voo e Controle de Aeronaves.

Orientador: Prof. Dr. Thiago Augusto Machado Guimarães

UBERLÂNDIA – MG

2019

A PROPOSAL OF TAIL AND CONTROL SURFACES DESIGN

Projeto de conclusão de curso **APROVADO** pelo Colegiado do Curso de Graduação em Engenharia Aeronáutica da Faculdade de Engenharia Mecânica da Universidade Federal de Uberlândia.

BANCA EXAMINADORA

_____

Prof. Dr. Thiago Augusto Machado Guimarães
Universidade Federal de Uberlândia

_____

Prof. Me. Felipe Machini Malachias Marques
Universidade Federal de Uberlândia

_____

Roberto Martins de Castro Neto
Universidade Federal de Uberlândia

UBERLÂNDIA – MG

2019

To my Mother and Father, for their unconditional support.

ACKNOWLEDGEMENTS

The conclusion of this work is a milestone in my academic and professional life. It would not be possible without the great support received from family and closest friends, who always believed in me. Special thanks to my mom and dad, Ester and Jose Maria, who always supported me in every single way.

During my college journey, two remarkable projects took place. The first one was the Tucano Aerodesign Team, where I participated for two years and had a great learning experience. Therefore, I would like to thank all those who were my teammates during those years. In addition, special thanks to our team mentor, Prof. Dr. Leonardo Sanches, who has also inspired me to develop this work.

The second project was my student exchange, which would not be possible without the support of the Federal University of Uberlândia and the support of CAPES, who sponsored my exchange. Furthermore, I would like to thank the ISAE-ENSMA personnel who received me and made me feel very welcome. I would also like to express my thanks to my internship mentor, Guillaume Baysset, for his patience and learnings.

Finally, I would like to thank my advisor, Prof. Dr. Thiago Guimarães, for his teachings and to my dear friend and colleague, Guilherme Miquelim, for the many useful comments and suggestions during this text development.

Gustavo Jorge Resende

RESENDE, G. J. **A Proposal of Tail and Control Surfaces Design.** 2019. 97p. Graduation Project, Federal University of Uberlândia, Uberlândia, Brazil.

ABSTRACT

This work presents an analytical procedure to size the tail and control surfaces of a fixed wing aircraft during the conceptual or preliminary design phases. The objective is to provide a better understanding on how the desired stability characteristics of the aircraft can help its design. Furthermore, it will be developed a methodology to size both empennages and the control surfaces, from Flight Mechanics theory, with minimal dependence on historical data. The main design constrain is determined from the aircraft mission and the desired stability characteristics. Whereas few geometrical data are available at the early design phases, it is proposed a new design procedure that take into account some simplifications. Firstly, from wing aerodynamic data and desirable characteristics for the airplane, the horizontal tail is designed. Additionally, it is possible to design both the elevator and the vertical tail. Then, certification requirements, drives the ailerons and rudder sizing. This procedure was incorporated into the conceptual design of a hybrid aircraft. After a preliminary sizing based on the proposed approach, a dynamic stability analysis was done to evaluate the aircraft's stability characteristics and flying qualities. Such characteristics were compared with airworthiness requirements and the evaluated requirements were met.

KEYWORDS: *flight dynamics, tail design, control surfaces, aeronautical design, static stability.*

RESENDE, G. J. **A Proposal of Tail and Control Surfaces Design.** 2019. 97p. Projeto de Conclusão de Curso, Universidade Federal de Uberlândia, Uberlândia, Brasil.

RESUMO

Este trabalho apresenta um procedimento analítico para dimensionar as superfícies estabilizadoras e de controle para uma aeronave de asa fixa durante as fases de projeto conceitual ou projeto detalhado. O principal objetivo é prover um melhor entendimento sobre como as características de estabilidade da aeronave podem ajudar em seu projeto. Além disso, será apresentado o desenvolvimento de uma metodologia para dimensionar ambas empenagens e as superfícies de controle, a partir da teoria de Mecânica do Voo, com dependência mínima de dados históricos. A principal restrição de projeto será determinada pelo tipo de missão da aeronave e as características de estabilidade desejadas. Visto que se trata de um procedimento adotado durante as primeiras fases de projeto da aeronave, poucos dados geométricos estão disponíveis e, portanto, algumas simplificações foram adotadas. Primeiramente, a partir de dados aerodinâmicos da asa e algumas características desejáveis para a aeronave, faz-se o projeto da empenagem horizontal. A partir desta etapa é possível projetar tanto o profundor quanto a empenagem vertical. Então, a partir de requisitos de certificação, providos pelas autoridades, realiza-se o dimensionamento dos ailerons e do leme. Por fim, o procedimento desenvolvido foi incorporado no projeto conceitual de uma aeronave hibrida. Uma vez que o projeto é finalizado, realiza-se uma análise de estabilidade dinâmica para avaliar as características de estabilidade e a qualidade de voo da aeronave. Tais características foram comparadas com requisitos de aeronavegabilidade e os requisitos analisados foram todos cumpridos.

PALAVRAS CHAVE: *dinâmica do voo, projeto de empenagem, superfícies de controle, projeto aeronáutico, estabilidade estática.*

List of Figures

List of Tables

List of Symbols

(O_I, x_I, y_I, z_I)	Inertial coordinate system
(O_w, x_w, y_w, z_w)	Wind coordinate system
(O_b, x_b, y_b, z_b)	Body fixed coordinate system
$[\Phi\ \Theta\ \Psi]^T$	Euler angles
$[p\ q\ r]^T$	Angular rates
$[u\ v\ w]^T$	Velocity components
$[X\ Y\ Z]^T$	Aero propulsive force components
$[L\ M\ N]^T$	Aero propulsive moment components
$\left[I_x\ I_y\ I_z\right]^T$	Moment of inertia about each axis
$\left[I_{yz}\ I_{xz}\ I_{xy}\right]^T$	Products of inertia
V_R	Rotation velocity
V_{TO}	Take-off velocity
V_∞	Free stream velocity
M_∞	Free stream Mach number
q_∞	Free stream dynamic pressure
q_{HT}	Local dynamic pressure at horizontal tail
q_{VT}	Local dynamic pressure at vertical tail
α	Aircraft angle of attack
β	Sideslip angle
α_w	Wing angle of attack
α_{HT}	Horizontal tail angle of attack
i_w	Wing incidence angle at the fuselage
i_{HT}	Horizontal tail incidence angle at the fuselage
$\bar{V}_{HT}$	Horizontal tail volume ratio
V_{VT}	Vertical tail volume ratio
η_{HT}	Horizontal tail efficiency
η_{VT}	Vertical tail efficiency
ϵ_w	Downwash angle
σ	Sidewash angle
ω_{SP}	Short-period mode frequency
ω_{PH}	Phugoid mode natural frequency
ω_{DR}	Dutch roll mode natural frequency

ξ_{SP}	Short-period damping ratio
ξ_{PH}	Phugoid mode natural frequency
ξ_{DR}	Dutch roll mode natural frequency
τ_{roll}	Roll time constant
T	Period of an oscillation
t_{half}	Time to half a signal amplitude
t_{double}	Time do double a signal amplitude
N_{half}	Number of cycles until the half signal amplitude
N_{double}	Number of cycles until the double signal amplitude
h	CG position relative to $\bar{c}_w$
h_n	Neutral point position relative to $\bar{c}_w$
l_{HT}	Distance between wing and HT aerodynamic center
l_{VT}	Distance between wing and VT aerodynamic center
W	Aircraft weight

For the following variables, sub-indices might be used to refers which component it belongs:

- $w \rightarrow wing$
- $HT \rightarrow horizontal\ tail$
- $VT \rightarrow vertical\ tail$
- $e \rightarrow elevator$
- $r \rightarrow rudder$
- $a \rightarrow aileron$

AR	Aspect ratio
S	Surface
b	Span
$\bar{c}$	Mean aerodynamic chord
c_r	Root chord
c_t	Tip chord
λ	Tip ratio or Eigenvalue (dynamic stability analysis)
δ	Control surface deflection
L	Lift force or Roll Moment
D	Drag force
C_L	Lift coefficient
C_D	Drag coefficient
C_l	2D lift coefficient
C_ℓ	Roll moment coefficient
C_m	Pitching moment coefficient
C_N	Yaw moment coefficient
C_{L_0}	Lift coefficient for zero angle of attack
C_{D_0}	Drag coefficient for zero angle of attack
C_{m_0}	Pitching moment coefficient for zero angle of attack
C_{L_α}	$\frac{\partial C_L}{\partial \alpha}$ → Lift coefficient derivative with respect to α
C_{m_α}	$\frac{\partial C_m}{\partial \alpha}$ → Pitch moment coefficient derivative with respect to α
C_{n_β}	$\frac{\partial C_N}{\partial \beta}$ → Yaw moment coefficient derivative with respect to β
C_{ℓ_β}	$\frac{\partial C_\ell}{\partial \beta}$ → Roll moment coefficient derivative with respect to β

$C_{L_{\delta_e}}$	$\frac{\partial C_L}{\partial \delta_e}$ → Lift coefficient derivative with respect to δ_e
$C_{m_{\delta_e}}$	$\frac{\partial C_m}{\partial \delta_e}$ → Elevator control effectiveness
$C_{n_{\delta_r}}$	$\frac{\partial C_N}{\partial \delta_r}$ → Rudder control effectiveness
C_{ℓ_β}	$\frac{\partial C_\ell}{\partial \delta_r}$ → Roll moment coefficient derivative with respect to δ_r
$C_{n_{\delta_a}}$	$\frac{\partial C_N}{\partial \delta_a}$ → Yaw moment coefficient derivative with respect to δ_a
$C_{\ell_{\delta_a}}$	$\frac{\partial C_\ell}{\partial \delta_a}$ → Roll moment coefficient derivative with respect to δ_a
C_{h_e}	Elevator hinge moment coefficient
C_{h_0}	Hinge moment coefficient for zero α_{HT} and δ_e
$C_{h_{\alpha_{HT}}}$	$\frac{\partial C_h}{\partial \alpha_{HT}}$ → Hinge moment coefficient derivative with respect to α_{HT}
$C_{h_{\delta_e}}$	$\frac{\partial C_h}{\partial \delta_e}$ → Hinge moment coefficient derivative with respect to δ_e
$\delta_{e_{free}}$	Elevator deflection for stick-free condition

Acronyms

AIAA	American Institute of Aeronautics and Astronautics
A.C.	Aerodynamic Center
M.A.C.	Mean Aerodynamic Chord
CFR	Code of Federal Regulations
RFP	Request of Proposal
ISA	International Standard Atmosphere
LLT	Lift Line Theory
HT	Horizontal tail
VT	Vertical tail

CONTENTS

CHAPTER I

INTRODUCTION

One of the main reasons that makes an aircraft's design such a challenge is its high level of complexity. A proper design takes into account the compromise between different areas, such as Aerodynamics, Structural, Performance and Flight Mechanics. The complexity lies in the fact that frequently this areas have different goals, sometimes even opposed ones. For instance, wings with a very high aspect ratio are great from an Aerodynamic point of view, but not so great from the Structural one. Thus, the aircraft designer must establish some trade-offs between all the areas of development, looking for overall optimal configuration. In this context, a common practice is to determinate the first dimensions from statistical and historical data, as presented by (Gudmundsson, 2014) and (Sadraey, 2013).

Although it is a good starting point, the design cannot be guided just from these kind of data. Otherwise, the designed aircraft would be very similar from those that already exists. In addition, historical values and statistical data have their bases on traditional aircrafts. With the advent of new fuel sources, hybrid and hybrid-electric propulsors, and new composite materials, some parameters may not be optimal as they

were in a traditional aircraft, e.g., the weight distribution in the airplane would probably be different. Nonetheless, a configuration that works well for a "traditional" aircraft may not be the best one for a hybrid one. In contradiction to a conventional design procedure, this work propose some alternatives to design the tail and control surfaces from Flight Mechanics theory and the aircraft mission, with minimal dependence on historical data.

For a better comprehension of the developed methodology, Chapters II and III address the basic Flight Mechanics theory, i.e., coordinate systems definition, aerodynamic coefficient definitions and so forth. This basic theory is a gathering of the content presented by Etkin (1996), Nelson (1998) and Roskam (2001). The most important equations are described in details in appendix A.

Chapter IV describes the tail and control surfaces design methodology. In addition to the references mentioned before, some design strategies were also adapted from (Gudmundsson, 2014). The Code of Federal Regulations (CFR), from (FAA, 2017), provide some guidelines that contributes for the design process as well.

Finally, in Chapter V, the proposed methodology is used in the development of a hybrid-electric aircraft based on the Request of Proposal (RFP) for the annual design competition held by the American Institute of Aeronautics and Astronautics (AIAA). With some initial available parameters, the empennage and the control surfaces are designed. The final aircraft configuration is then presented and followed by a dynamic stability analysis, which is useful to evaluate the aircraft's flying qualities and to verify if the FAA requirements[1] are met.

[1] Since the RFP is from an American institution, the certification requirements used for the designed aircraft would be those from FAA.

CHAPTER II

AXIS SYSTEMS AND EQUATIONS OF MOTION

Modeling a fixed wing vehicle to analyze and simulate its motion is not a trivial task. An airplane in flight is a very complex dynamic system. Therefore, in order to accomplish this, a consistent mathematical model of the aircraft and its subsystems must be used. This model allows to evaluate the stability characteristics[2] of the airplane, which is of particular interest to the pilot and designer.

For such mathematical model, well-defined coordinate systems must be specified as well as some aerodynamic definitions. The equations of motion discussed in the following sections are widely accepted by aeronautical engineers and researchers. In addition, several assumptions were made along the development of the equations, e.g. the treatment of the aircraft as a single rigid body and Earth is treated as flat and stationary in inertial space.

It is out of the scope of this work to develop the set of equations that will be presented. Although, a detailed development is presented by Etkin (1996), Nelson (1998) and Roskam (2001).

[2] Stability definitions are presented in Chapter III.

2.1 AERODYNAMIC NOMENCLATURE AND AXIS SYSTEMS

In order to describe the motion of an airplane, many different coordinate systems may be used. In this work, only three will be considered.

The first one is considered to be fixed on Earth[3] and, for the purpose of aircraft motion analysis, will be regarded as the *Inertial Coordinate System* (O_I, x_I, y_I, z_I). Its origin is arbitrarily located to suit the particularity of each problem, the axis $O_I z_I$ points vertically downwards, the axis $O_I x_I$ points horizontally to a convenient direction, for instance, North, or along a runway (Etkin & Reid, 1996). The second one is the *Body Coordinate System* (O_b, x_b, y_b, z_b) and is attached to the airplane's body as shown in Figure 2.1, note that the xz plane is coincident with the airplane's symmetry plane.

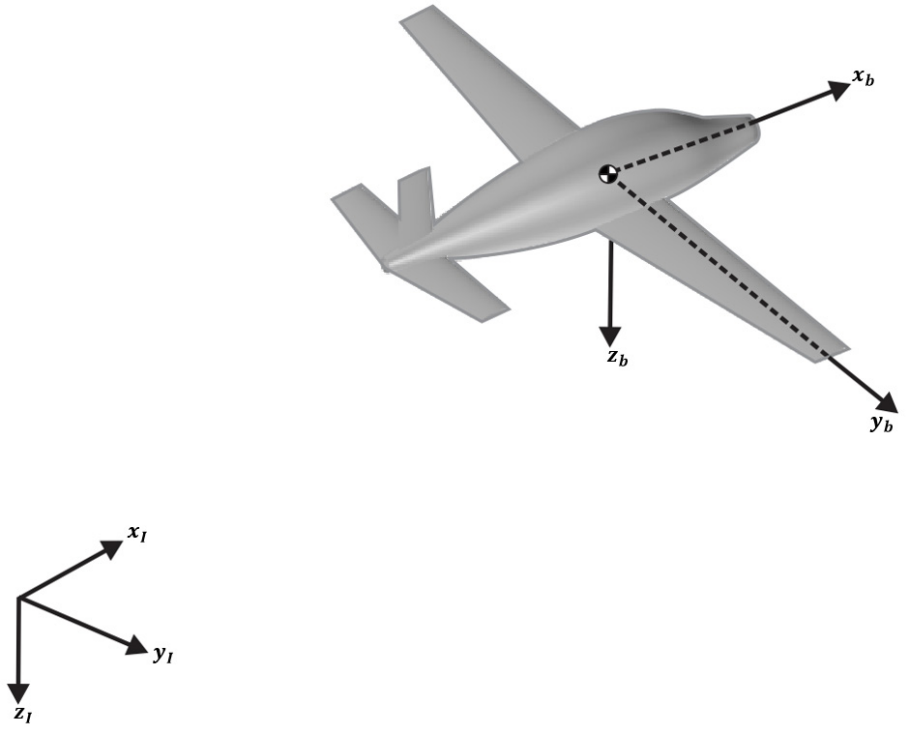

Figure 2.1: Inertial and body coordinate systems.

The last one is the *Wind Coordinate System* (O_w, x_w, y_w, z_w), also attached to the body, but the axis $O_w x_w$ points towards the relative wind direction (Figure 2.2). Both *Body* and *Wind* has their origins at the airplane's center of gravity (CG).

[3] In these analyses, Earth curvature and motions may not be considered.

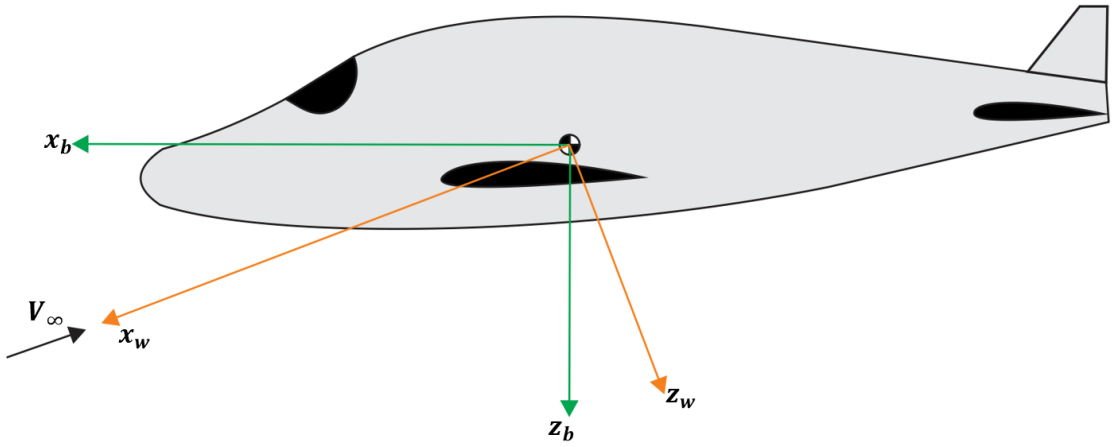

Figure 2.2: Body and wind coordinate systems.

The main forces acting during an airplane's flight are the aerodynamic, thrust and gravitational. These forces can be decomposed along an axes fixed to the airplane's center of gravity, as illustrated in Figure 2.3. The aerodynamic and thrust forces are represented by X, Y and Z components along the x_b, y_b and z_b axes.

Table 2.1 summarizes the forces, moments, velocities and inertia properties denominations of an airplane.

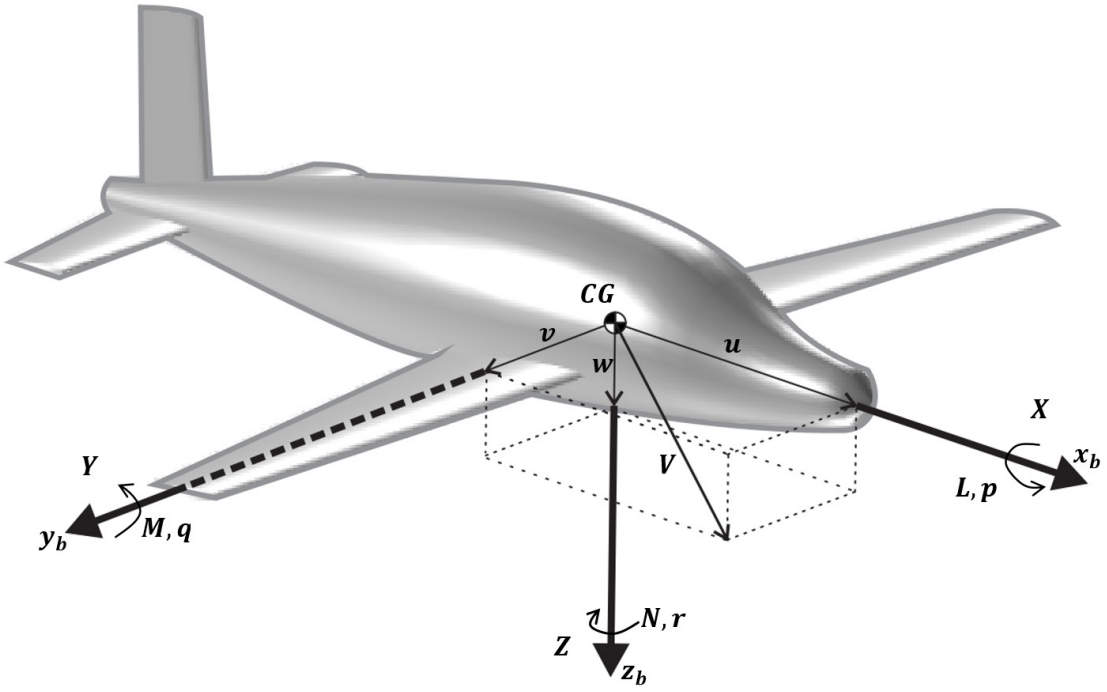

Figure 2.3: Definition of velocity components, forces and moments in a body fixed coordinate system.

Table 2.1: Definition of velocity components, forces and moments in a body fixed coordinate system.

	Roll Axis x_b	**Pitch Axis** y_b	**Yaw Axis** z_b
Angular rates [rad/s]	p	q	r
Velocity components [m/s]	u	v	w
Aero propulsive force components [N]	X	Y	Z
Aero propulsive moment components [N.m]	L	M	N
Moment of inertia about each axis [kg.m²]	I_x	I_y	I_z
Products of inertia [kg.m²]	I_{yz}	I_{xz}	I_{xy}

The aerodynamic forces are defined by dimensionless coefficients, the flight dynamic pressure (q_∞) and the wing area (S_w). Usually these forces are written in the *Wind Coordinate System* (as lift and drag, for example) and then decomposed in the *Body Coordinate System*. In a similar manner, the aerodynamic moments are defined by dimensionless coefficients, the flight dynamic pressure, wing area and a reference length. For the pitching moment, the reference length is the wing's mean aerodynamic chord (M.A.C.). For rolling and yaw moments, this reference is the wingspan (b_w).

The dimensionless coefficients are mainly functions of the Reynolds and Mach numbers, angle of attack and sideslip angle. As illustrated in Figure 2.4, these aerodynamic angles are defined by:

$$\alpha = \tan^{-1}\left(\frac{w}{u}\right) \tag{2.1}$$

and

$$\beta = \sin^{-1}\left(\frac{v}{V}\right) \tag{2.2}$$

where

$$V = \sqrt{u^2 + v^2 + w^2} \tag{2.3}$$

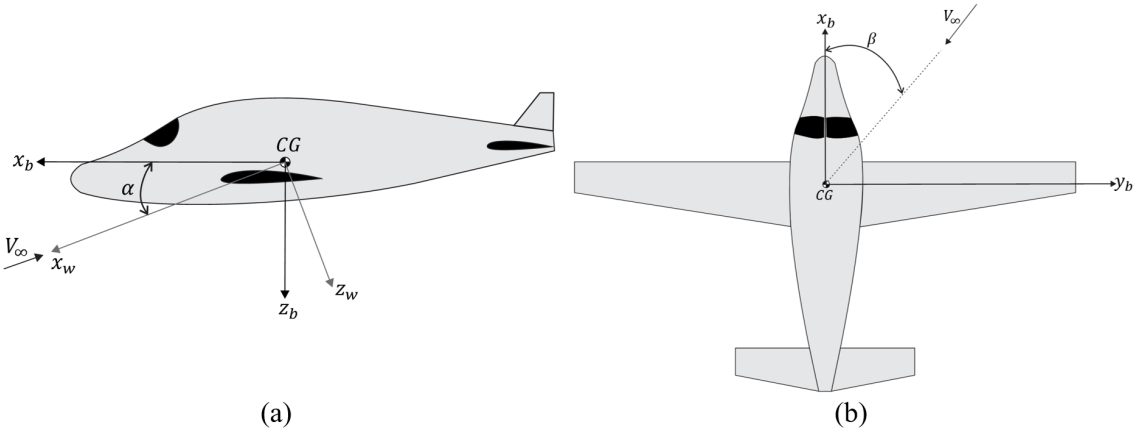

(a) (b)

Figure 2.4: Definition of (a) angle of attack and (b) sideslip angle.

2.2 Orientation of the Airplane

Defining the orientation of the airplane with respect to the *Inertial Coordinate System* is equivalent to define the orientation its *Body Coordinate System*. The procedure consists in a series of three consecutive rotations, the Euler angles (or orientation angles), whose order are very important. Etkin (1996), Nelson (1998) and Roskam (2001) develops detailed explanation on how those rotations must took place.

For simplicity, Figure 2.5 illustrates three specific positions of an airplane presenting the difference between aerodynamic (α, β), orientation (Φ, Θ, Ψ) and trajectory angles (Γ_2, Γ_3).

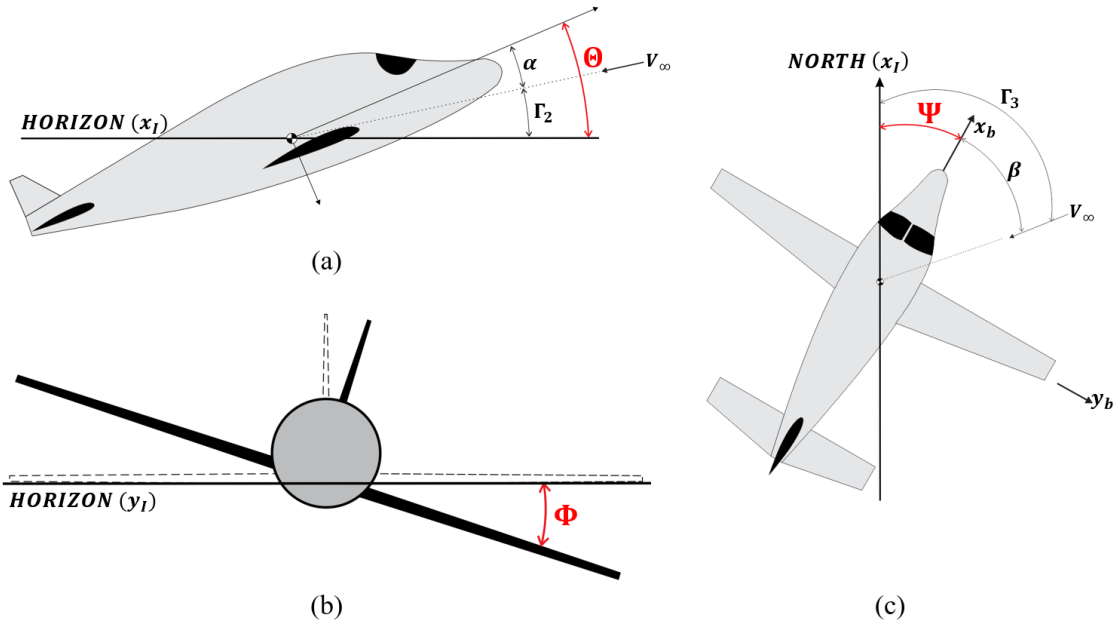

Figure 2.5: Airplane orientation angles, in red, with respect to the inertial frame of reference.

2.3 General Equations of Motion

As stated earlier, the general equations of motion of an airplane are the fundamental basis to study its static and dynamic behavior. The present section is dedicated to discuss the main remarks about those equations. In addition, some particular flight conditions, where the equations of motion are simplified, is of interest.

To obtain the dynamic equations presented in appendix B, the main assumptions are that the aircraft is one single rigid body with known geometry and constant mass. Then the equations of Newton-Euler are applied and integrated for the entire airplane.

$$\vec{F}_{A,P,W} = m.\begin{bmatrix} du/dt \\ dv/_{dt} \\ dw/_{dt} \end{bmatrix} \tag{2.4}$$

$$\vec{M}_{A,P} = \left(\frac{d\vec{H}}{dt}\right)_{\substack{Inertial \\ frame}} \tag{2.5}$$

where $\vec{F}_{A,P,W}$ Is the resultant of aerodynamic, propulsive and gravitational forces.

$\vec{M}_{A,P}$ Is the resultant of aerodynamic and propulsive moments acting on the aircraft's CG.

$\vec{H}$ Is the airplane's angular momentum.

To include the aeroelastic properties, the model must accounts for an aeroelastic equilibrium from which the external shape variation of the airplane can be determined (Roskam, 2001). Those properties, however, will not be considered in the methodology presented in later chapters.

The set of equations obtained from equations (2.4) and (2.5) results in a non-linear system of differential equations. For stability analyses, it is common to linearize this system of equations, around a given equilibrium condition, by the small perturbation's approach. This technique assumes that any variable can be decomposed in a steady term (non-perturbed) and a perturbed term:

$$\mathcal{X}(t) = \mathcal{X}_0 + \Delta\mathcal{X}(t)$$

Another assumption is that perturbation terms of higher orders are considered negligible. In this way, the equations of the perturbed motion can be described in a vector stead-space form:

$$\{\dot{x}\} = \mathbf{A}.\{x\}$$

where the matrix **A** represents the dynamic characteristics of the system. Appendix B presents this set of equations for the longitudinal and lateral motions with more details.

2.3.1 Equations of Motion for Steady State Rectilinear Flight

For the purposes of control surfaces design, the steady state rectilinear flight condition is assumed, being characterized by:

$$\frac{d\vec{V}}{dt} = \vec{0} \qquad\qquad \vec{\omega} = [p\ q\ r]^T = 0$$

Then, the force and moment equations (B.1) to (B.6) becomes:

$$X - m.g.\sin(\Theta) = 0 \tag{2.6}$$

$$Y + m.g.\sin(\Phi).\cos(\Theta) = 0 \tag{2.7}$$

$$Z + m.g.\cos(\Phi).\cos(\Theta) = 0 \tag{2.8}$$

$$L = 0 \tag{2.9}$$

$$M = 0 \tag{2.10}$$

$$N = 0 \tag{2.11}$$

CHAPTER III

STATIC STABILITY THEORY

This chapter will briefly introduce some basic definitions regarding Aerodynamics and Flight Mechanics, which will be constantly used in the subsequent chapters. The objective is to define the forces and moments coefficients of a fixed wing aircraft and show how they describe its static behavior.

For the following sections, it is important to remind that stability is a property of an equilibrium state of a system (Nelson, 1998). For an aircraft, when the resultant force as well as the resultant moment at the center of gravity are simultaneously zero the flight will be steady and uniform. This characteristic defines an equilibrium state of the airplane (or a trim flight condition). In the literature, this subject is divided into static and dynamic stability.

Static stability responds if the system will return to its initial condition after a perturbation. Figure 3.1 illustrates some different conditions of static stability. Figure 3.1(d) brings a good remark that a system can be static stable in a specific direction (the y direction for this case) and unstable in another one (x direction). This characteristic is commonly present in an airplane, where it can be stable with respect to one degree of freedom and unstable with respect to another (Etkin & Reid, 1996).

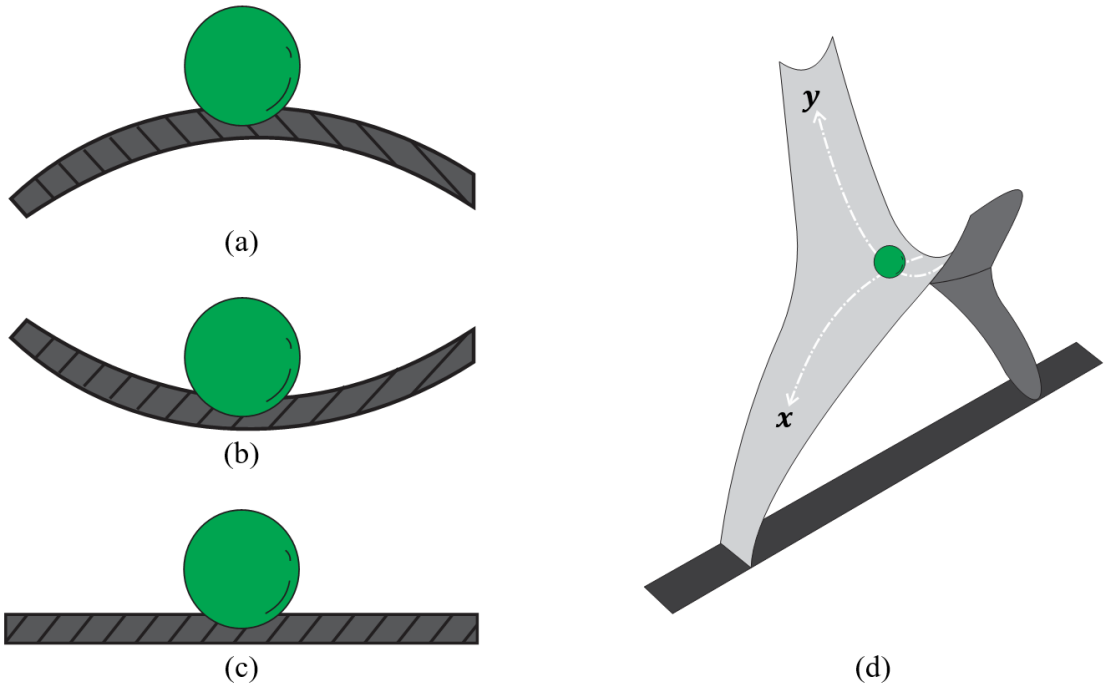

Figure 3.1 - (a) Ball on a hill - unstable equilibrium; (b) Ball in a bowl - stable equilibrium; (c) Ball on a plane - neutral equilibrium; (d) Ball on a saddle surface - unstable equilibrium. Adaption from (Etkin & Reid, 1996).

While static stability, basically, answers the question "Is it stable? Yes or no? ", dynamic stability describes more characteristics of the airplane's transient behavior, such as if there will be oscillations, how long it will take to half the oscillatory signal, how long to return to the equilibrium condition and so on.

3.1 Longitudinal Forces and Moments

Lift and drag forces and the pitching moment are the main efforts presented in the longitudinal motion of an airplane. One can combine the wing and horizontal tail contributions[4] to compute the resultant force and moment acting in the airplane's CG (*Build-up* method).

3.1.1 Wing Contribution

The wing contribution to the longitudinal aerodynamic forces can be computed by decomposing its lift and drag forces from the *Wind Coordinate System* to the *Body Coordinate System* (Figure 3.2). One may notice that these coordinate systems are shifted from one to another by the angle of attack (α) of the airplane, which may not be the same as the angle of attack of the wing (α_w).

[4] At this first moment the thrust force and fuselage interference are not being considered.

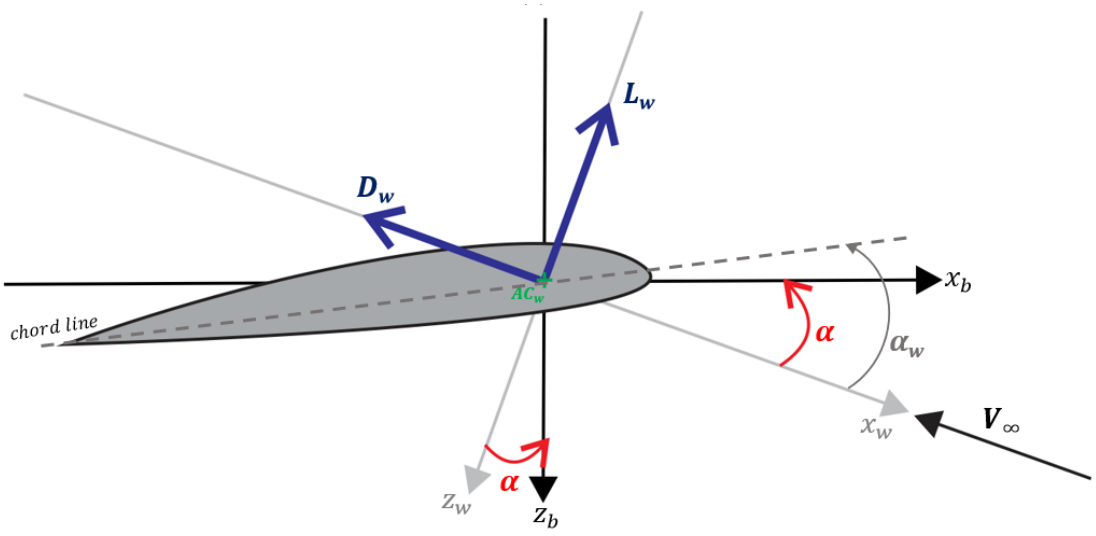

Figure 3.2: Sketch of lift and drag acting in the wing.

The sum of the moments about the CG leads to the following equation for the pitching moment coefficient (see appendix A.1):

$$(C_m)_w = \frac{(h - h_{AC_w})}{\bar{c}_w}.C_{L_w} + \frac{z_w}{\bar{c}_w}\left(-C_{D_w} + \alpha.C_{L_w}\right) - C_{m_{AC_w}} \tag{3.1}$$

Which, as shown in appendix A.1, is simplified by:

$$(C_m)_w = \frac{(h - h_{AC_w})}{\bar{c}_w}.C_{L_w} - C_{m_{AC_w}} \tag{3.2}$$

3.1.2 Tail Contribution

The tail contribution to the longitudinal effort at the airplane's CG is obtained in a similar way to the wing's contribution. The main difference lies in the flow deviation made by the wing, which induces a downwash velocity[5] at the air stream that reaches the horizontal tail. This downwash velocity implies a reduction of the horizontal tail's effective angle of attack (α_{HT}) by a downwash angle (ϵ). Therefore, α_{HT} may be defined by (Figure 3.3):

$$\alpha_{HT} = \alpha + i_{HT} - \epsilon_w \tag{3.3}$$

An estimation for ϵ_w is:

$$\epsilon_w = \epsilon_0 + \epsilon_\alpha.\alpha_w \tag{3.4}$$

Hence,

$$\alpha_{HT} = (1 - \epsilon_\alpha).\alpha + i_{HT} - \epsilon_0 - \epsilon_\alpha.i_w \tag{3.5}$$

[5] This is valid for conventional airplanes. For airplanes with canard, the wing in induce an upward velocity (see (Nelson, 1998) for details).

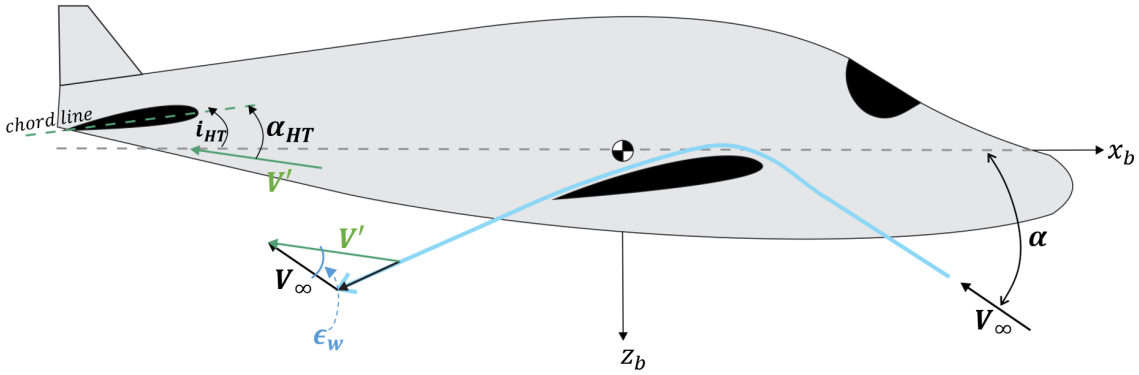

Figure 3.3: Wing downwash affecting the flow field at the horizontal tail.

In addition, the effects of the engine's position with respect to the tail may changes the tail's dynamic pressure. The ratio between the wing and the tail aerodynamic pressure is given by:

$$\eta_{HT} = \frac{q_{HT}}{q_w} = \frac{\frac{1}{2}.\rho_{HT}.V_{HT}^2}{\frac{1}{2}.\rho_\infty.V_\infty^2} \tag{3.6}$$

The total lift acting in the CG generated by the horizontal tail is given by:

$$(C_L)_{HT} = \eta_{HT}.\frac{S_{HT}}{S_w}.\left(C_{L_{0_{HT}}} + C_{L_{\alpha_{HT}}}.\alpha_{HT}\right)$$

$$(C_L)_{HT} = \eta_{HT}.\frac{S_{HT}}{S_w}.\left[C_{L_{0_{HT}}} + C_{L_{\alpha_{HT}}}.\left((1-\epsilon_\alpha).\alpha + i_{HT} - \epsilon_0 - \epsilon_\alpha.i_w\right)\right] \tag{3.7}$$

The sum of the moments about the CG, due to the aerodynamic effort acting in the tail, leads to the following equation for the pitching moment coefficient (see appendix A.1):

$$(C_m)_{HT} = -\eta_{HT}.\left(\bar{V}_{HT} - \left(h - h_{AC_w}\right).\frac{S_{HT}}{S_w}\right).C_{L_{HT}} - \eta_{HT}.\frac{\bar{c}_{HT}.S_{HT}}{\bar{c}_w.S_w}.C_{m_{AC_{HT}}} \tag{3.8}$$

where $\bar{V}_{HT}$ is the horizontal tail volume ratio.

3.1.3 Total Effects in the CG

Considering the wing and the horizontal tail, the total lift of the aircraft is:

$$C_L = (C_L)_w + (C_L)_{HT} \tag{3.9}$$

Equation (3.9) can be rewritten as $C_L = C_{L_0} + C_{L_\alpha}.\alpha$, where:

$$C_{L_0} = \left(C_{L_{0_w}} + C_{L_{\alpha_w}}.i_w\right) + \eta_{HT}.\frac{S_{HT}}{S_w}.\left[C_{L_{0_{HT}}} + C_{L_{\alpha_{HT}}}.(i_{HT} - \epsilon_0 - \epsilon_\alpha.i_w)\right] \tag{3.10}$$

$$C_{L_\alpha} = C_{L_{\alpha_w}} + \eta_{HT}.\frac{S_{HT}}{S_w}.C_{L_{\alpha_{HT}}}.(1-\epsilon_\alpha) \tag{3.11}$$

Similarly, for the pitching moment in the airplane's CG:

$$C_m = (C_m)_w + (C_m)_{HT} \tag{3.12}$$

Rewriting equation (3.12) as $C_m = C_{m_0} + C_{m_\alpha}.\alpha$:

$$C_{m_0} = (h - h_{AC_w}).C_{L_0} - \eta_{HT}.\bar{V}_{HT}.\left[C_{L_{0_{HT}}} + C_{L_{\alpha_{HT}}}.(i_{HT} - \epsilon_0 - \epsilon_\alpha.i_w)\right] - \left(C_{m_{AC_w}} + \eta_{HT}.\frac{\bar{c}_{HT}.S_{HT}}{\bar{c}_w.S_w}\right) \tag{3.13}$$

$$C_{m_\alpha} = (h - h_{AC_w}).C_{L_\alpha} - \eta_{HT}.\bar{V}_{HT}.C_{L_{\alpha_{HT}}}.(1-\epsilon_\alpha) \tag{3.14}$$

Notice that, from equation (3.14), C_{m_α} depends on the CG location (h). The limit of static stability of an airplane is when the C_{m_α} approaches to zero, where it will be in a neutral equilibrium. The CG position that makes $C_{m_\alpha} = 0$ is called neutral point (h_N).

$$h_N = h_{AC_w} + \eta_{HT}.\bar{V}_{HT}.\frac{C_{L_{\alpha_{HT}}}}{C_{L_\alpha}}.(1-\epsilon_\alpha) \tag{3.15}$$

Equations (3.11), (3.14) and (3.15) will be very useful for the horizontal tail sizing in Chapter IV.

3.2 LONGITUDINAL CONTROL

Longitudinal control of an airplane can be achieved, mainly, by providing an incremental lift force on the horizontal tail[6]. The incremental lift force can be produced by a deflection of an all move tail or by an elevator (Nelson, 1998). Because the control surface is located at some distance from the CG, the incremental lift force creates a moment about the airplane's CG.

As demonstrated by (Nelson, 1998), the deflection of the elevator (δ_e) increases the airplane's lift coefficient by ΔC_L.

$$\Delta C_L = C_{L_{\delta_e}}.\delta_e$$

[6] Other lifting surfaces can also be used to provide this incremental lift, but in this work the focus will remain at the horizontal tail and elevator.

$$\Delta C_L = \eta_{HT}.\frac{S_{HT}}{S_w}.C_{L_{\alpha_{HT}}}.\tau.\delta_e \tag{3.16}$$

The term $\left(C_{L_{\alpha_{HT}}}.\tau\right)$ is the elevator effectiveness. The parameter τ can be determined from Figure 3.4. It is important to highlight that the surface ratio in Figure 3.4 can also be considered a local chord ratio.

On the other hand, the change in the pitching moment coefficient is:

$$\Delta C_m = C_{m_{\delta_e}}.\delta_e$$

$$\Delta C_m = -\eta_{HT}.\bar{V}_{HT}.C_{L_{\alpha_{HT}}}.\tau.\delta_e \tag{3.17}$$

The stability derivative $C_{m_{\delta_e}}$ is the elevator control power (Nelson, 1998). The larger the control power, the more effective the elevator in creating control moment.

Hence, the total lift and moment coefficients becomes:

$$C_L = C_{L_0} + C_{L_\alpha}.\alpha + C_{L_{\delta_e}}.\delta_e \tag{3.18}$$

and

$$C_m = C_{m_0} + C_{m_\alpha}.\alpha + C_{m_{\delta_e}}.\delta_e \tag{3.19}$$

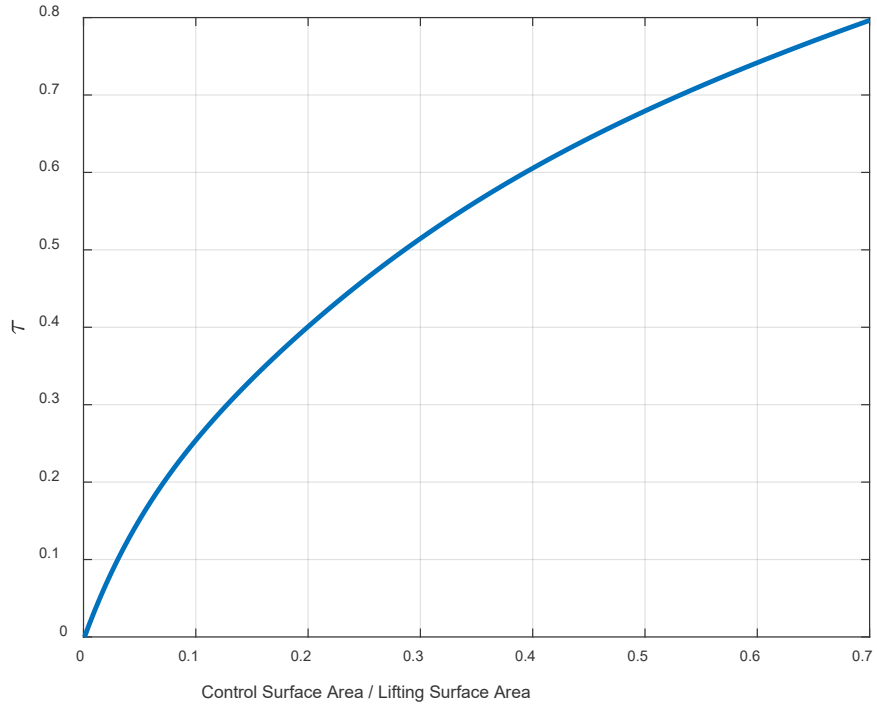

Figure 3.4: Flap effectiveness parameter. Adapted from (Nelson, 1998).

3.3 Latero-Directional Forces and Moments

Latero-directional stability is concerned with the static stability of the aircraft about the x and z-axis, also known as roll stability and directional stability respectively. Similarly to the case of longitudinal static stability, it is desirable that the aircraft has a tendency to return to its initial condition after a yawing perturbation or a roll perturbation.

The main contribution to directional stability comes from the vertical tail, which produces a lift-like force parallel to the xy plane when the aircraft is flying at sideslip. The assembly wing-fuselage has a destabilizing, although it is very small when compared to the vertical tail contribution.

Since this side force, acting in the vertical tail, has a moment arm in both x and z-axis (with respect to the CG), a flight in sideslip condition deals with side-force, rolling and yaw moment. Therefore, a bank angle may also be associated (see appendix B.1). In another words, one may state that the existence of a β angle generates some Φ angle and the contrary is equally true.

3.3.1 Tail Contribution

As show in Figure 3.5, when the aircraft is flying with a positive sideslip angle, the angle of attack experienced by the vertical tail is given by:

$$\alpha_{VT} = \beta + \sigma \tag{3.20}$$

where σ is the sidewash angle created by the wing distortion in the flow field. It is analogous to the downwash for the horizontal tail.

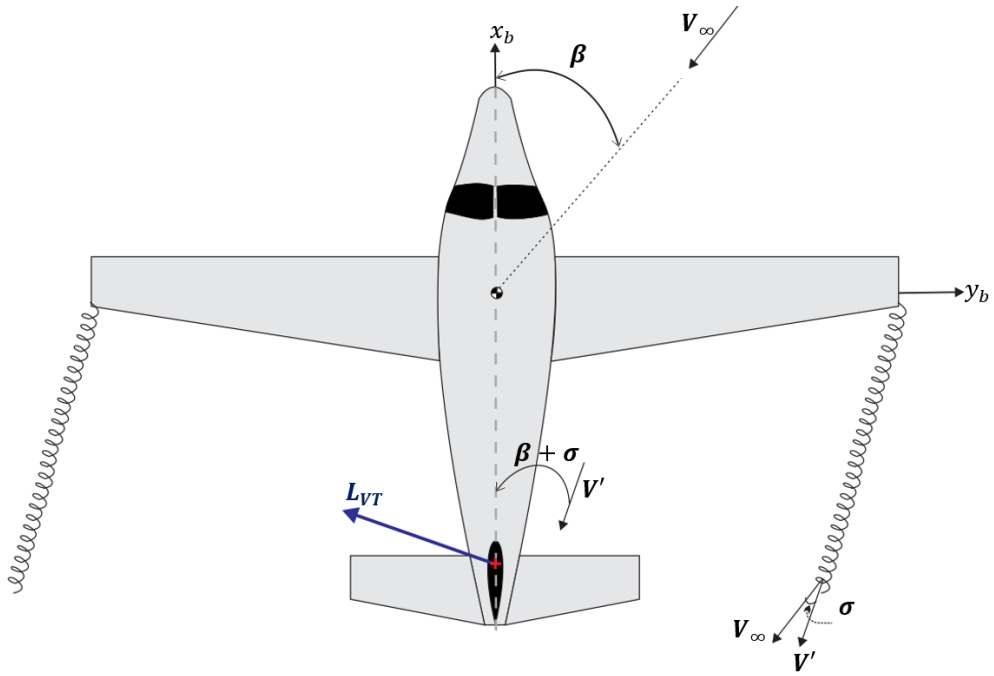

Figure 3.5: Vertical tail contribution to directional stability and illustration of sidewash due to wing vortices.

As demonstrated in appendix A.2, the force and moments produced by the vertical tail are:

$$Y_{VT} = -C_{L_{\alpha_{VT}}}.(\beta+\sigma).q_{VT}.S_{VT} \tag{3.21}$$

$$L_{VT} = -|z_{VT}|.C_{L_{\alpha_{VT}}}.(\beta+\sigma).q_{VT}.S_{VT} \tag{3.22}$$

$$N_{VT} = l_{VT}.C_{L_{\alpha_{VT}}}.(\beta+\sigma).q_{VT}.S_{VT} \tag{3.23}$$

Or, in the coefficient form:

$$(C_Y)_{VT} = \frac{Y_{VT}}{q_\infty.S_w} = -\eta_{VT}.C_{L_{\alpha_{VT}}}.\frac{S_{VT}}{S_w}(\beta+\sigma) \tag{3.24}$$

$$(C_\ell)_{VT} = \frac{L_{VT}}{q_\infty.S_w.b_w} = \frac{-|z_{VT}|.S_{VT}}{b_w.S_w}.\eta_{VT}.C_{L_{\alpha_{VT}}}.(\beta+\sigma) \tag{3.25}$$

$$(C_n)_{VT} = \frac{N_{VT}}{q_\infty.S_w.b_w} = \eta_{VT}.V_{VT}.C_{L_{\alpha_{VT}}}.(\beta+\sigma) \tag{3.26}$$

where $$\eta_{VT} = \frac{q_{VT}}{q_\infty} \tag{3.27}$$

and $$V_{VT} = \frac{l_{VT}.S_{VT}}{b_w.S_w} \tag{3.28}$$

Notice that for the lateral stability, the reference length becomes the wingspan (b_w), which is more representative than the mean aerodynamic chord for the motions outside the longitudinal plane.

Taking the derivative of equations (3.24) to (3.26) with respect to β allows one to evaluate the contribution of the vertical tail to roll and directional stability.

$$C_{Y_\beta} = -\eta_{VT}.C_{L_{\alpha_{VT}}}.\frac{S_{VT}}{S_w}.\left(1+\frac{d\sigma}{d\beta}\right) \tag{3.29}$$

$$C_{\ell_\beta} = \frac{-|z_{VT}|.S_{VT}}{b_w.S_w}.\eta_{VT}.C_{L_{\alpha_{VT}}}.\left(1+\frac{d\sigma}{d\beta}\right) \tag{3.30}$$

$$C_{n_\beta} = V_{VT}.\eta_{VT}.C_{L_{\alpha_{VT}}}.\left(1+\frac{d\sigma}{d\beta}\right) \tag{3.31}$$

There is no analytical equation to evaluate the sidewash dependence on the slip angle. However, (USAF, 1978) presents an algebraic equation for estimating the combined effect of the tail efficiency (η_{VT}) and the sidewash:

$$\eta_{VT}.\left(1+\frac{d\sigma}{d\beta}\right) = 0.724 + 3.06.\frac{S_{VT}/S_w}{1+\cos(\Lambda_{c/4w})} + 0.4\frac{z_w}{d} + 0.009.AR_w \tag{3.32}$$

where d = the maximum fuselage depth
z_w = the distance, parallel to the z-axis, from wing root quarter chord point to fuselage centerline
$\Lambda_{c/4w}$ = sweep of wing quarter chord.

It is important to emphasize that the derivatives presented here are the major contributors for the total derivatives of the airplane, but they are not the only ones. For example, a more complete model for the C_{n_β} may be:

$$C_{n_\beta} = \left(C_{n_\beta}\right)_{fuselage} + \left(C_{n_\beta}\right)_{wing} + \left(C_{n_\beta}\right)_{HT} + \left(C_{n_\beta}\right)_{VT} + \ ...$$

The same goes for all other derivative terms. However, while in early design process, it is reasonable to simplify these models in order to be able estimate some values. Then, as the design progresses, more data are available and those derivatives can be calculated with more accuracy.

3.4 Lateral Control

Similarly, to the basic longitudinal control presented in section 3.2, lateral control may be achieved by an increment in the side force on the vertical tail. This incremental force, produced by a rudder deflection (δ_r), acts in a distance from the airplane's CG producing the moment responsible for the control. According to the coordinate system presented in section 2.1, a positive side force will produce a negative yawing moment.

As demonstrated by (Nelson, 1998), the side force and yawing moment coefficients due to the rudder's actuation are:

$$(C_Y)_{\delta_r} = C_{Y_{\delta_r}}.\delta_r \tag{3.33}$$

$$(C_n)_{\delta_r} = C_{n_{\delta_r}}.\delta_r \tag{3.34}$$

where,
$$C_{Y_{\delta_r}} = \eta_{VT}.\frac{S_{VT}}{S_w}.C_{L_{\alpha_{VT}}}.\tau \tag{3.35}$$

and
$$C_{n_{\delta_r}} = -\eta_{VT}.V_{VT}.C_{L_{\alpha_{VT}}}.\tau \tag{3.36}$$

$C_{n_{\delta_r}}$ is the rudder control effectiveness and determines the rate of change of yawing moment with δ_r. The factor τ can be estimated from Figure 3.4.

The rudder is, therefore, the primary control surface responsible for directional control. However, when asymmetrically deflected, the ailerons produces an adverse yaw due to difference in local drag (see Figure 3.6), given by:

$$(C_n)_{\delta_a} = C_{n_{\delta_a}}.\delta_a \tag{3.37}$$

with,

$$C_{n_{\delta_a}} = 2.K.C_L.C_{\ell_{\delta_a}} \tag{3.38}$$

where K Is an empirical factor, depending upon planform geometry, obtained from (USAF, 1978). Its value is negative and is in a range of -0.1 to -0.35, approximetly.

C_L Is the aircraft lift coefficient for zero aileron deflection.

$C_{\ell_{\delta_a}}$ Is the aileron's roll control power, presented in the next section.

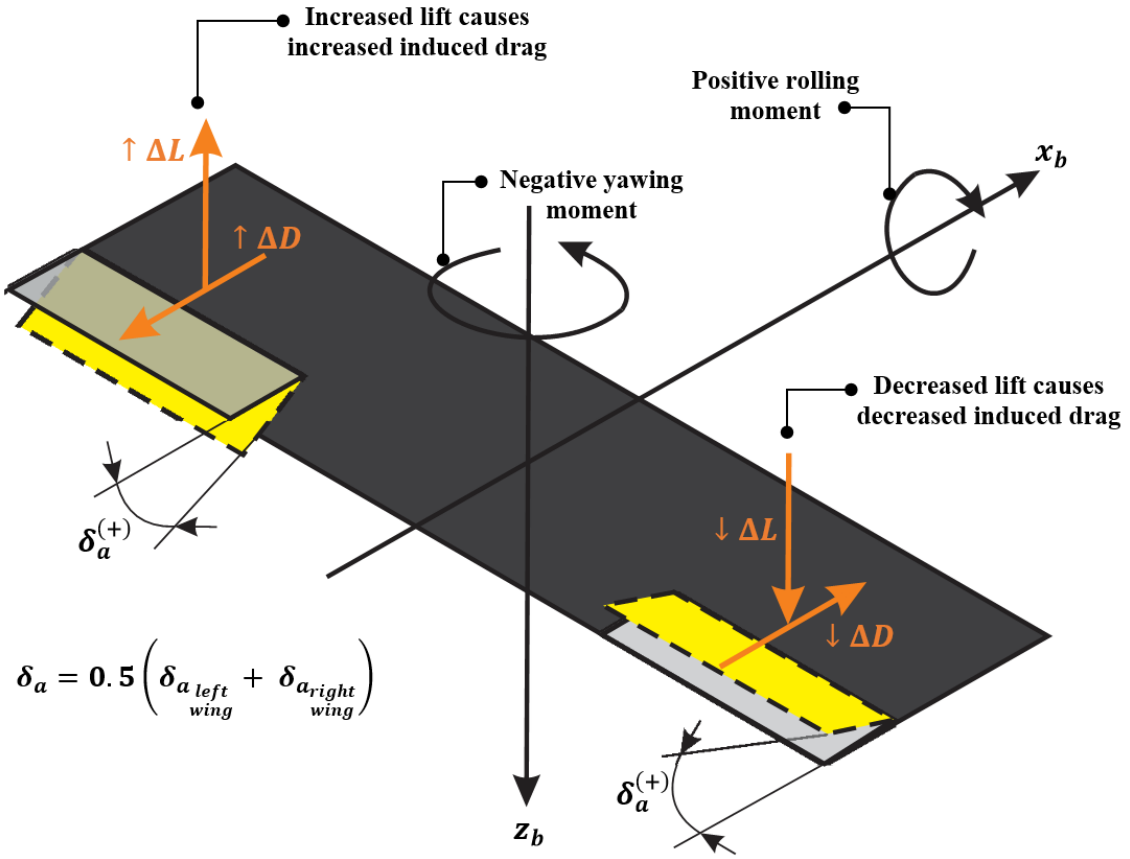

Figure 3.6: Yawing moment due to aileron deflection. Adapted from (Roskam, 2001).

One last observation about the role played by the ailerons in the directional stability is that they produce a negligible side force variation. Then:

$$C_{Y_{\delta_a}} = \frac{\partial C_Y}{\partial \delta_a} \approx 0 \tag{3.39}$$

Hence, the total side force coefficient and yaw moment coefficient, in a sideslip flight condition are:

$$C_Y = C_{Y_\beta}.\beta + C_{Y_{\delta_a}}.\delta_a + C_{Y_{\delta_r}}.\delta_r \tag{3.40}$$

$$C_n = C_{n_\beta}.\beta + C_{n_{\delta_a}}.\delta_a + C_{n_{\delta_r}}.\delta_r \tag{3.41}$$

3.5 Roll Control

The main surfaces responsible for the roll control are the ailerons and spoilers[7]. Its primary function is to produce a rolling moment[8], by modifying the spanwise lift distribution so that there will be an increase in lift on one side and a decrease in the opposite side. Nelson (1998) and Gudmundsson (2014) estimates the roll control power $\left(C_{\ell_{\delta_a}}\right)$ by a strip integration method, illustrated in Figure 3.7.

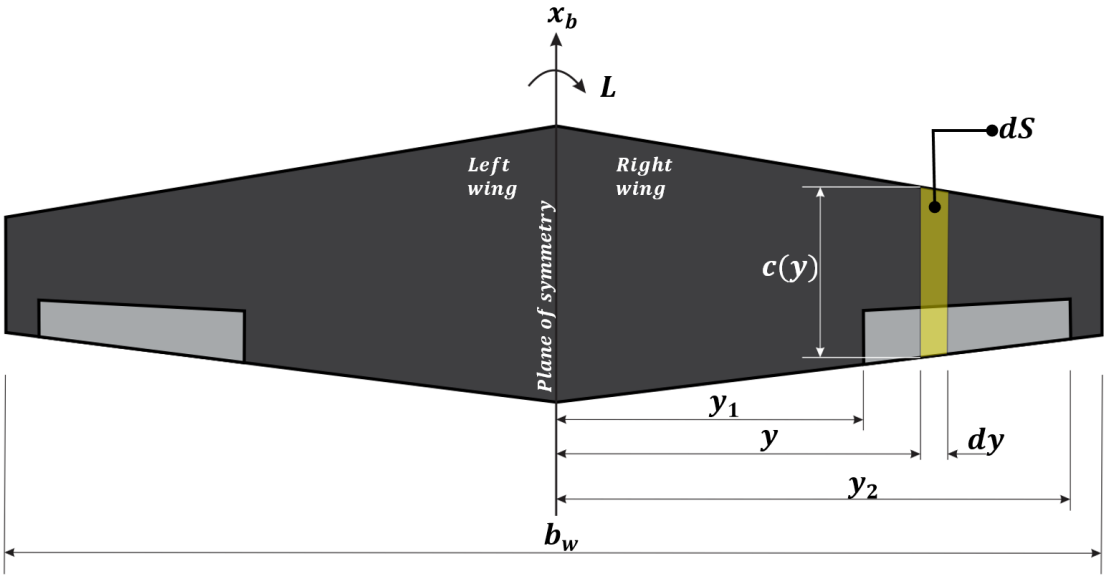

Figure 3.7: Definition of the aileron geometry. Adapted from (Gudmundsson, 2014).

The roll coefficient moment is given by (see (Nelson, 1998) for demonstration):

$$C_\ell = C_{\ell_{\delta_a}}.\delta_a \tag{3.42}$$

where,

$$C_{\ell_{\delta_a}} = \frac{2.C_{L_{\alpha_w}}.\tau}{S.b}.\int_{y_1}^{y_2} c(y).y.dy \tag{3.43}$$

[7] Although the spoilers helps to provide roll moment in a comparable manner to the ailerons, in the present work they will not be considered during the sizing methodology.

[8] They frequently introduce a yawing moment as well, but this effect will be neglected for the sizing procedures.

As expected, a secondary surface responsible for roll control is the rudder. Its actuation provides roll moment for the same reason that the vertical tail side force does: the z_{VT} distance from the CG (see Figure A.4, appendix A.2). The roll moment created by a rudder deflection can be calculated by:

$$(C_\ell)_{\delta_r} = C_{\ell_{\delta_r}}.\delta_r \tag{3.44}$$

where,

$$C_{\ell_{\delta_r}} = \eta_{VT}.\frac{|z_{VT}|.S_{VT}}{b_w.S_w}.C_{L_{\alpha_{VT}}}.\tau \tag{3.45}$$

Hence, the total roll moment coefficient, in a sideslip flight condition is:

$$C_\ell = C_{\ell_\beta}.\beta + C_{\ell_{\delta_a}}.\delta_a + C_{\ell_{\delta_r}}.\delta_r \tag{3.46}$$

Equations (3.40), (3.41) and (3.46) will be very useful for the rudder sizing in Chapter IV.

CHAPTER IV

TAIL AND CONTROL SURFACES SIZING

The previous chapter was an introduction to the theory that will be applied in the following methodology. As presented in the diagram of Figure 4.1, the procedure consists, basically, in designing the horizontal tail from wing aerodynamic data and desirable characteristics for the airplane (e.g. neutral point, $C_{L_{\alpha_{HT}}}$). For the elevator design, additional data is needed, e.g. CG envelope and stall characteristics. From this procedure, for a conventional configuration, where the aerodynamic center of horizontal and vertical tails can be considered equal (Gudmundsson, 2014), it is possible to estimate an initial size for the vertical tail. To achieve the final configuration of vertical tail, its design must be simultaneous to the rudder design to ensure that all lateral stability requirements are met.

Then, airworthiness requirements imposed by aeronautic authorities (e.g. FAA, ANAC) propose the guidelines to size aileron and rudder. The subsequent sections will treat each design procedure individually. The choice of which requirement will be followed, depends on the type of aircraft that is being designed.

The following procedure, when realized throughout an aircraft design since its beginning and few geometrical data are available, must be accomplished side by side with the team in charge of the CG envelope conception.

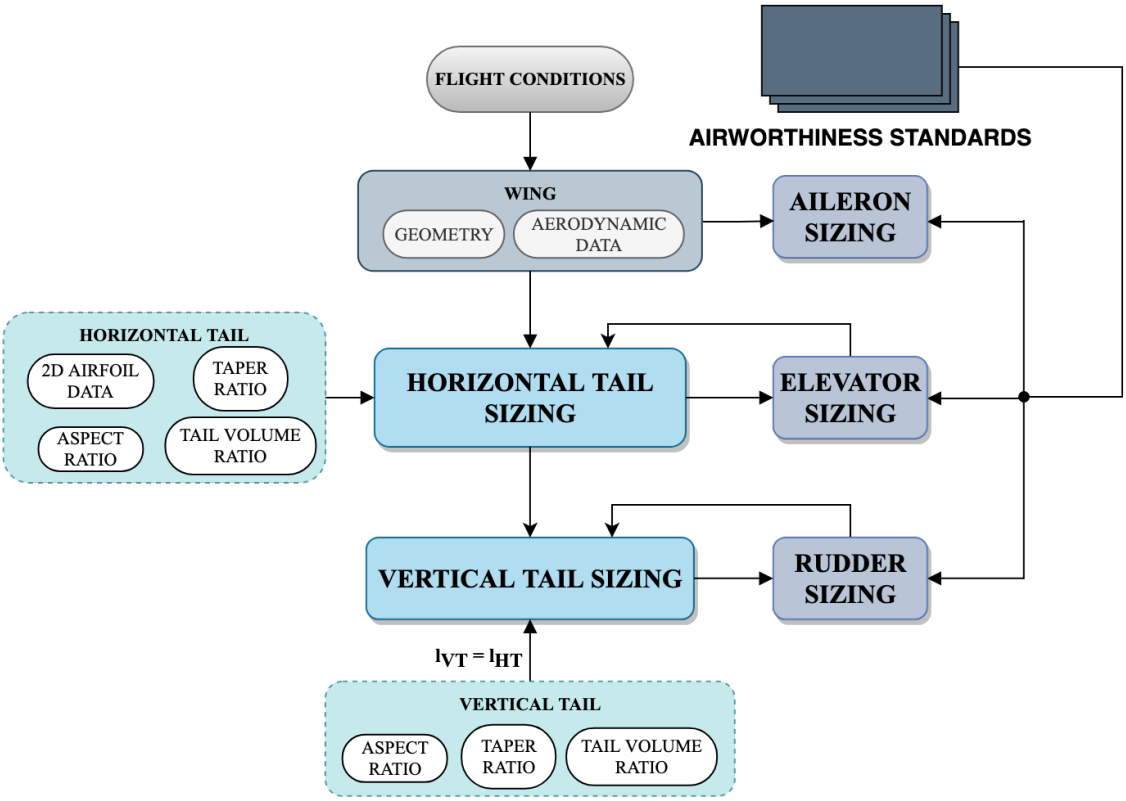

Figure 4.1: Overlay procedure structure.

4.1 HORIZONTAL TAIL

The design of horizontal tail can be accomplished by the combination of equations (3.11) and (3.15). From Figure 4.1, one can infer that the only unknown is the horizontal tail surface.

Thus, substituting the C_{L_α} equation into the neutral point equation, one may obtain:

$$S_{HT} = \frac{S_w}{\eta_{HT}.C_{L_{\alpha_{HT}}}.(1-\epsilon_\alpha)}.\left[\frac{\eta_{HT}.\bar{V}_{HT}.C_{L_{\alpha_{HT}}}.(1-\epsilon_\alpha)}{h_n - h_{AC_w}} - C_{L_{\alpha_w}}\right] \tag{4.1}$$

It is usual to have h_n as an imposed parameter, since the minimal statical stability margin and the most forward CG position are given. When it is not the case, one must evaluate the effects of the neutral point in the horizontal tail sizing (see Figure 4.2).

Notice that $\bar{V}_{HT}$ is a parameter that depends on S_{HT}. Then, one must perform a parametric evaluation of the tail volume ratio before determine the tail surface area. The

term between brackets in equation (4.1) restricts the value chosen for $\bar{V}_{HT}$, since one must guarantee that this term is grater then zero. Hence,

$$\bar{V}_{HT} > (\bar{V}_{HT})_{critical} = C_{L_{\alpha_w}} . \frac{(h_n - h_{AC_w})}{\eta_{HT} . C_{L_{\alpha_{HT}}} . (1 - \epsilon_\alpha)} \tag{4.2}$$

Figure 4.2 illustrates how S_{HT} and l_{HT} varies for different values of $\bar{V}_{HT}$ and h_n. For the sake of comparison, the graph shows non-dimensional values that gives a better idea of how big is the tail compared to the wing and how big is the distance between wing and tail compared to the fuselage length. The x-axis shows how greater the tail volume ratio is from the critical value $(\bar{V}_{HT})_{critical}$. In this example, there are two different values of h_n and, therefore, two different values for the critical tail volume ratio. Here $\bar{V}_{HT}$ is considered 5% to 25% greater than the critical value in each case.

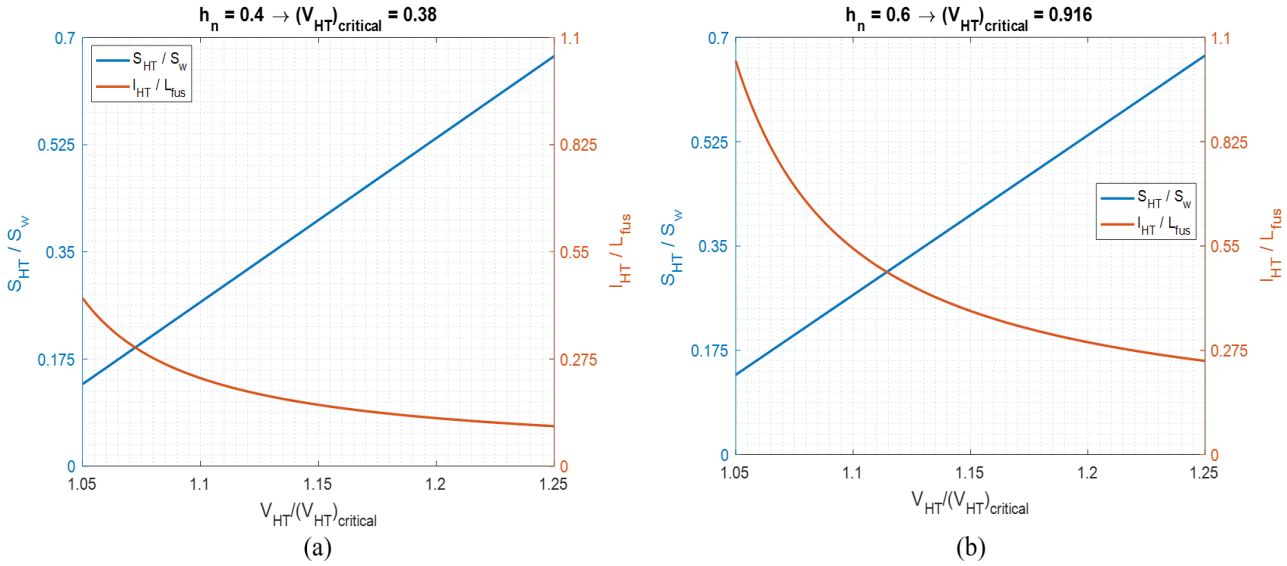

Figure 4.2: Effect of $\bar{V}_{HT}$ in S_{HT} and l_{HT} for a given neutral point.

In initial phases of design, the same analysis may help to determine other parameters, such as AR_{HT} and the airfoil used in the horizontal tail.

4.1.1 The Slope of HT Lift Curve

To estimate the lift curve slope of a 3D lifting surface, there is a good approximation that relates only the slope of the airfoil section (C_{l_α}) and its aspect ratio (AR).

$$\frac{\partial C_L}{\partial \alpha} = C_{L_\alpha} = \frac{C_{l_\alpha}}{1 + \frac{C_{l_\alpha}}{AR}} \tag{4.3}$$

This correlation is a fine first guess for $C_{L_{\alpha_{HT}}}$[9]. Once the horizontal tail is designed, a more accurate value of the slope of the lift curve can be calculated via an aerodynamic analysis, such as the lift line theory (LLT). Then, the new value of $C_{L_{\alpha_{HT}}}$ will be used to re-size the horizontal tail. This procedure must be iterative until the convergence of $C_{L_{\alpha_{HT}}}$.

It is important to remark that the choice of horizontal tail airfoil has an import role in the tail's design, since it affects directly the value of $C_{L_{\alpha_{HT}}}$. From equation (4.1) it is clear that a high $C_{L_{\alpha_{HT}}}$ provides a smaller S_{HT}. However, other characteristics of the airfoil section must be taken into account such as its drag and pitching moment. Hence, an aerodynamic study about the horizontal tail airfoil section is highly recommended during the tail's design. This study helps to ensure the best configuration was chosen (e.g. a configuration that reduces the airplane total drag and meet the stability needs).

4.2 ELEVATOR

The strategy to size the elevator is based on guarantee that the aircraft will be able to stablish a trim condition at V_{stall}. Trim condition is achieved by a combination of angle of attack and elevator deflection (δ_e) that provides enough C_L to compensate the aircraft's weight at the flight velocity and with zero pitching moment. To find this combination one must solve equations (3.18) and (3.19) simultaneously[10].

However, at this point, one does not have the elevator dimensions, which means that its effectiveness parameter (τ) is also unknown. As the elevator deflection at V_{stall} is expected to be the most negative, one remains with two equations and two unknowns. Re-writing equations (3.18) and (3.19) in matrix form and, with α and τ as the dependent variables, yields:

$$\begin{bmatrix} C_{L_\alpha} & \eta_{HT}.\frac{S_{HT}}{S_w}.C_{L_{\alpha_{HT}}}.\delta_{e_{min}} \\ C_{m_\alpha} & -\eta_{HT}.\bar{V}_{HT}.C_{L_{\alpha_{HT}}}.\delta_{e_{min}} \end{bmatrix}.\begin{Bmatrix} \alpha \\ \tau \end{Bmatrix} = \begin{Bmatrix} C_{L_{@V_{stall}}} - C_{L_0} \\ -C_{m_0} \end{Bmatrix} \tag{4.4}$$

where, $C_{L_{@V_{stall}}} = 2.W/(\rho.V_{stall}^2.S_w)$. The calculated value of τ can be used to define the elevator surface (S_e) with the aid of Figure 3.4.

[9] This correlation gives good approximation for lifting surfaces with $AR \geq 4$. For lower aspect ratio approximations, see (Anderson, 2011).

[10] One should notice that equations (3.18) and (3.19) are the same as equations (2.8) and (2.10), but in a coefficient form.

In addition, one must verify if the elevator designed is able to produce enough pitching moment during the take-off run at the rotation velocity ($V_R \cong 0.8.V_{TO}$). A simplified way to do this verification is to evaluate the moment around the main landing gear as shown in Figure 4.3[11].

If the moment is positive (nose up), the elevator design is satisfactory. Otherwise, an iteration process must augment the elevator surface, until this requirement is satisfied. Despite of the simplicity of this criterion, which does not take account for the rate of pitching, it leads to satisfactory results at the early stage design.

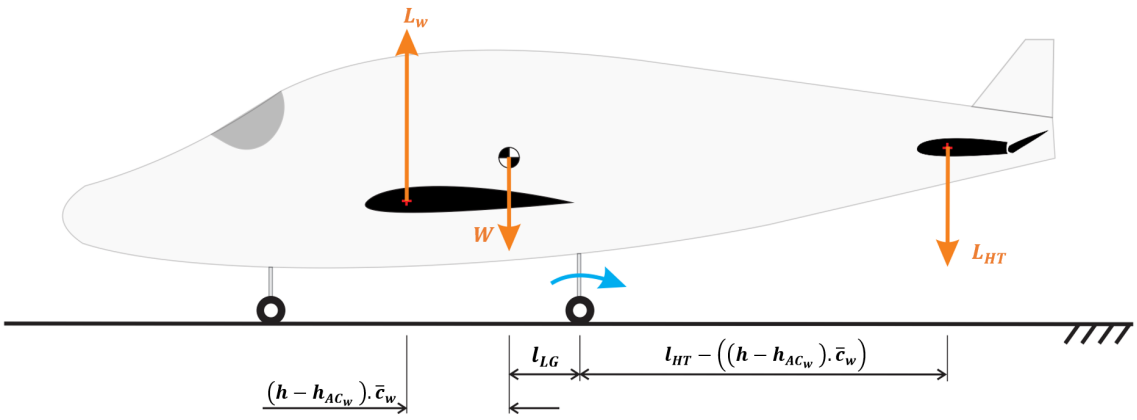

Figure 4.3: Rotation about the main landing gear during take-off run.

4.3 VERTICAL TAIL

The assumption that both vertical and horizontal tails has their aerodynamic center aligned (at the longitudinal axis, Figure 4.4), is not a strong one for conventional configuration (Gudmundsson, 2014). Hence, with l_{VT} determined, the vertical tail surface is:

$$S_{VT} = \frac{V_{VT}.b_w.S_w}{l_{VT}} \tag{4.5}$$

The choice of the vertical tail volume ratio (V_{VT}) is such that, there will be enough area for the rudder on the vertical tail, so the lateral stability requirements can be fulfilled. Therefore, their design are interdependent, as said earlier in this chapter.

[11] Note that, since de aircraft is on the ground, before rotating the angle of attack of the wing is its own incidence at the fuselage. For the horizontal tail, it is: $\alpha_{HT} = i_{HT} - \epsilon$.

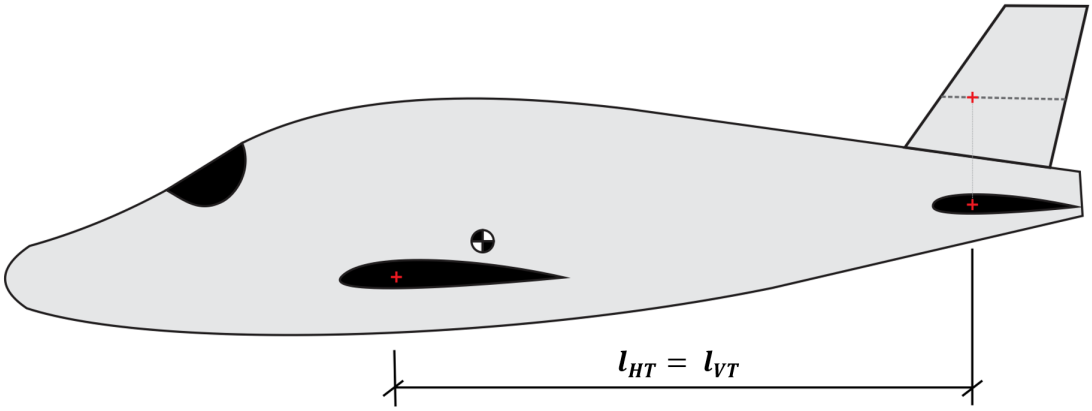

Figure 4.4: Illustration of vertical and horizontal tail lift centers alignments.

4.4 AILERON

Two major steps defines the aileron design, the choice of its span and location along the wingspan and the evaluation of the its area. The first one is made in such a way that the rolling moment produced by the ailerons deflection will be optimal. The second step is based on the steady-state roll helix angle $\left(\frac{pb_w}{2V_\infty}\right)$.

In order to achieve maximum responsiveness, the aileron position at the wingspan must be where the local rolling moment is maximized. As shown in Figure 4.5, for the specific wing geometry simulated, the region around 80% of the span presents a peak of rolling moment with the aileron in neutral position. This peak location is highly dependent on the wing geometry (Gudmundsson, 2014). The designer should choose this position as the centroid of the aileron. Then, the choice of the span can be made based on a threshold value with respect to the maximum local rolling moment for the wing with zero aileron deflection (e.g. 95% of max$[C_\ell(y)]$).

The second step is to calculate the aileron's area. This calculation is based on the steady-state roll helix angle $\left(\frac{\mathrm{p.b_w}}{2.\mathrm{V_\infty}}\right)$, defined by:

$$\left(\frac{p.\,b_w}{2.\,V_\infty}\right) = -\frac{C_{\ell_{\delta_a}}}{C_{\ell_p}}.\,\delta_a \tag{4.6}$$

where p is the roll rate in rad/s, $C_{\ell_{\delta_a}}$ is the aileron authority derivative (see Section 3.5) and C_{ℓ_p} is the roll damping. An approximation for C_{ℓ_p} is proposed by (Gudmundsson, 2014) and is given by:

$$C_{\ell_p} = -\frac{4\left(C_{l_\alpha} + C_{d_0}\right)}{S_w b_w^2} \int_0^{b/2} y^2\, c(y)\, dy \tag{4.7}$$

C_{l_α} and C_{d_0} are the mean lift curve slope and drag coefficients of the local airfoils sections.

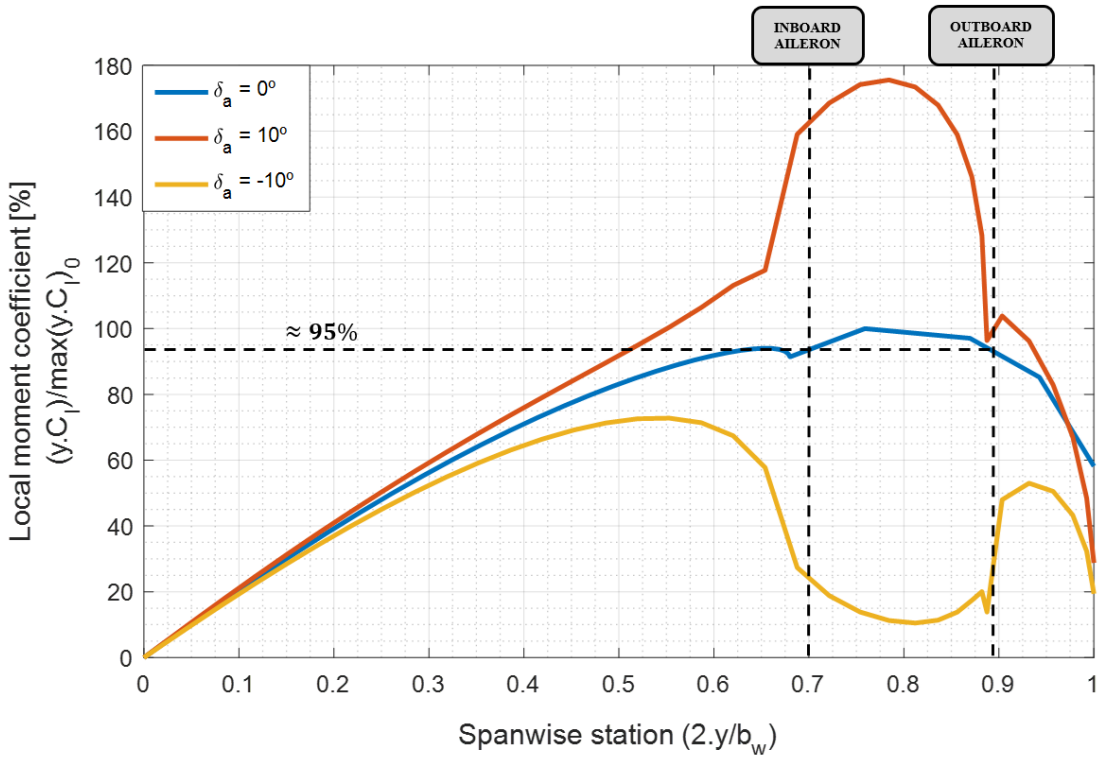

Figure 4.5: Normalized spanwise distribution of local rolling moment coefficients. Simulation made with XFLR5© software, with LLT method, for a wing with: λ=0.45, AR=10, α=2°.

According to (Nelson, 1998), the minimal value for the ratio $\left(\frac{p.b_w}{2.V_\infty}\right)$ should be at least 0.07 for cargo and transport airplanes. Thus, after evaluating the value of the roll damping and choosing the value of the steady-state roll helix angle, it is possible to calculate τ by introducing the $C_{\ell_{\delta_a}}$ equation (3.43) into equation (4.6):

$$\tau = -C_{\ell_p} . \frac{b_w\, S_w}{2\, C_{L_{\alpha_w}}\, \delta_{a_{max}} \int_{y_1}^{y_2} c(y).y\, dy} . \left(\frac{p.b_w}{2.V_\infty}\right) \tag{4.8}$$

Equation (4.8) assumes that the specified value for $\left(\frac{p.b_w}{2.V_\infty}\right)$ will be reached with maximum aileron deflection ($\delta_{a_{max}}$). Once the ailerons position and span are known, one can calculate its effectiveness parameter (τ) and, with help of Figure 3.4, evaluate its inboard and outboard chords.

4.5 RUDDER

A symmetrical airplane, with positive yaw stiffness (C_{n_β}) tend to fly in a zero β condition, which is desired in most cases. The need for a yaw control is to guarantee that the aircraft is able to keep this condition when yawing moments may act upon the airplane

(Table 4.1). Since the rudder is the surface that provides this control, its design needs to cover all the requirements presented in Table 4.1.

Table 4.1: Requirements for directional control. Adapted from (Nelson, 1998).

Rudder requirements	Implication for rudder design
Crosswind landings	The rudder must be able to permit the pilot to trim the airplane and maintain alignment with the runaway during a crosswind landing, for the specified crosswinds. Landing may be carried out for 90º crosswinds up to $0.2V_{stall}$ (FAR 23 Section 233, (FAA, 2017)), for general aviation airplanes, and 25kts, for transport airplanes (FAR 25 Section 233, (FAA, 2017)).
Asymmetric power condition	For multiengine airplanes, the rudder must be able to overcome the yawing moment produced by asymmetric thrust triggered by the failure of one or more engines at low flight speeds.
Adverse yaw	While a turning maneuver, when the airplane is banked, the ailerons may create an adverse yawing moment that opposes the turn. The critical condition occurs at low flight speeds. The rudder must overcome this adverse yaw so that the airplane may achieve a coordinated turn.
Spin recovery	The rudder must be powerful enough to oppose the spin recovery.

Although there were presented four requirements that the rudder must accomplish, for rudder design purposes one may consider only the two most critical, crosswind landings and asymmetric power condition. The other two may be verified after the rudder design is ready.

The strategy to size the rudder is based on guaranteeing that the aircraft will be able to be in a lateral trim condition in both critical cases. Lateral trim condition is achieved by a combination of bank angle (Φ), sideslip angle (β), aileron deflection (δ_a) and rudder deflection (δ_r) that provides zero roll and yaw moments and compensates the lateral component of the weight (due to the bank angle). To find this combination one must solve equations (2.7), (2.9) and (2.11) simultaneously. Those equations may also be written in a coefficient matrix form as:

$$\begin{bmatrix} C_{Y_\beta} & C_{Y_{\delta_a}} & C_{Y_{\delta_r}} \\ C_{\ell_\beta} & C_{\ell_{\delta_a}} & C_{\ell_{\delta_r}} \\ C_{n_\beta} & C_{n_{\delta_a}} & C_{n_{\delta_r}} \end{bmatrix} . \begin{Bmatrix} \beta \\ \delta_a \\ \delta_r \end{Bmatrix} = \begin{Bmatrix} \dfrac{-m.g.\sin(\Phi).\cos(\Theta) + F_{Y_T}}{q_\infty . S_w} \\ \dfrac{-L_T}{q_\infty . S_w . b_w} \\ \dfrac{-N_T}{q_\infty . S_w . b_w} \end{Bmatrix} \tag{4.9}$$

where, F_{Y_T} Is the thrust component of the aero-propulsive force Y.

L_T Is the thrust component of the aero-propulsive roll moment L.

N_T Is the thrust component of the aero-propulsive yaw moment N.

Since there are four variables and only three equations, one of them needs to be specified. In addition, at this point, one does not have the rudder dimensions, meaning that its effectiveness parameter (τ) is also unknown. However, as stated before, the sizing procedure considers a critical flight condition. Therefore, it is assumed that the rudder deflection is known, being its maximum value (which one of the parameters defined by the designer).

The following sub-sections describes how to design the rudder for a crosswind landing and for an asymmetric power condition, respectively, by modifying equation (4.9). The chosen rudder will be the greater one, which will be capable to fulfill both requirements.

4.5.1 CROSSWIND LANDING

As mentioned in Table 4.1, during the crosswind landing, rudder control is applied to align the aircraft with the runway heading allowing the airplane to be trimmed at the specified crosswind condition (see Figure 4.6). To accomplish this requirement, the rudder must be able to allow the airplane to fly with a sideslip angle defined by:

$$\beta = \arcsin\left(\frac{V_{wind}}{V_\infty}\right) \tag{4.10}$$

where V_∞ is the aircraft total speed:

$$V_\infty = \sqrt{u_0^2 + V_{wind}^2} \tag{4.11}$$

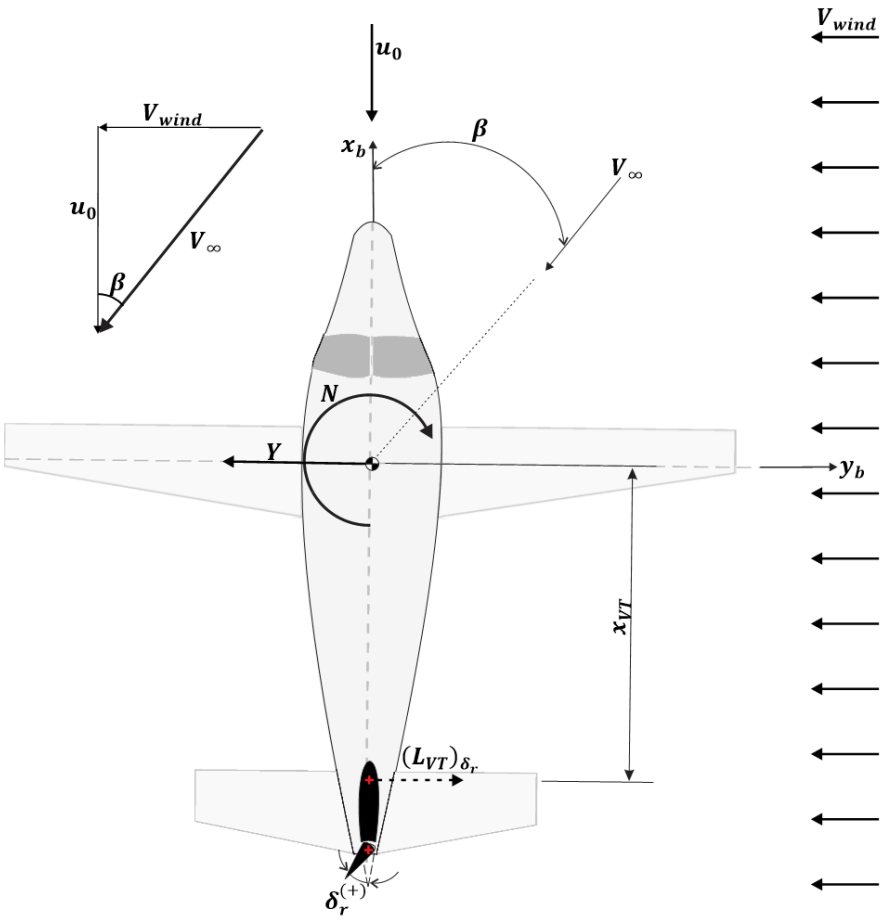

Figure 4.6: Free body diagram for a crosswind landing. Note that the dashed force (L_{VT})δr is embedded in the side force Y formulation, but acts in a different point.

Thus, the first modification on equation (4.9) is that the sideslip angle is known. Hence, the unknowns are: Φ, δ_a and τ. Note that the term τ is embedded in the rudder's derivatives:

$$C_{Y_{\delta_r}} = \eta_{VT}.\frac{S_{VT}}{S_w}.C_{L_{\alpha_{VT}}}.\tau$$

$$C_{\ell_{\delta_r}} = \eta_{VT}.\frac{|z_{VT}|.S_{VT}}{b_w.S_w}.C_{L_{\alpha_{VT}}}.\tau$$

$$C_{n_{\delta_r}} = -\eta_{VT}.V_{VT}.C_{L_{\alpha_{VT}}}.\tau$$

In crosswind landings, both the bank and the approximation angles are expected to be small. Hence, it is reasonable to approximate:

$$sin(\Phi) \approx \Phi$$

$$\cos(\Theta) \approx 1$$

Furthermore, for the crosswind problem, the engines are assumed to work properly.

$$F_{Y_T} = L_T = N_T = 0$$

Then, the modified version of equation (4.9) for the rudder design by the crosswind-landing criterion is:

$$\begin{bmatrix} \frac{m.g}{q_\infty.S_w} & C_{Y_{\delta_a}} & \eta_{VT}.\frac{S_{VT}}{S_w}.C_{L_{\alpha_{VT}}}.\delta_{r_{max.}} \\ 0 & C_{\ell_{\delta_a}} & \eta_{VT}.\frac{|z_{VT}|.S_{VT}}{b_w.S_w}.C_{L_{\alpha_{VT}}}.\delta_{r_{max.}} \\ 0 & C_{n_{\delta_a}} & -\eta_{VT}.V_{VT}.C_{L_{\alpha_{VT}}}.\delta_{r_{max.}} \end{bmatrix} . \begin{Bmatrix} \Phi \\ \delta_a \\ \tau \end{Bmatrix} = \begin{Bmatrix} -C_{Y_\beta}.\beta \\ -C_{\ell_\beta}.\beta \\ -C_{n_\beta}.\beta \end{Bmatrix} \quad (4.12)$$

Solving the linear system of equation (4.12), one will found the effectiveness parameter needed for the rudder to be able to trim the aircraft at a 90º crosswind approximation. Then, with the help of Figure 3.4, the rudder's surface can be determined. In addition, one must verify that the aileron deflection obtained does not exceeds its maximum deflection and that the bank angle is acceptable (lower than 10º, (FAA, 2017)).

4.5.2 Asymmetric Power Condition

Because the present method is meant to be applied during the early stage of the aircraft design, some assumptions need to be made. Among them, the engines are considered to be aligned with the fuselage centerline and with the CG[12]. Therefore, even in the case of an asymmetric power condition, the side force and the rolling moment due to the propulsive system remains zero. The yaw moment, however, is given by:

$$N_T = \sum_{i=1}^{n} -T_i.y_i \quad (4.13)$$

where, n represents the number of operative engines, T_i is the thrust of *i-th* the operating engine and y_i is its position along the wingspan. For design purposes, the worst condition must always be presumed and, therefore, it is reasonable to assume the failure of all engines of one side.

As mentioned before, to close the linear system from equation (4.9), one of the four variables must be specified. For the engine failure case, the certification requirements

[12] If more detailed data with respect to the engines position are available, (Roskam, 2001) provides a more complete model, capable to account for propulsive side force and rolling moment.

states that the aircraft must remain trimmed with a bank angle that do not exceed five degrees for speeds above $1.2.V_{stall}$ (FAA, 2017).

Similarly to the case of cross wind landing, the maximum rudder deflection is assumed. The unknowns will be the sideslip angle, aileron deflection and the rudders efficiency parameter. Then, the modified version of equation (4.9) for the rudder design by the asymmetric power criterion is:

$$\begin{bmatrix} C_{Y_\beta} & C_{Y_{\delta_a}} & \eta_{VT}.\frac{S_{VT}}{S_w}.C_{L_{\alpha_{VT}}}.\delta_{r_{max.}} \\ C_{\ell_\beta} & C_{\ell_{\delta_a}} & \eta_{VT}.\frac{|z_{VT}|.S_{VT}}{b_w.S_w}.C_{L_{\alpha_{VT}}}.\delta_{r_{max.}} \\ C_{n_\beta} & C_{n_{\delta_a}} & -\eta_{VT}.V_{VT}.C_{L_{\alpha_{VT}}}.\delta_{r_{max.}} \end{bmatrix} . \begin{Bmatrix} \beta \\ \delta_a \\ \tau \end{Bmatrix} = \begin{Bmatrix} -\frac{m.g.\sin(\Phi)}{q_\infty.S_w} \\ 0 \\ \frac{-\sum_{i=1}^{n} -T_i.y_i}{q_\infty.S_w.b_w} \end{Bmatrix} \quad (4.14)$$

CHAPTER V

APPLICABILITY

The methodology presented in Chapter IV was developed during a hybrid-electric aircraft conceptual design. The design requirements were determined by a Request of Proposal (RFP) for the annual design competition sponsored by The American Institute of Aeronautics and Astronautics (AIAA Technical Committee, 2018). To accomplish the project, there were eight teams: Conceptual Design, Interior, Market, Aerodynamics, Flight Mechanics, Structural, Propulsive and Systems.

The RFP for the 2018-2019's competition requires the design of a hybrid-electric aircraft capable to transport up to six passengers plus a single pilot, with total payload of 626 kg, certificated according to 14 CFR Part 23 (FAA, 2017) . Its mission is for short haul or on-demand operations servicing small airports. Missions are flown at ISA+0, zero wind conditions, with sea level field elevation for takeoffs and landings. The whole list of requirements and constraints for this project can be found at (AIAA Technical Committee, 2018).

Based on the RFP the Aerodynamic team, along with the Interior and Conceptual Design teams, defined the wing-fuselage configuration. The tail and control surfaces

design were developed along with the aircraft's CG envelope. The following sections presents the aircraft configuration before the tail design and each step of the methodology presented in Chapter IV.

To automate the design process, an algorithm was coded in MATLAB® language. Furthermore, in order to avoid excessive need of external software, a lift line theory (LLT) routine was implemented in order to evaluate the aerodynamic characteristics of the wing and the horizontal tail. This LLT algorithm is based on the notes of (Ba, 2017). However, to account for the fuselage presence in some stability coefficients, the USAF Digital DATCOM software was utilized. This software was also used to calculate the stability derivatives after the aircraft design in order to perform the dynamic stability analysis on section 5.4. In addition, the software XFLR5© was utilized to evaluate some airfoil sections characteristics for the horizontal tail.

5.1 AIRCRAFT DATA

The Conceptual Design team defined the wing load, providing the basis for the Aerodynamic team to define the wing's characteristics. In addition, the Interior team designed the distribution of passengers and crew inside the aircraft, defining the fuselage's external shape. The initial configuration of the aircraft is presented at Table 5.1. The wing airfoil section is the NACA63$_1$412, which main characteristics are presented in Table 5.2 and Figure 5.1.

Table 5.1: Aircraft characteristics.

Variable name	Symbol	Value	Unit	Defined by
Fuselage length	L_{fus}	9.00	[m]	Interior design and Aerodynamic team
Stall velocity	V_{stall}	31.4	[m/s]	Regulation requirements (FAA, 2017)
Cruise velocity	V_{cruise}	97.8	[m/s]	RFP
Wing data				
Position[(1)]	X_{wing}	3.50	[m]	Interior design
Area	S_w	15.40	[m^2]	Aerodynamic team
Span	b_w	12.41	[m]	
Root chord	c_{r_w}	1.71	[m]	
M.A.C.[(2)]	$\bar{c}_w$	1.30	[m]	
A.C. position	h_{AC_w}	0.258	-	
Aspect ratio	AR_w	10.00	-	
Taper ratio	λ_w	0.45	-	
Sweep angle[(3)]	$(\Lambda_w)_{1/4}$	0	[deg]	
Twist angle	θ_w	0	[deg]	
Dihedral angle	Γ_w	0	[deg]	

(1) With respect to the fuselage nose.
(2) Mean Aerodynamic Chord.
(3) With respect to the ¼ chord line.

Table 5.2: Wing airfoil section characteristics at Re = 6e+06.

$C_{l_\alpha}\ [rad^{-1}]$	C_{d_0}	$C_{m_{AC}}$	$C_{l_{max}}$	$\alpha_{stall}\ [deg]$
6.0092	0.0055	-0.0800	1.7700	15

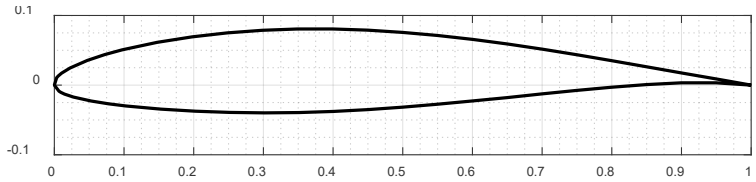

Figure 5.1: NACA63$_1$412.

In addition, the Propulsive team had defined four engines on each semi-wing. The inboard engine have a take-off power of 36.3 kW and the other three have 32.6 kW.

5.1.1 THE CG ENVELOPE

The size of the empennage interferes with the total aircraft weight and, hence, with the CG position. On the other hand, the CG position interferes with the empennage sizing. Thus, the both of them must be construct together and iteratively. Figure 5.2 presents the final CG envelope with two scales: as a percentage of the M.A.C. and the position with respect to the aircraft nose. The range (most forward and most aft position) is determined by quantity of passengers and amount of fuel.

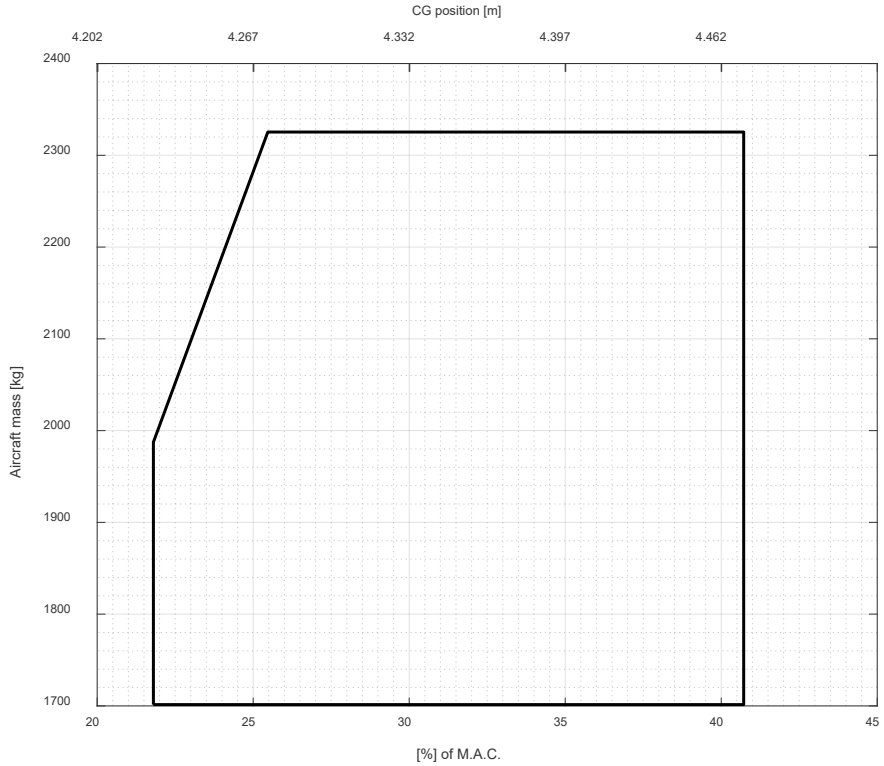

Figure 5.2: Aircraft CG envelope.

5.2 EMPENNAGE DESIGN

5.2.1 HORIZONTAL TAIL

Also in the course of the conceptual design, it was decided that a conventional tail configuration would be applied. This decision was based on a study done by the Market team and, with help of a decision matrix, the team realized that this configuration was suitable for other areas of the project. The variables used as input for the horizontal empennage are summarized in Table 5.3.

Table 5.3: Horizontal tail input parameters.

Variable name	Symbol	Value	Unit
Aircraft			
Location of stick-fixed neutral point(1)	h_n	0.5	-
Wing-fuselage			
Wing area	S_w	15.4	[m^2]
Lift slope	$(C_{L_\alpha})_{wf}$	6.084	[rad^{-1}]
Downwash slope	ϵ_α	0.474	[rad^{-1}]
Horizontal tail			
Aspect ratio	AR_{HT}	6.5	-
Taper ratio	λ_{HT}	0.6	-
Angle of incidence at the fuselage	i_{HT}	0	[deg]
Twist angle	θ_{HT}	0	[deg]
Sweep angle	$(\Lambda_{HT})_{1/4}$	0	[deg]
Dihedral angle	Γ_{HT}	0	[deg]
HT efficiency	η_{HT}	0.95	-

(1) With respect to the leading edge of the M.A.C. and normalized by its chord ($\bar{c}_w$).

The choice of h_n was based on the parametrical study recommended in section 4.1. For this study, an average value of $C_{L_{\alpha_{HT}}}$ was used (considering that the airfoil section was not chosen at this point). It was clear that, even with a variation of $C_{L_{\alpha_{HT}}}$, h_n=0.5 was the neutral point position which would provide the best trade-off between S_{HT} and l_{HT}.

The initial range of aspect ratio (AR_{HT}) and taper ratio (λ_{HT}) analyzed was based on historical values of airplanes with similar characteristics. However, as an attempt to reduce the tail induced drag, which was one of the main goals of the project, a slightly higher value of aspect ratio was chosen for the horizontal tail. For the taper ratio, a mean value was considered in order to preserve good stall characteristics at the tail.

Twist, sweep and dihedral angles were not considered relevant due to the flight speed range of the aircraft. As for the incidence angle at the fuselage, it would be

considered only if the angle of attack of the tail approaches to its stall angle at critical trim condition. Further analysis after the design process had shown that it was not the case.

The airfoil section was chosen after an aerodynamic study of its influence in the final S_{HT} and in the aircraft drag coefficient during cruise flight. Table 5.4 presents the airfoils analyzed and their relevant aerodynamic characteristics. All airfoils within this table were simulated with inverted camber. Among then, the AH21 presented the best characteristics, with reasonable stall angle, and good trade-off between drag, lift and pitching moment. In addition, with the AH21, the final area of the horizontal tail is bigger than with other airfoils, without great increase of drag, which means that it can better accommodate the elevator.

Table 5.4: Characteristics of several airfoil sections and their impact on S_{HT} and the aircraft total drag in cruise flight. Airfoil characteristics simulated in XFLR5©, with inverted camber.

	NACA 6412	**NACA 4412**	**NACA 4410**	**NACA 65-410**	**AH21**
$\boldsymbol{\alpha_0}$	5.64º	4.272º	4.273º	3.13º	3.7º
$\boldsymbol{\alpha_{stall}}$	13.0º	15.0º	11.5º	11.0º	11.75º
$\boldsymbol{C_{l_0}}$	-0.6260	-0.5070	-0.5070	-0.3650	-0.3870
$\boldsymbol{C_{l_\alpha}}$	0.1105	0.1181	0.1181	0.1161	0.1042
$\boldsymbol{C_{m_{AC}}}$	0.1410	0.1070	0.1070	0.0820	0.1030
$\boldsymbol{C_{d_0}}$	0.0070	0.0064	0.0064	0.0058	0.0054
$\boldsymbol{S_{HT}}$	3.19	3.07	3.04	3.08	3.33
$\boldsymbol{C_{D_{cruise}}}$ (1)	0.01299	0.01287	0.01278	0.01274	0.01275

(1) Total drag coefficient of the aircraft, considering the elevator deflection.

With all parameters properly set, the next step is the choice of $\bar{V}_{HT}$. As mentioned in section 4.1, this choice is made considering an analytical approximation of $C_{L_{\alpha_{HT}}}$ and a percentage of $(\bar{V}_{HT})_{critical}$. It was found that a tail volume ratio 9.5% greater than the critical value was a reasonable value[13]. Then, after the $C_{L_{\alpha_{HT}}}$ correction, with the LLT algorithm, the final value of $\bar{V}_{HT}$ was 0.698. Table 5.5 summarizes the final horizontal tail geometric characteristics.

[13] Note that after the $C_{L_{\alpha_{HT}}}$ correction, the critical volume ratio will change. However, the tail volume ratio remains the same.

Table 5.5: Horizontal tail geometric characteristics.

Variable name	Symbol	Value	Unit
Surface	S_{HT}	3.16	[m²]
Span	b_{HT}	4.53	[m]
Root chord	$c_{r_{HT}}$	0.87	[m]
Tip chord	$c_{t_{HT}}$	0.52	[m]
M.A.C.	$\bar{c}_{HT}$	0.71	[m]
HT volume ratio	$\bar{V}_{HT}$	0.698	-
Distance between wing and HT A.C.'s	l_{HT}	4.42	[m]

5.2.2 VERTICAL TAIL

According to the methodology presented in section 4.3, once the horizontal tail is designed, the vertical tail can be easily sized. Table 5.6 condense the vertical tail geometric parameters.

Simulations with DATCOM software have shown that the wing-fuselage group have a destabilizing contribution, relatively high, to lateral stability ($C_{n_\beta} \approx -0.107\,\text{rad}^{-1}$). Therefore, the vertical tail volume ratio (V_{VT}) was chosen to size a vertical tail capable to overcome this negative contribution and provide a positive C_{n_β} for the airplane.

The sweep angle of 30º was chosen in order to fit the vertical tail root chord within the fuselage limits, while respecting the constrain: $l_{HT} = l_{VT}$. Both, the aspect ratio and taper ratio, were chosen as average values from similar aircrafts.

Table 5.6: Vertical tail geometric characteristics.

Variable name	Symbol	Value	Unit
Aspect ratio	AR_{VT}	3	-
Taper ratio	λ_{VT}	0.3	-
Sweep angle	Λ_{VT}	30	[deg]
Surface	S_{VT}	1.95	[m²]
Span	b_{VT}	2.42	[m]
Root chord	$c_{r_{VT}}$	1.24	[m]
Tip chord	$c_{t_{VT}}$	0.37	[m]
M.A.C.	$\bar{c}_{VT}$	0.88	[m]
VT volume ratio	$\bar{V}_{VT}$	0.045	-
Distance between wing and VT A.C.'s	l_{VT}	4.42	[m]

5.3 CONTROL SURFACES DESIGN

5.3.1 ELEVATOR DESIGN

Following the procedure described in section 4.2, the first criterion designed an elevator capable to trim the aircraft at stall velocity. However, it was not sufficient for the rotation criterion during the take-off run. Thus, an iterative process took place and the elevator area was augmented gradually, until both criteria were satisfied. Note that according to the procedure description, the elevator design considered the most aft CG position with the most unfavorable aircraft weight (see Figure 5.2).

Table 5.7 summarizes the elevator characteristics. The elevator span and the deflection range were design decision made on literature recommendations.

Table 5.7: Elevator characteristics.

Variable name	Symbol	Value	Unit
Surface	S_e	0.86	[m²]
Span	b_e	4.53	[m]
Root chord	c_{r_e}	0.24	[m]
Tip chord	c_{t_e}	0.14	[m]
Minimum deflection	$\delta_{e_{min}}$	-25	[deg]
Maximum deflection	$\delta_{e_{max}}$	20	[deg]
Effectiveness parameter	τ	0.488	-

5.3.2 AILERON DESIGN

For the aileron design, a value of 85% was set as the threshold value with respect to the maximum local rolling moment. As presented in Figure 5.3, this criterion positions the aileron between 67% and 95% of the wingspan. Table 5.8 presents the ailerons characteristics.

Table 5.8: Aileron characteristics.

Variable name	Symbol	Value	Unit
Inboard position	y_1	4.15	[m]
Outboard position	y_2	5.90	[m]
Surface	S_a	0.34	[m²]
Deflection range	δ_a	± 15	[deg]
Effectiveness parameter	τ	0.412	-

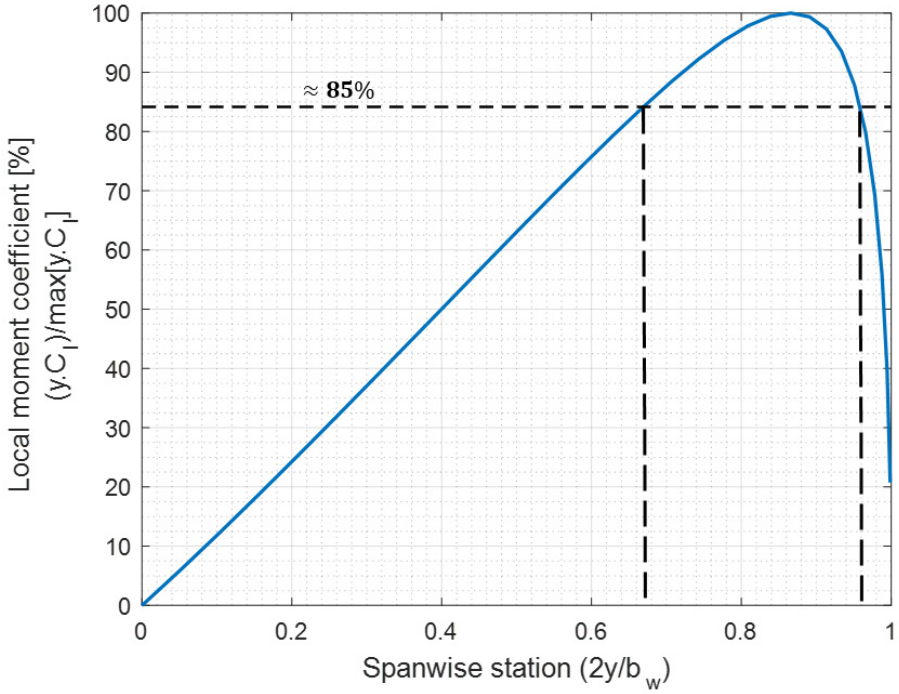

Figure 5.3: Normalized spanwise distribution of local rolling moment coefficients. Distribution calculated with the LLT algorithm.

5.3.3 RUDDER DESIGN

The rudder sizing considered the critical cases of crosswind landing and asymmetric power condition, as mentioned on section 4.5. Usually, for small aircrafts, the second one is the severest. As stated on 14 CFR Part 23 (FAA, 2017), the asymmetric power condition is characterized by the failure of the critical engine. For safety reasons, however, the rudder design was done considering the failure of two critical engines. Table 5.9 shows the rudder characteristics.

Table 5.9: Rudder geometric characteristics.

Variable name	Symbol	Value	Unit
Surface	S_r	0.85	[m²]
Span	b_r	2.42	[m]
Root chord	c_{r_r}	0.54	[m]
Tip chord	c_{t_r}	0.16	[m]
Deflection range	δ_r	$\pm$ 30	[deg]
Effectiveness parameter	τ	0.631	-

Important Note

During the rudder design, it was found that the linear system of equation (4.14) could result in unreal results for the sideslip angle and the effectiveness parameter. After further investigation, the problem was in the β derivatives considerations, which were calculated considering only the vertical tail effects. Rewriting the matrix on the left-hand side of equation (4.14):

$$\begin{bmatrix} C_{Y_\beta} & C_{Y_{\delta_a}} & \eta_{VT}.\frac{S_{VT}}{S_w}.C_{L_{\alpha_{VT}}}.\delta_{r_{max.}} \\ C_{\ell_\beta} & C_{\ell_{\delta_a}} & \eta_{VT}.\frac{|z_{VT}|.S_{VT}}{b_w.S_w}.C_{L_{\alpha_{VT}}}.\delta_{r_{max.}} \\ C_{n_\beta} & C_{n_{\delta_a}} & -\eta_{VT}.V_{VT}.C_{L_{\alpha_{VT}}}.\delta_{r_{max.}} \end{bmatrix}$$

$$\begin{bmatrix} -\eta_{VT}.\left(1+\frac{d\sigma}{d\beta}\right).\frac{S_{VT}}{S_w}.C_{L_{\alpha_{VT}}} & C_{Y_{\delta_a}} & \eta_{VT}.\frac{S_{VT}}{S_w}.C_{L_{\alpha_{VT}}}.\delta_{r_{max.}} \\ -\eta_{VT}.\left(1+\frac{d\sigma}{d\beta}\right).\frac{|z_{VT}|.S_{VT}}{b_w.S_w}.C_{L_{\alpha_{VT}}} & C_{\ell_{\delta_a}} & \eta_{VT}.\frac{|z_{VT}|.S_{VT}}{b_w.S_w}.C_{L_{\alpha_{VT}}}.\delta_{r_{max.}} \\ \eta_{VT}.V_{VT}.C_{L_{\alpha_{VT}}} & C_{n_{\delta_a}} & -\eta_{VT}.V_{VT}.C_{L_{\alpha_{VT}}}.\delta_{r_{max.}} \end{bmatrix}$$

Since the term $\left(1+\frac{d\sigma}{d\beta}\right)$ is almost one, it is clear that in this matrix the third column is proportional to the first by a factor of approximately $-\delta_{r_{max}}$. Thus, the determinant of this matrix is practically zero, making the system unsolvable.

Therefore, at this step of the design it is advisable to use a higher fidelity source for those derivatives calculations, which considers other components effects on the β derivatives.

5.4 Aircraft Characteristics and Flight Qualities

The following sections will present the final geometry of the aircraft as well as its inertia properties. In order to verify if the CG range does not cross the stick-free neutral point, a simple evaluation of the longitudinal stability when the elevator is completely free to rotate about its hinge is also done.

Furthermore, once the design of the tail and control surfaces is complete, one must evaluate the aircraft flight qualities. Since it is an extensive subject and can vary from country to country according to their own regulatory agency, the present work will treat only about the main flight qualities evaluation (presented by (Nelson, 1998) and (Roskam,

2001)). This evaluation involves a dynamic stability analysis considering the small-disturbance theory, briefly discussed in appendix B.2. In case of poor flying qualities, state feedback control can be used to improve stability characteristics (Nelson, 1998).

The flying qualities (or handling qualities) of an airplane are related to its stability and control characteristics and are the main definers of the pilot's impression of the airplane (Nelson, 1998). These qualities must be such that the pilot is able to complete the mission purposes with reasonable physical and mental efforts (Roskam, 2001).

To predict, whether or not an airplane will have acceptable handling qualities, a rate scale must be adopted, which pilots can use to rate the flying qualities of a given aircraft in a given mission segment. Furthermore, the handling qualities expected by the pilot depend on the type of aircraft and the flight phase. Aircrafts may be classified according to size and maneuverability (Table 5.10). Flight phases are defined as shown in Table 5.11. Category A deals exclusively with military aircraft and Category B and C are applicable to either commercial or military aircraft.

Table 5.10: Classification of airplanes.

Class I	**Small, light airplanes, such as:**	
	▪ Light utility; ▪ Primary trainer;	▪ Light observation aircraft.
Class II	**Medium-weight, low-to-medium maneuverability airplanes, such as:**	
	▪ Heavy utility / search and rescue; ▪ Light or medium transport / cargo / tanker; ▪ Early warning / electronic counter-measures / airborne command, control or communications relay;	▪ Anti-submarine; ▪ Assault transport; ▪ Reconnaissance; ▪ Tactical bomber; ▪ Heavy attack; ▪ Trainer for Class II.
Class III	**Large, heavy, low-to-medium maneuverability airplanes, such as:**	
	▪ Heavy transport / cargo / tanker; ▪ Heavy bomber; ▪ Trainer for Class III;	▪ Patrol / early warning / electronic counter-measures / airborne command, control or communications relay;
Class IV	**High maneuverability airplanes, such as:**	
	▪ Fighter / interceptor; ▪ Attack; ▪ Tactical reconnaissance;	▪ Observation; ▪ Trainer for Class IV.

Table 5.11: Flight phases categories. Adapted from (Nelson, 1998).

Nonterminal flight phases	
Category A	Nonterminal flight phase that require rapid maneuvering, precision tracking, or precise flight-path control. Included in the category are air-to-air combat ground attack, weapon delivery-launch, aerial recovery, reconnaissance, in-flight refueling (tanker), terrain-following, antisubmarine search, and close-formation flying.
Category B	Nonterminal flight phases that are normally accomplished using gradual maneuvers and without precision tracking, although accurate flight-path control may be required. Included in the category are climb, cruise, loiter, in-flight refueling (tanker), descent, emergency descent, emergency deceleration, and aerial delivery.
Terminal flight phases	
Category C	Terminal flight phases are normally accomplished using gradual maneuvers and usually require accurate flight-path control. Included in this category are take-off, catapult takeoff, approach, wave-off / go-around and landing.

The Cooper-Harper pilot rating scale is widely accepted. However, presenting in details the whole Cooper-Harper scale is out of scope of this work. Although, it is important to highlight that in this scale, the flying qualities are specified in terms of three levels:

Level 1 Flying qualities clearly adequate for the mission flight phase

Level 2 Flying qualities adequate to accomplish the mission flight phase, but with some increase in pilot workload or degradation in mission effectiveness, or both, exists.

Level 3 Flying qualities such that the airplane can be controlled safely but pilot workload is excessive or mission effectiveness is inadequate, or both. Category A flight phases can be terminated safely and Category B and C flight phases can be completed.

In addition, the designer should always aim the project to achieve a Level 1 flight quality.

According to the RFP (AIAA Technical Committee, 2018), the present aircraft is Class II. The flying qualities analyzed in the next sub-sections will refer to a Class B flight phase (cruise). The following analysis will focus on the cruise phase, which occurs at an altitude of 36576 m (12000 ft) and is flown at 97.8 m/s. Since cruise is when most

of the flight take place, it is reasonable to ensure that the pilot will have a plane with good flying qualities during this phase.

5.4.1 GEOMETRY

Figure 5.4 recapitulates the final surfaces values and illustrates the aircraft's appearance. In addition, Table 5.12 presents the inertia properties, necessary for the dynamic stability analysis.

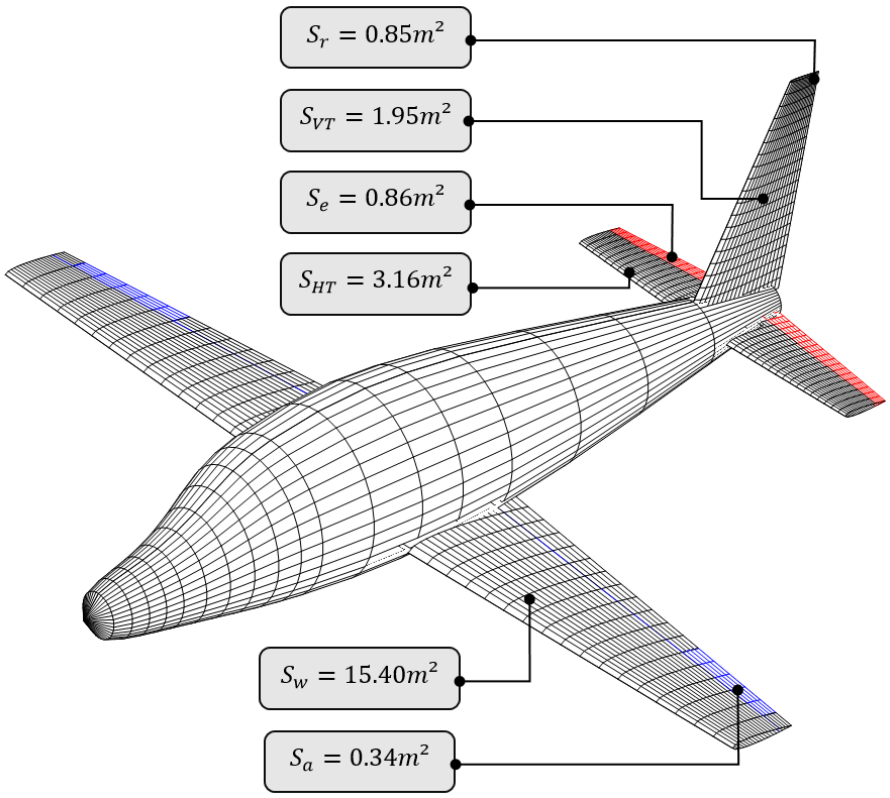

Figure 5.4: Aircraft final geometry.

These properties were calculated with OpenVSP software. This software is a parametric aircraft geometry tool, allowing the user to create, by common engineering parameters, a 3D model of an aircraft (NASA, 2019). The calculation have considered all the components weight and position, including fuel, passengers, air condition system, avionics and so forth.

Table 5.12: Aircraft inertia properties.

I_x [kg.m²]	I_y [kg.m²]	I_z [kg.m²]	I_{xz} [kg.m²]
1698.5	6228.8	7661.4	196.1

5.4.2 Elevator-Free Neutral Point

From the point of view of handling qualities, a characteristic of interest is the airplane stability when the elevator is completely free to rotate about its hinge line under the influence of the aerodynamic pressure distribution that act upon it (Etkin & Reid, 1996). This condition is commonly called a stick-free condition. As shown in appendix A.1, the stick-free stability is less than with the fixed controls. It is desirable, however, that this difference is small. Which is the case for the designed aircraft (Figure 5.5).

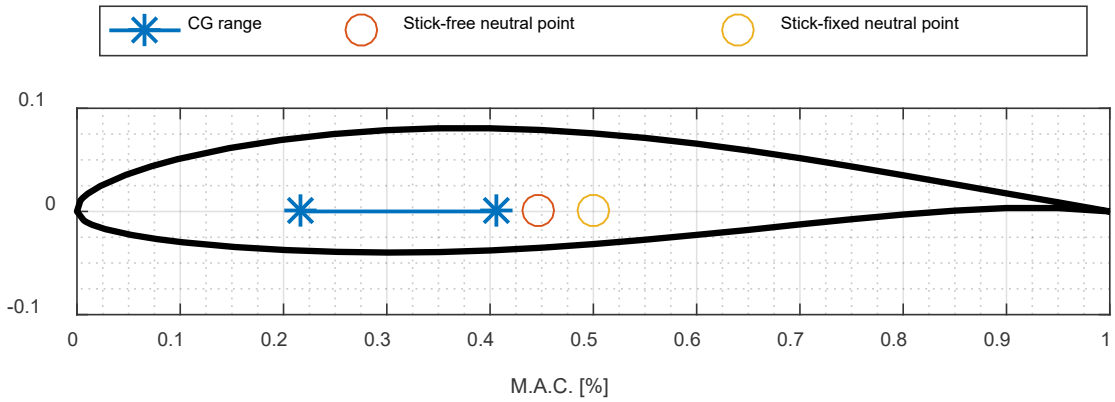

Figure 5.5: Comparison of the CG range and neutral points for the cases of stick free and fixed, with respect to the M.A.C..

Static margin is a term that appears frequently in the literature. It is simply the distance between the neutral point and the actual CG position, in percentage of the M.A.C. (Nelson, 1998). For the designed aircraft, the minimum stick fixed static margin is 9.42% and the stick-free static margin is 4%.

According to (Nelson, 1998), for most aircraft designs it is desirable to have a stick fixed static margin of approximately, or greater than 5% of the M.A.C. Therefore, it can be concluded that the presented method for designing the horizontal tail produced good longitudinal static stability characteristics.

5.4.3 Longitudinal Flying Qualities

In order to predict the aircraft handling qualities for longitudinal motion, a dynamic stability analyze must be evaluated. As shown in appendix B.2, the matrix that describes the dynamic behavior of the aircraft depends on the coefficients and derivatives presented in Table 5.13. From those coefficients and the inertia properties presented before, the aircraft longitudinal state vector equations for uncontrolled motion (meaning no control input) will be:

$$\begin{Bmatrix} \Delta\dot{u} \\ \dot{w} \\ \dot{q} \\ \Delta\dot{\Theta} \end{Bmatrix} = \mathbf{A_{longitudinal}} \cdot \begin{Bmatrix} \Delta u \\ w \\ q \\ \Delta\Theta \end{Bmatrix}$$

where, $$\mathbf{A_{longitudinal}} = \begin{bmatrix} -0.0242 & 0.0492 & 0 & -9.81 \\ -0.2092 & -2.0658 & 95.1267 & 0 \\ 0.0020 & -0.2072 & -2.9648 & 0 \\ 0 & 0 & 1 & 0 \end{bmatrix}$$

Table 5.13: Aerodynamic characteristics at 36576 m (12000 ft) and V∞ =97.8 m/s. (All derivatives are per radian). Longitudinal.

Coefficient	Value	Coefficient	Value
C_L	0.3203	$C_{L_{\dot{\alpha}}}$	3.0688
C_D	0.0258	$C_{m_{\dot{\alpha}}}$	-10.7510
C_{L_α}	6.6107	C_{L_q}	10.0400
C_{m_α}	-1.6999	C_{m_q}	-23.7000

The solution of the eigenvalue problem yields to two natural modes, quite typical for fixed wing aircrafts. They are two damped oscillations, one of long period and lightly damped (phugoid), the other of short period and heavily damped (short-period). The eigenvalues of $\mathbf{A_{longitudinal}}$ are:

Mode 1 (Phugoid mode): $\lambda_{1,2} = -0.0111 \pm 0.1338\, i$

Mode 2 (Short-period mode): $\lambda_{3,4} = -2.5163 \pm 4.4164\, i$

From the eigenvalues and equations (see appendix C), it is possible to calculate the "undamped" circular frequency (ω_n), the damping ratio (ξ). As complementary data, the period of the oscillation (T), time to half (t_{half}) the signal amplitude and cycles to half (N_{half}), are also of interest. These parameters are summarized in Table 5.14 for both modes.

Table 5.14: Longitudinal modes characteristics.

	ω_n [rad/s]	ξ	T [s]	t_{half} [s]	N_{half}
Phugoid	0.134	0.083	46.959	62.193	1.321
Short-period	5.083	0.495	1.423	0.275	0.193

Short-period frequency criterion:

According to Roskam (Roskam, 2001), the FAR do not set specific limits on ω_{SP} and, when it is the case, common practice is to adopt military requirements. Then, Figure 5.6 illustrates the requirement of MIL-F-8785C, adapted from (Roskam, 2001). The adaptation considered only flight phase Category B.

The region between lines indicates where the respectively flight Level is achieved. If necessary, a linear extrapolation can be made for the boundaries of n/α. Note that both axis of the graph are in log scale. The red "*" indicates where the designed aircraft fits on this region.

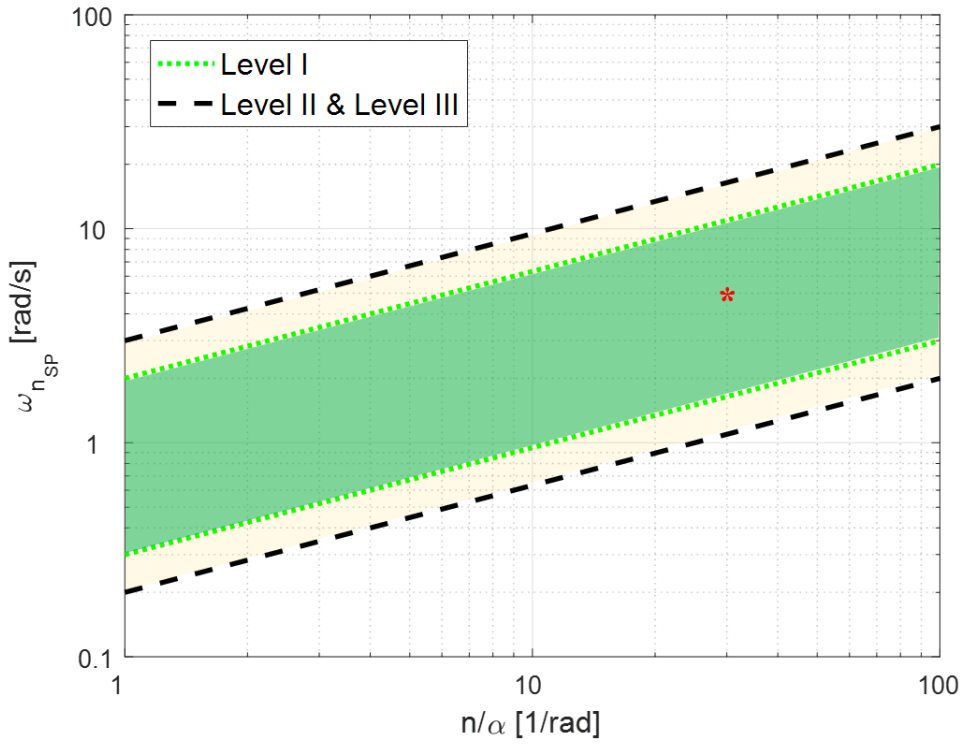

Figure 5.6: Short-period undamped natural frequency requirement, for flight phase Category B. Adapted from (Roskam, 2001).

The parameter n/α may be found from:

$$\frac{n}{\alpha} = \frac{q_\infty . C_{L_\alpha}}{W/S_w} \tag{5.1}$$

Then:

$$\omega_{SP} = 5.083$$

$$\frac{n}{\alpha} = 29.779$$

Damping ratio criterion:

The short-period damping ratio, ξ_{SP}, must be within the limits presented in Table 5.15. Note that damping ratios larger than 1.0 are admitted. A damping ratio larger than 1.0 indicates that the phugoid mode has collapsed into two stable real roots.

According to Table 5.13, the designed aircraft meets the requirement for both modes in a Category B flight phase.

Table 5.15: Longitudinal flying qualities: damping ratio limits. Adapted from (Nelson, 1998).

Phugoid mode				
	Level 1	$\xi_{PH} > 0.04$		
	Level 2	$\xi_{PH} > 0$		
	Level 3[(1)]	$T_{double} > 55\ s$		
Short-period mode				
	Categories A and C		**Category B**	
Level	$(\xi_{SP})_{min}$	$(\xi_{SP})_{max}$	$(\xi_{SP})_{min}$	$(\xi_{SP})_{max}$
1	0.35	1.30	0.30	2.00
2	0.25	2.00	0.20	2.00
3	0.15	–	0.15	–

[(1)] Here, T_{double} represents the time to double a signal amplitude (e.g. pitch rate) in case of an unstable phugoid mode.

5.4.4 LATERAL FLYING QUALITIES

Just as for the longitudinal motion, the handling qualities for lateral motion are predicted by a dynamic stability analysis. The matrix that describes the dynamics of the aircraft's lateral behavior depends on the coefficients presented in Table 5.16. From those coefficients and inertia properties presented earlier, the lateral state vector equations is:

$$\begin{Bmatrix} \dot{v} \\ \dot{p} \\ \dot{r} \\ \dot{\Phi} \end{Bmatrix} = \mathbf{A_{lateral}} \cdot \begin{Bmatrix} \mathrm{v} \\ p \\ r \\ \Phi \end{Bmatrix}$$

where,

$$\mathbf{A_{lateral}} = \begin{bmatrix} -0.2328 & -0.0525 & -97.7800 & 9.81 \\ -0.2346 & -16.8591 & 3.2955 & 0 \\ 0.0296 & -0.5995 & -0.6819 & 0 \\ 0 & 1 & 0 & 0 \end{bmatrix}$$

Table 5.16: Aerodynamic characteristics at 36576 m (12000 ft) and V∞ =97.8 m/s. (All derivatives are per radian). Lateral.

Coefficient	Value	Coefficient	Value
C_{y_β}	-0.7430	C_{n_p}	-0.0261
C_{l_β}	-0.0510	C_{y_r}	0
C_{n_β}	0.0344	C_{ℓ_r}	0.1164
C_{y_p}	-0.0270	C_{n_r}	-0.1192
C_{ℓ_p}	-0.5793		

The solution of the eigenvalue problem yields three natural modes, quite typical for fixed wing aircrafts. Two of them are convergences, one very fast (roll mode), one very slow (spiral mode), and one that is a lightly damped oscillation (Dutch roll mode) with a period similar to that of the longitudinal short-period mode. Table 5.17 summarizes these characteristics, which are evaluated from the following eigenvalues of $\mathbf{A_{lateral}}$:

Mode 1 (Spiral mode): $\lambda_1 = -0.0090$

Mode 2 (Rolling mode): $\lambda_2 = -16.7979$

Mode 3 (Dutch Roll mode): $\lambda_{3,4} = -0.4834 \pm 1.9499\, i$

Table 5.17: Lateral modes characteristics.

	ω_n [rad/s]	T [s]	t_{half} [s]	N_{half}
Spiral	-	-	76.718	-
Roll	-	-	0.041	-
Dutch Roll	2.009	3.222	1.434	0.444

Dutch roll frequency and damping

The main requirements for the Dutch roll mode are summarized in Table 5.18. For the designed aircraft, the frequency and damping characteristics are as follows:

ξ_{DR}: 0.24

$\omega_{n_{DR}}$: 2.01[rad/s]

$\xi_{DR}.\omega_{n_{DR}}$: 0.48[rad/s]

Therefore, as a Class II airplane in a Category B flight phase, the designed aircraft meets all requirements.

Table 5.18: Dutch roll flying qualities. Adapted from (Nelson, 1998).

Level	Category	Class	Min. ξ_{DR}	Min. $\xi_{DR} \cdot \omega_{n_{DR}}$ [rad/s]	Min $\omega_{n_{DR}}$ [rad/s]
1	A	I,IV	0.19	0.35	1.0
		II,III	0.19	0.35	0.4
	B	All	0.08	0.15	0.4
	C	I,II-C and IV	0.08	0.15	1.0
		II-L, III	0.08	0.15	0.4
2	All	All	0.02	0.05	0.4
3	All	All	0.02	-	0.4

Where C and L denote carrier- or land-based aircraft.

Spiral stability

According to (Roskam, 2001), there are no specific civil requirements regarding the spiral stability in any type of airplane. Nonetheless, the military requirements stablishes limits for the allowable spiral divergence mode (Table 5.19). As stated before, it is common practice to use military requirements when civil requirements are not specified. Since the spiral mode of the designed airplane, at cruise flight, is stable, there will be no divergence.

Table 5.19: Spiral mode flying characteristics: minimum time to double amplitude. Adapted from (Nelson, 1998).

Class	Category	Level 1	Level 2	Level 3
I and IV	A	12 s	12 s	4 s
	B and C	20 s		
II and III	All	20 s		

Roll mode time constant

The airplane roll mode time constant (τ_{roll}) is a measure of how fast is the roll response. A small τ_{roll} signifies a rapidly increase of roll rate after a lateral control input. The requirements presented in Table 5.20 were adapted from (Nelson, 1998), which, by its turn, had adapted the military requirement MIL-F-8785C.

The time constant can be evaluated from:

$$\tau_{roll} = -\frac{1}{(L_p/I_x)} \tag{5.2}$$

where, $$L_p = 0.25\rho_\infty . V_\infty . b_w^2 . S_w . C_{\ell_p}$$

L_p is the dimensional derivative of the rolling moment with respect to a change on the angular velocity p. For the designed aircraft, the roll mode time constant is found to be 0.059 s, which meets the requirement.

Table 5.20: Roll mode flying qualities: maximum allowable roll time constant. Adapted from (Nelson, 1998).

Class	Category	Level I	Level II	Level III
I and IV	A and C	1.0 s	1.4 s	10 s
II and III		1.4 s	3.0 s	
All	B	1.4 s	3.0 s	

Despite meeting the requirements, the time constant is too small when compared with other aircrafts. This might indicates that the aircraft will be oversensitive for the small perturbations on the roll mode.

CHAPTER VI

CONCLUSIONS

In the previous chapters, it was demonstrated how the empennage and control surfaces design can be drive by the aircraft's mission and flight dynamics characteristics. The proposed methodology in Chapter IV have addressed, systematically, how to accomplish the design procedure.

The final aircraft configuration has shown to be satisfactory, both visually and qualitatively. According to Roskam (2001), good visual characteristics are as important as good flying characteristics in aircraft design. Throughout the design procedure, the chosen parameters were, in majority, based on the desired dynamic characteristics of the aircraft. Moreover, as stated in Chapter V, the aircraft behavior at cruise flight phase met all requirements presented. In addition, for longitudinal static stability, the aircraft is capable to establish trim flight condition at stall velocity. Therefore, it is reasonable to say that the developed methodology fulfilled its objective.

Further work is in progress to evaluate, with more details, the aircraft behavior at low speed regime ($1.2V_{stall}$). At this point results have shown that, in low speed regime, the aircraft still have good flying qualities for longitudinal motion and, for the lateral motion, the roll and Dutch roll modes are also satisfactory. The spiral mode, however,

has shown to be unstable and, according to requirements present on Table 5.19, the level flight would be Level 3. Which would require a stability augmentation system (SAS) to enhance the flight qualities and provide Level I classification. Moreover, despite the DATCOM model ensures that the stall angle at $1.2V_{stall}$ is about 17º, at this flight condition the airplane is trimmed at α = 14.5º. Therefore, the calculated results, especially regarding the small perturbation theory equations, should be looked very carefully. In other words, since the trim angle is near the stall region, the applied mathematical model begins to "collapse" and the results begins to be less accurate.

Although the results are satisfactory, it is important to emphasize that the use of empirical and analytical evaluations of aerodynamic coefficients and their derivatives are acceptable in a first moment. However, even if those are reasonable, experimental data should always be taken into account to evaluate the stability and control characteristics (ABBOTT, DOENHOFF, & Jr., 1945).

Finally, in a future work it is desired to improve the MATLAB® algorithm used to code the presented methodology. Such improvement may leads to a design algorithm almost independent on external sources and historical data. Among the possible improvements, one could list:

- Engine influence on longitudinal calculations, especially regarding the elevator design;
- Introduce an aerodynamic solver more complex than LLT, capable of include the fuselage contribution in the aerodynamic coefficients;
- Implement a Mach correction for flight phases with Mach number greater than 0.3 (which were not the case for the studied project);
- Enhance the algorithm used for the evaluation of CG position.

REFERENCES

ABBOTT, I. H., DOENHOFF, A. E., & Jr., L. S. (1945). *Report Nº. 824 - Summary of Airfoil Data.* National Advisory Committee for Aeronautics, Langley Memorial Aeronautical Laboratory.

AIAA Technical Committee. (2018). Request for Proposal - Thin Haul Transport and Air Taxi. Retrieved 2018, from https://www.aiaa.org/designcompetitions/

Anderson, J. D. (2011). *Fundamentals of Aerodynamics* (5th ed.). McGraw-Hill.

Ba, M. (2017). Cours Aérodynamic d'Aile. ISAE - ENSMA.

Etkin, B., & Reid, L. D. (1996). *Dynamics of Flight - Stability and Control* (3ª ed.). John Wiley & Sons, INC.

FAA, F. A. (2017). *Federal Aviation Regulations* . Department of Transportation. Retrieved from www.faa.gov

Gudmundsson, S. (2014). *General Aviation Aircraft Design: Applied Methods and Procedures.* Elsevier.

Mc Donnel Douglas Astronautics Company. (1979). *The USAF Stability and Control Digital DATCOM, Volume I, Users Manual.* Technical report, Air Force Systems Command, Air Force Fligth Dynamics Laboratory, St. Louis.

NASA. (2019). *OpenVSP*. Retrieved 2019, from www.openvsp.org

Nelson, R. C. (1998). *Flight Stability and Automatic Control* (2ª ed.). WCB McGraw-Hill.

Roskam, J. (2001). *Airplane Flight Dynamics and Automatic Flight Controls - Part I.* Lawrence: DARcorporation.

Sadraey, M. H. (2013). *Aircraft Design - A Systems Engineering Approach.* New Hampshire, USA: John Wiley & Sons.

USAF. (1978). *STABILITY AND CONTROL DATCOM.* Air Force Systems Command, Flight Dynamics Laboratory, Ohio.

APPENDIX A – EQUATIONS DEVELOPMENTS

A.1 LONGITUDINAL FORCES AND MOMENTS

To the following equations, consider:

$$C_{L_w} = C_{L_{0_w}} + C_{L_{\alpha_w}}.\alpha_w \tag{A.1}$$

$$C_{D_w} = C_{D_{0_w}} + k.C_{L_w}^{\ 2} \tag{A.2}$$

$$C_{m_w} = C_{m_{0_w}} + C_{m_{\alpha_w}}.\alpha_w \tag{A.3}$$

where,

$$\alpha_w = \alpha + i_w \tag{A.4}$$

- **WING CONTRIBUTION**

The aerodynamic forces acting at the wing, decomposed in the *Body Coordinate System* are (Figure A.1):

$$\overrightarrow{F_{A_w}}^{(b)} = \begin{Bmatrix} -D_w.\cos(\alpha) + L_w.\sin(\alpha) \\ 0 \\ -D_w.\sin(\alpha) - L_w.\cos(\alpha) \end{Bmatrix} \tag{A.5}$$

Assuming that α is a small angle and that the wing has a good aerodynamic efficiency, the following simplifications can be made (Nelson, 1998):

$\cos(\alpha) \cong 1$, $\sin(\alpha) \cong \alpha$, $L_w \gg D_w$

Thus, equation (A.5) becomes:

$$\overrightarrow{F_{A_w}}^{(b)} = \begin{Bmatrix} -D_w + L_w.\alpha \\ 0 \\ -L_w \end{Bmatrix} \tag{A.6}$$

The moment in the airplane's CG caused by the wing is given by:

$$\vec{M}^b = \vec{r}_{AC_w}^{\,b} \times \vec{F}_{A_w}^{\,b} + \vec{M}_{AC_w}^{\,b} \tag{A.7}$$

where,

$$\vec{r}_{AC_w}^{\,b} = [x_w \quad 0 \quad z_w]^T \tag{A.8}$$

and

$$\vec{M}_{AC_w}^{\,b} = [0 \quad m_{AC_w} \quad 0]^T \tag{A.9}$$

Thus,

$$\vec{M}^b = \begin{Bmatrix} 0 \\ x_w.L_w + z_w(-D_w + \alpha.L_w) + m_{AC_w} \\ 0 \end{Bmatrix} \tag{A.10}$$

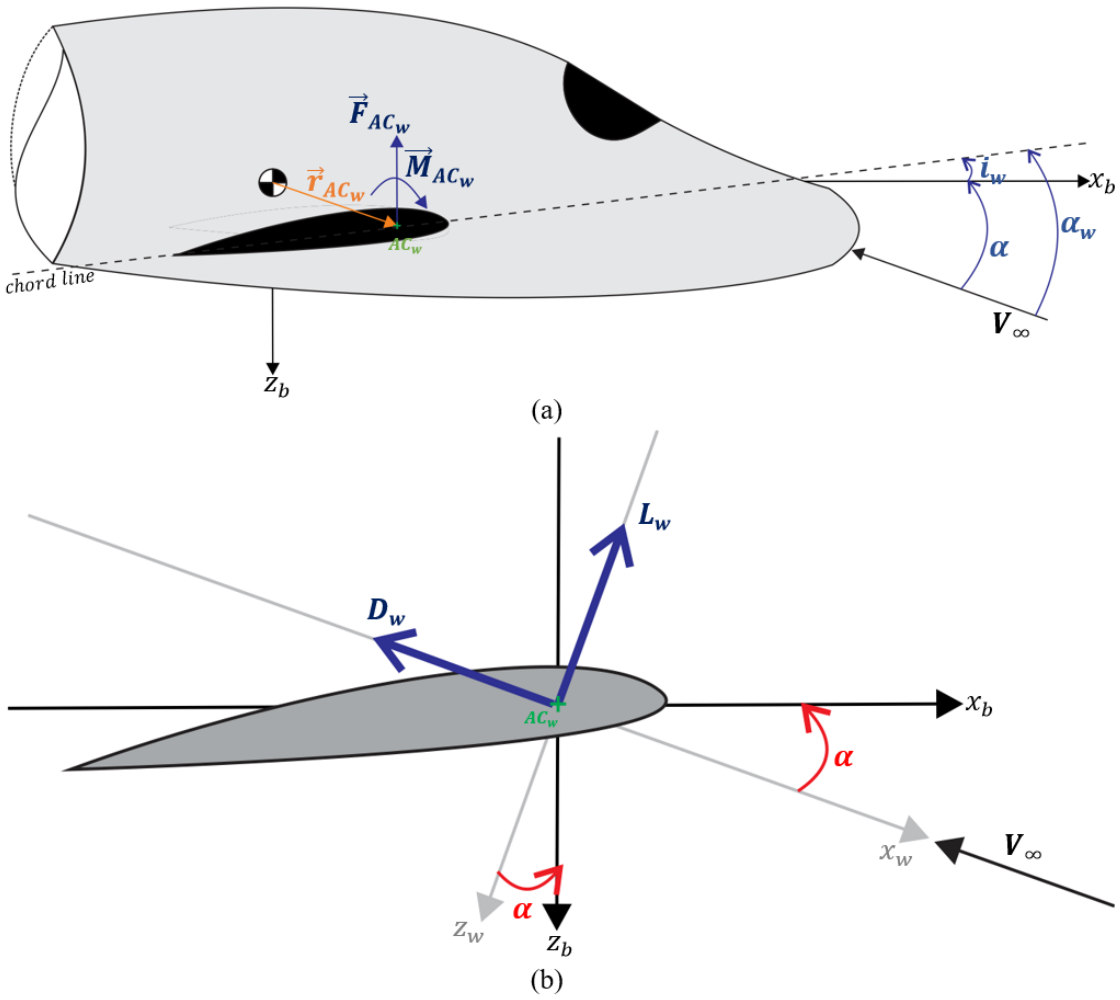

Figure A.1: Aerodynamic force and moment created by the wing at: (a) the airplane CG and (b) the wing itself.

Dividing equation (A.10) by $\frac{1}{2}\rho_\infty . V_\infty^2 . S_w . \bar{c}_w$ yields:

$$(C_m)_w = \frac{x_w}{\bar{c}_w}\left[\frac{L_w}{\frac{1}{2}\rho_\infty V_\infty^2 S_w}\right] + \frac{z_w}{\bar{c}_w}\left(\left[\frac{-D_w}{\frac{1}{2}\rho_\infty V_\infty^2 S_w}\right] + \alpha\left[\frac{L_w}{\frac{1}{2}\rho_\infty V_\infty^2 S_w}\right]\right) - \left[\frac{m_{AC_w}}{\frac{1}{2}\rho_\infty V_\infty^2 S_w \bar{c}_w}\right] \quad \text{(A.11)}$$

Which becomes:

$$(C_m)_w = \frac{x_w}{\bar{c}_w}\left[C_{L_w}\right] + \frac{z_w}{\bar{c}_w}\left(\left[-C_{D_w}\right] + \alpha\left[C_{L_w}\right]\right) - \left[C_{m_{AC_w}}\right] \quad \text{(A.12)}$$

Organizing equation (A.12) in terms of $(C_{m_0})_w$ and $(C_{m_\alpha})_w$, and applying equations (A.1) to (A.4):

$$(C_m)_w = (C_{m_0})_w + (C_{m_\alpha})_w . \alpha$$

$$\left(C_{m_0}\right)_w = \frac{x_w}{\bar{c}_w}.C_{L_{0_{\tilde{w}}}} + C_{m_{AC_w}} \tag{A.13}$$

$$\left(C_{m_\alpha}\right)_w = \frac{x_w}{\bar{c}_w}.C_{L_{\alpha_w}} + \frac{z_w}{\bar{c}_w}.\left(-2.k.C_{L_{0_{\tilde{w}}}}.C_{L_{\alpha_w}} + C_{L_w} + \alpha.C_{L_{\alpha_w}}\right) \tag{A.14}$$

where,

$$C_{L_{0_{\tilde{w}}}} = \left(C_{L_{0_w}} + C_{L_{\alpha_w}}.i_w\right) \tag{A.15}$$

Note that $\left(C_{m_\alpha}\right)_w$ is a function of α. It is common to consider $z_w \approx 0$, to simplify some analysis and neglect this dependence of α. Figure A.2 compares the impact of all simplifications made through the development of these equations, showing the graph of $(Cm)_w \; vs. \; \alpha$ of a random aircraft. The hypothesis are:

- Hypothesis I is the one made in equation (A.6)

$$\cos(\alpha) \cong 1, \qquad \sin(\alpha) \cong \alpha, \qquad L_w \gg D_w$$

- Hypothesis II:

$$\cos(\alpha) \cong 1 \qquad \sin(\alpha) \cong \alpha$$

- Hypothesis III:

$$\cos(\alpha) \cong 1, \quad \sin(\alpha) \cong \alpha, \quad L_w \gg D_w, \quad z_w \approx 0$$

It is clear, comparing the three curves, that the assumptions made has minor impacts in the final valor of $(C_m)_w$ in angles of attack on the linear region.

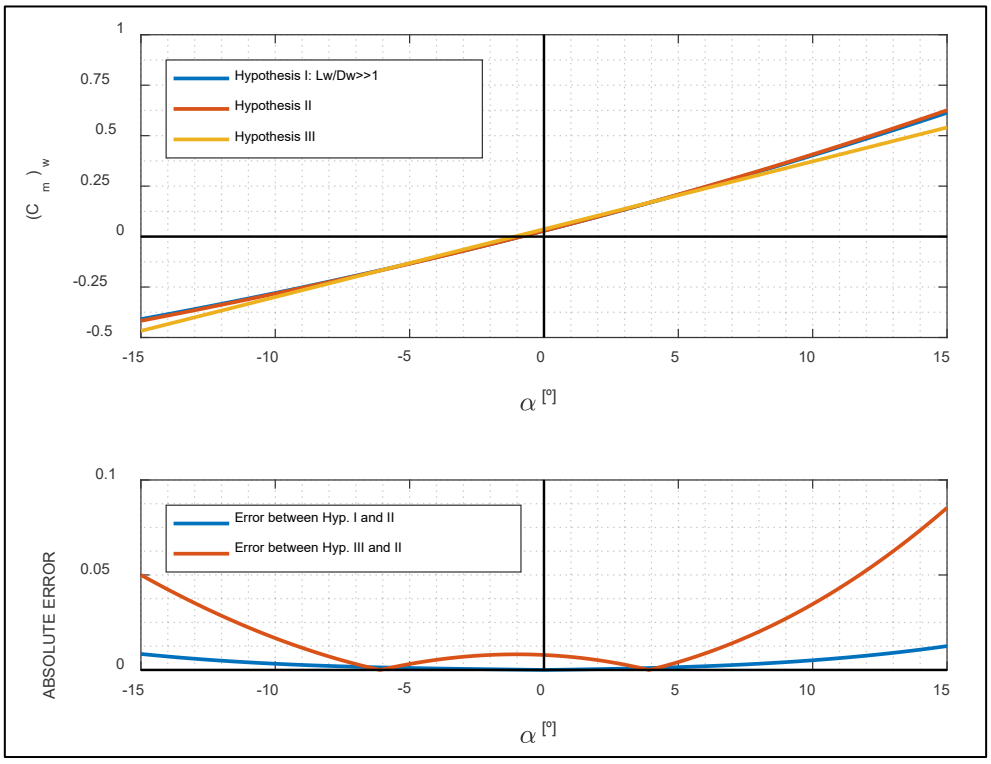

Figure A.2: Effect of different hypotheses in the value of $(C_m)_w$.

- **TAIL CONTRIBUTION**

As shown in Figure A.3, the wing disturbs the flow field that arrives at the horizontal tail. Consequently, the angle of attack experienced by the tail is different by the one experienced by the wing. The aerodynamic forces acting at the horizontal tail, decomposed in the *Body Coordinate System* are:

$$\overrightarrow{F_{A_{HT}}}^{(b)} = \begin{Bmatrix} -D_{HT}.\cos(\alpha_{HT}) + L_{HT}.\sin(\alpha_{HT}) \\ 0 \\ -D_{HT}.\cos(\alpha_{HT}) - L_{HT}.\cos(\alpha_{HT}) \end{Bmatrix} \tag{A.16}$$

Assuming that α_{HT} is a small angle and, the following simplifications can be made (Nelson, 1998):

$$\cos(\alpha_{HT}) \cong 1, \qquad \sin(\alpha_{HT}) \cong \alpha_{HT}, \qquad \frac{L_{HT}}{D_{HT}} \gg 1$$

Thus, equation (A.16) becomes:

$$\overrightarrow{F_{A_{HT}}}^{(b)} = \begin{Bmatrix} 0 \\ 0 \\ -L_{HT} \end{Bmatrix} \tag{A.17}$$

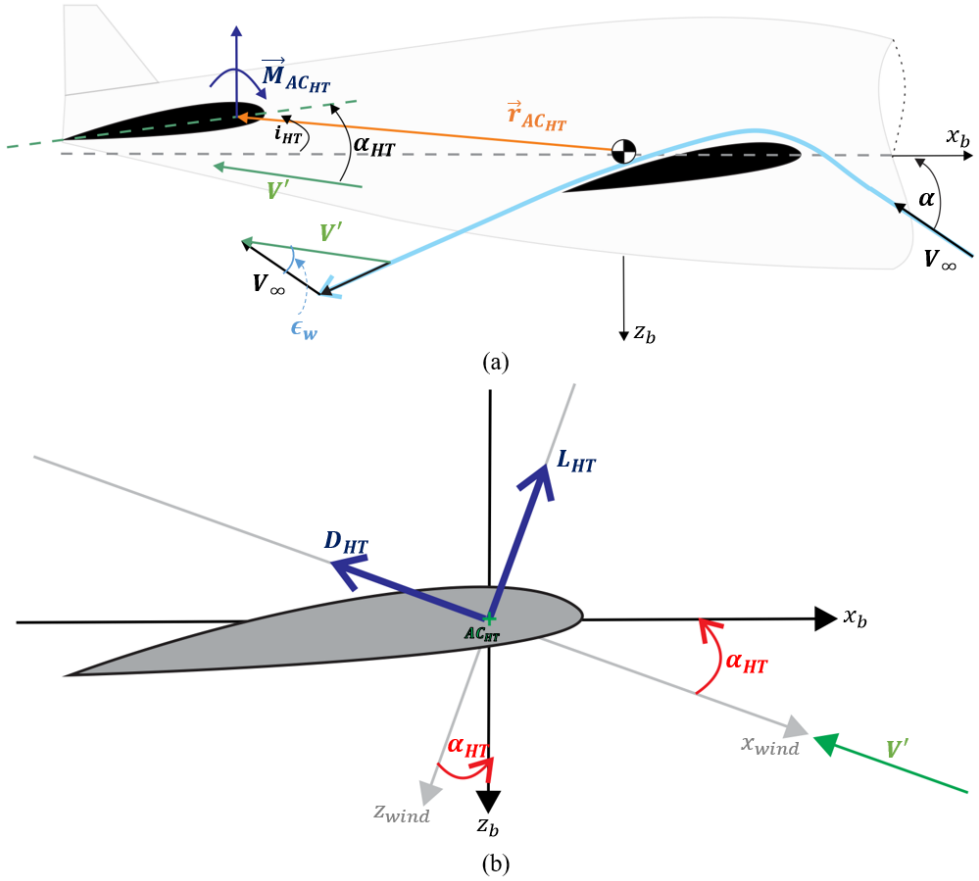

Figure A.3: Flow field around the wing-horizontal tail assembly and aerodynamic forces acting at the tail.

The moment in the airplane's CG caused by the horizontal tail is given by:

$$\vec{M}^b = \vec{r}^b_{AC_{HT}} \times \vec{F}^b_{A_{HT}} + \vec{M}^b_{AC_{HT}} \tag{A.18}$$

where,

$$\vec{r}^b_{AC_w} = [x_{HT} \quad 0 \quad z_{HT}]^T \tag{A.19}$$

and

$$\vec{M}^b_{AC_{HT}} = [0 \quad m_{AC_{HT}} \quad 0]^T \tag{A.20}$$

Thus,

$$\vec{M}^b = \begin{Bmatrix} 0 \\ x_{HT}.L_{HT} + m_{AC_{HT}} \\ 0 \end{Bmatrix} \tag{A.21}$$

Dividing equation (A.21) by $q_\infty.S_w.\bar{c}_w.\left(\frac{q_{HT}.S_{HT}.\bar{c}_{HT}}{q_{HT}.S_{HT}.\bar{c}_{HT}}\right)$ and organizing the therms:

$$(C_m)_{HT} = -\frac{q_{HT}}{q_\infty}.\frac{|x_{HT}|.S_{HT}}{\bar{c}_w.S_w}.\frac{L_{HT}}{q_\infty.S_{HT}} - \frac{q_{HT}}{q_\infty}.\frac{\bar{c}_{HT}.S_{HT}}{\bar{c}_w.S_w}.\frac{m_{AC_{HT}}}{q_{HT}.S_{HT}.\bar{c}_{HT}} \tag{A.22}$$

Which becomes:

$$(C_m)_{HT} = -\eta_{HT}.V_{HT}.C_{L_{HT}} - \eta_{HT}.\frac{\bar{c}_{HT}.S_{HT}}{\bar{c}_w.S_w}.C_{m_{AC_{HT}}} \tag{A.23}$$

Note that $C_{L_{HT}}$ is:

$$C_{L_{HT}} = C_{L_{0_{HT}}} + C_{L_{\alpha_{HT}}}.\alpha_{HT} \tag{A.24}$$

where

$$\alpha_{HT} = \alpha + i_{HT} - \epsilon_w \tag{A.25}$$

The downwash angle may be modeled by:

$$\epsilon = 2.k.C_{L_w}$$

$$\epsilon = 2.k.(C_{L_{0_w}} + C_{L_{\alpha_w}}.\alpha_w)$$

Hence,

$$\epsilon = \epsilon_0 + \epsilon_\alpha.\alpha_w \tag{A.26}$$

where

$$\epsilon_0 = 2.k.C_{L_{0_w}} \tag{A.27}$$

$$\epsilon_\alpha = 2.k.C_{L_{\alpha_w}} \tag{A.28}$$

and

$$k \approx \frac{1}{\pi AR} \tag{A.29}$$

Dividing equation (A.17) by $q_\infty.S_w.\left(\frac{q_{HT}.S_{HT}}{q_{HT}.S_{HT}}\right)$, the lift coefficient of the horizontal tail acting at the airplane is then:

$$(C_L)_{HT} = \eta_{HT}.\frac{S_{HT}}{S_w}.C_{L_{HT}} \tag{A. 30}$$

Note the difference in notation where $(C_L)_{HT}$ stands for lift coefficient contribution for the airplane, while $C_{L_{HT}}$ is the lift coefficient of the horizontal tail as an isolated aerodynamic body.

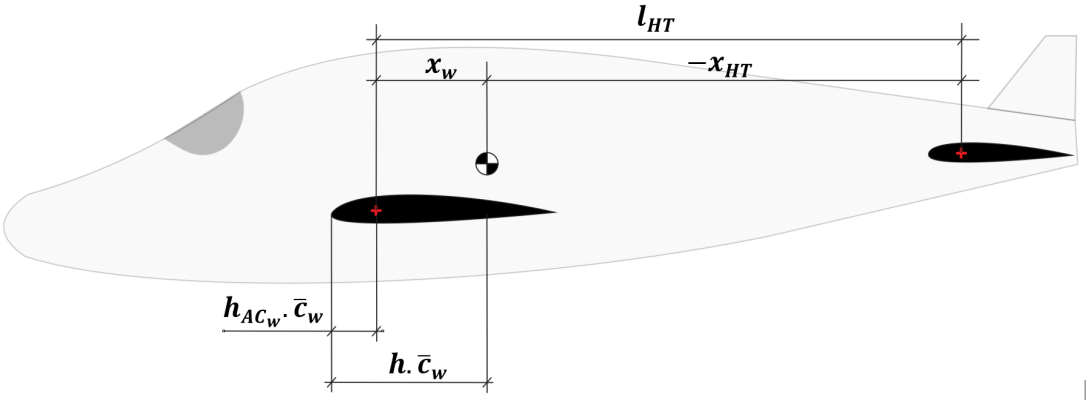

Figure A.4: Aircraft reference lengths definitions.

According to Figure A.4, $x_w = \left(h - h_{AC_w}\right).\bar{c}_w$ and $x_{HT} = l_{HT} - \left(h - h_{AC_w}\right).\bar{c}_w$. Thus, equation (A.23) may be rewritten as:

$$(C_m)_{HT} = -\eta_{HT}.\left(\bar{V}_{HT} - \left(h - h_{AC_w}\right).\frac{S_{HT}}{S_w}\right).C_{L_{HT}} - \eta_{HT}.\frac{\bar{c}_{HT}.S_{HT}}{\bar{c}_w.S_w}.C_{m_{AC_{HT}}} \quad \text{(A. 31)}$$

where

$$\bar{V}_{HT} = \frac{l_{ht}.S_{HT}}{\bar{c}_w.S_w} \quad \text{(A. 32)}$$

is the horizontal tail volume ratio.

- **INFLUENCE OF A FREE ELEVATOR ON LIFT AND MOMENT**

When a fix deflection angle is imposed to the control surface, the aerodynamic force distribution over it creates a moment about its hinge line. Therefore, the control system must be able to overcome this hinge moment in order to maintain the fixed deflection.

The hinge moment acting on the elevator (H_e) is defined by:

$$H_e = C_{h_e}.\frac{1}{2}.\rho.V_\infty^2.S_e.\bar{c}_e \quad \text{(A. 33)}$$

In many practical cases it is very reasonable to assume that the hinge moment coefficient (C_{h_e}) is a linear function of α_{HT} and δ_e (Etkin & Reid, 1996). However, as stated by (Etkin & Reid, 1996), there are important exceptions in which strong nonlinearities are present.

Assuming that C_{h_e} is linear, it follows that:

$$C_{h_e} = C_{h_0} + C_{h_{\alpha_{HT}}}.\alpha_{HT} + C_{h_{\delta_e}}.\delta_e \quad \text{(A. 34)}$$

A stick-free situation implies that there is no actuator effort to overcome the hinge moment, which yields $C_{h_e} = 0$. Thus, in another words, this means that the elevator deflection (δ_e) is no longer imposed, it is actually a consequence of the aerodynamic force distribution over it. Then,

$$\delta_{e_{free}} = -\frac{C_{h_{\alpha_{HT}}}.\alpha_{HT}}{C_{h_{\delta_e}}} \quad \text{(A. 35)}$$

Equation (A. 34) assumes $C_{h_0} \approx 0$. It is clear from this equation that the elevator position is determined by α_{HT}.

Then it is possible to analyze the influence of a free elevator on lift and pitching moment. For the tail's lift:

$$C_{L_{HT}} = C_{L_{0_{HT}}} + C_{L_{\alpha_{HT}}}.\alpha_{HT} + C_{L_{HT_{\delta_e}}}.\delta_{e_{free}}$$

Then, combining with equation (A. 34) results in:

$$C_{L_{HT}} = C_{L_{0_{HT}}} + F_{\delta_{e_{free}}}.C_{L_{\alpha_{HT}}}.\alpha_{HT} \quad \text{(A. 36)}$$

where,
$$F_{\delta_{e_{free}}} = \left(1 - \frac{C_{L_{HT_{\delta_e}}}}{C_{L_{\alpha_{HT}}}}.\frac{C_{h_{\alpha_{HT}}}}{C_{h_{\delta_e}}}\right) \quad \text{(A. 37)}$$

is the free elevator factor for a tail.

Now, inserting equation (A.35) into the pitching moment coefficient equation yields:

$$C_m = C_{m_{AC_w}} + \left(h - h_{AC_w}\right).C_L - \eta_{HT}.\bar{V}_{HT}.\left(C_{L_{0_{HT}}} + F_{\delta_{e_{free}}}.C_{L_{\alpha_{HT}}}.\alpha_{HT}\right) \quad \text{(A. 38)}$$

Then, deriving with respect to the aircraft angle of attack (α):

$$\left(C_{m_\alpha}\right)_{\delta_{e_{free}}} = \left(h - h_{AC_w}\right).C_{L_\alpha} - \eta_{HT}.\bar{V}_{HT}.F_{\delta_{e_{free}}}.C_{L_{\alpha_{HT}}}.(1 - \epsilon_\alpha) \quad \text{(A. 39)}$$

From equation (A. 38), one can infers that the aircraft static stability is degraded in function of the factor $F_{\delta_{e_{free}}}$, when compared to the fixed-stick situation. Also from equation (A. 38), the neutral point for a stick-free condition can also be evaluated:

$$h_{n_{free}} = h_{AC_w} + \eta_{HT}.\bar{V}_{HT}.F_{\delta_{e_{free}}}.\frac{C_{L_{\alpha_{HT}}}}{C_{L_\alpha}}.(1-\epsilon_\alpha) \quad \text{(A. 40)}$$

A.2 Lateral Forces and Moments

As illustrated in Figure A.5, the aerodynamic forces acting in the vertical tail are decomposed in the *Body Coordinate System* as:

$$\vec{F}_{VT}^{(b)} = \begin{Bmatrix} -D_{VT}.\cos(\alpha_{VT}) + Lift_{VT}.\sin(\alpha_{VT}) \\ -D_{VT}.\sin(\alpha_{VT}) - Lift_{VT}.\cos(\alpha_{VT}) \\ 0 \end{Bmatrix} \quad \text{(A. 41)}$$

where $\alpha_{VT} = \beta + \sigma$

Assuming the small angle approximation and that $Lift_{VT} \gg D_{VT}$ yields:

$$\overrightarrow{F_{A_{VT}}}^{(b)} = \begin{Bmatrix} 0 \\ -Lift_{VT} \\ 0 \end{Bmatrix} \quad \text{(A. 42)}$$

where, $Lift_{VT} = -C_{L_{\alpha_{VT}}}.\alpha_{VT}$

Dividing the side force by $q_\infty.S_w.\left(\frac{q_{VT}.S_{VT}}{q_{VT}.S_{VT}}\right)$:

$$(C_y)_{VT} = \frac{Lift_{VT}}{q_\infty.S_w} = \frac{-C_{L_{\alpha_{VT}}}.(\beta+\sigma)q_{VT}.S_{VT}}{q_\infty.S_w}$$

$$(C_y)_{VT} = -C_{L_{\alpha_{VT}}}.(\beta+\sigma).\eta_{VT}.\frac{S_{VT}}{S_w} \quad \text{(A. 43)}$$

This is the side force coefficient of the aircraft produced by the vertical tail.

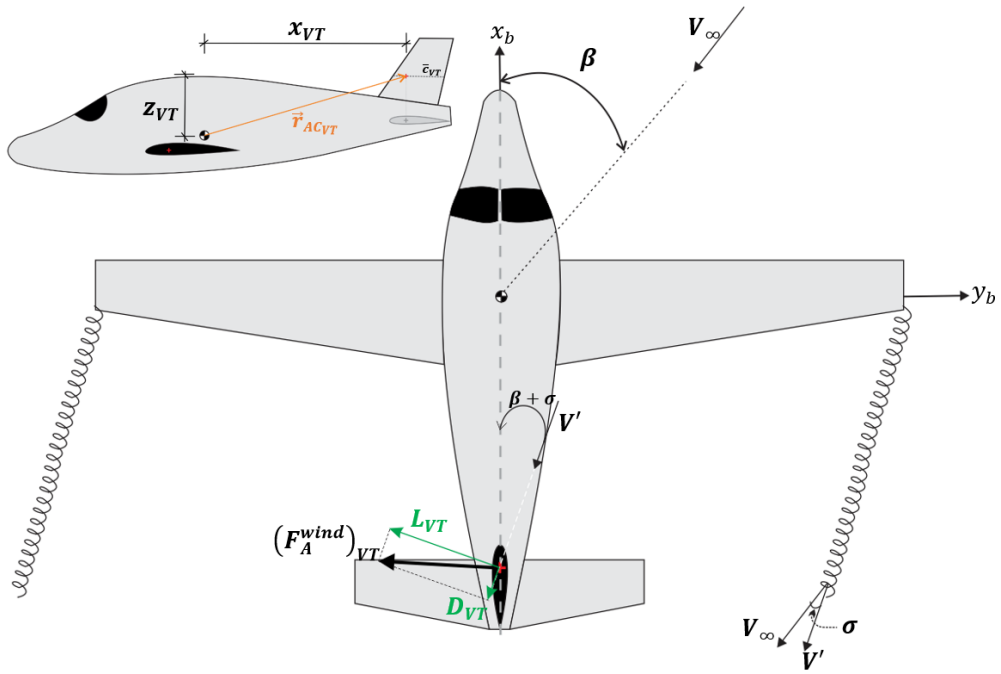

Figure A.5: Lateral force acting on the vertical tail and illustration of the sidewash created by the wing vortices.

The moment in the airplane's CG caused by the vertical tail is given by[14]:

$$\vec{M}^b = \vec{r}^b_{AC_{VT}} \times \vec{F}^b_{A_{VT}} + \vec{M}^b_{AC_{VT}} \quad \text{(A. 44)}$$

where,

$$\vec{r}^b_{AC_{VT}} = [x_{VT} \quad 0 \quad z_{VT}]^T \quad \text{(A. 45)}$$

and, since the vertical tail airfoil must be symmetric, $\vec{M}^b_{AC_{VT}} = \vec{0}$.

Thus,

$$\vec{M}^b = \begin{Bmatrix} z_{VT}.Lift_{VT} \\ 0 \\ -x_{VT}.Lift_{VT} \end{Bmatrix} \quad \text{(A. 46)}$$

Dividing the moment components of equation (A. 46) by $q_\infty.S_w.b_w.\left(\frac{q_{VT}.S_{VT}.b_{VT}}{q_{VT}.S_{VT}.b_{VT}}\right)$ yields, respectively:

$$(C_\ell)_{VT} = \frac{-|z_{VT}|.S_{VT}}{b_w.S_w}.\frac{q_{VT}}{q_\infty}.\frac{Lift_{VT}}{q_{VT}.S_{VT}.b_{VT}}$$

$$(C_\ell)_{VT} = \frac{-|z_{VT}|.S_{VT}}{b_w.S_w}.\eta_{VT}.C_{L_{VT}} \quad \text{(A. 47)}$$

And,

$$(C_n)_{VT} = \frac{|x_{VT}|.S_{VT}}{b_w.S_w}.\frac{q_{VT}}{q_\infty}.\frac{Lift_{VT}}{q_{VT}.S_{VT}.b_{VT}}$$

$$(C_n)_{VT} = V_{VT}.\eta_{VT}.C_{L_{VT}} \quad \text{(A. 48)}$$

[14] x_{VT} may also be written as l_{VT}.

APPENDIX B – EQUATIONS OF MOTION

B.1 GENERAL EQUATIONS OF MOTION

The equations presented below are adapted from (Etkin & Reid, 1996), but they may be found in most books of Flight Dynamics. They are quite general and contain few assumptions, such as that the effects of spinning rotors are negligible and that the airplane is considered to be one single rigid body and has a plane of symmetry (plane xz).

Table B.1: Summary of kinematic and dynamic equations.

Force equations	$X - mg\ sin(\Theta) = m.(\dot{u}^I + qw^I - rv^I)$	(B.1)
	$Y + mg\sin(\Phi)\cos(\Theta) = m.(\dot{v}^I + ru^I - pw^I)$	(B.2)
	$Z + mg\cos(\Phi)\cos(\Theta) = m.(\dot{w}^I + pv^I - qu^I)$	(B.3)
Moment equations	$L = I_x\dot{p} - I_{zx}\dot{r} + qr(I_z - I_y) - I_{zx}pq$	(B.4)
	$M = I_y\dot{q} + rp(I_x - I_z) + I_{zx}(p^2 - r^2)$	(B.5)
	$N = I_z\dot{r} - I_{zx}\dot{p} + pq(I_y - I_x) - I_{zx}qr$	(B.6)
Body angular velocities in terms of Euler angles and Euler rates	$p = \dot{\Phi} - \dot{\Psi}\sin(\Theta)$	(B.7)
	$q = \dot{\Theta}\cos(\Phi) + \dot{\Psi}\cos(\Theta)\sin(\Phi)$	(B.8)
	$r = \dot{\Psi}\cos(\Theta)\cos(\Phi) - \dot{\Theta}\sin(\Phi)$	(B.9)
Euler rates in terms of Euler angles and body angular velocities	$\dot{\Phi} = p + \left(qsin(\Phi) + rcos(\Phi)\right)\tan(\Theta)$	(B.10)
	$\dot{\Theta} = qcos(\Phi) - rsin(\Phi)$	(B.11)
	$\dot{\Psi} = \left(qsin(\Phi) + rcos(\Phi)\right)\sec(\Theta)$	(B.12)

Velocity of the aircraft in the inertial frame in terms of Euler angles and body velocity components[15]

$$\begin{Bmatrix} \dot{x}^I \\ \dot{y}^I \\ \dot{z}^I \end{Bmatrix} = \begin{bmatrix} C_\Theta C_\Psi & S_\Phi S_\Theta C_\Psi - C_\Phi S_\Psi & C_\Phi S_\Theta C_\Psi - S_\Phi S_\Psi \\ C_\Theta S_\Psi & S_\Phi S_\Theta S_\Psi - C_\Phi C_\Psi & C_\Phi S_\Theta C_\Psi - S_\Phi C_\Psi \\ -S_\Theta & S_\Phi C_\Theta & C_\Phi C_\Psi \end{bmatrix} . \begin{Bmatrix} u^I \\ v^I \\ w^I \end{Bmatrix} \quad \text{(B.13)}$$

[15] C and S are shortenings for cosine and sine, respectively.

B.2 LINEAR EQUATIONS OF MOTION

Despite their generality, equations (B.1) to (B.12), consist in a system of 12 coupled nonlinear ordinary differential equations in the independent variable t, which can be quite complex to solve. For this reason, this system is frequently linearized for use in stability and control analysis. According to (Etkin & Reid, 1996), the use of small-disturbance theory has been found in practice to give good results and able to predict with satisfactory precision the stability of unaccelerated flight.

It is assumed that the airplane motion is composed by a reference condition steady flight and small deviations from it. The reference values of all variables are denoted by a subscript zero, and the small perturbations by prefix Δ. The equation below is a generalization, where $\mathcal{X}$ may be substituted by any variable:

$$\mathcal{X}(t) = \underbrace{\mathcal{X}_0}_{reference\ condition} + \underbrace{\Delta\mathcal{X}(t)}_{small\ pertubation} \tag{B.14}$$

When the reference value is zero, the Δ may be omitted. This convention is adopted by (Etkin & Reid, 1996) and may vary for other authors. The reasons for the success of the method are: (1) in many cases, the major aerodynamic effects are nearly linear functions of the disturbances, and (2) disturbed flight of considerable violence can occur with quite small values of the linear and angular velocity disturbances. Nonetheless, there are limitations to the theory, such as solutions for problems with large disturbance angle are not suitable.

All disturbance quantities are assumed to be small, so that their squares and products are negligible compared to first-order terms. Additionally, for trigonometric functions, the following relations are used:

$$\sin(\Delta\mathcal{X}) = \Delta\mathcal{X}$$
$$\cos(\Delta\mathcal{X}) = 1$$

The reference flight condition is assumed to be symmetric and with no angular velocity (typical trim condition). Thus $v_0 = p_0 = q_0 = r_0 = \Phi_0 = \Psi_0 = 0$. Furthermore, for dynamic stability analysis it is common to choose the stability axis as the fixed-body coordinate system, which sets $w_0 = 0$, $u_0 = V_\infty$ and Θ_0 will coincide with the reference angle of climb.

- **REFERENCE STEADY STATE EQUATIONS**

When applying the small disturbance form from (B.14) into equations (B.1) to (B.12), it is possible to separate the system in two other: one that is time independent (steady state) and another that is time dependent (disturbed motion). The reference steady state equations are then:

$$X_0 - m.g.\sin(\Theta_0) = 0 \quad \text{(B.15)}$$

$$Y_0 = 0 \quad \text{(B.16)}$$

$$Z_0 + m.g.\cos(\Theta_0) = 0 \quad \text{(B.17)}$$

$$L_0 = 0 \quad \text{(B.18)}$$

$$M_0 = 0 \quad \text{(B.19)}$$

$$N_0 = 0 \quad \text{(B.20)}$$

Before writing the time dependent set of equations, it is necessary to introduce a few more assumptions.

- **THE LINEAR AIR REACTIONS**

The main factor that distinguishes the flight mechanic equations of motion from other branches of mechanics is the evaluation of the external forces, which are the aerodynamic forces for a flying vehicle. From many studies, it has been found that a good estimative for the aerodynamic forces can be made by the following linear approximations:

$$\Delta X = X_u.\Delta u + X_w.w \quad \text{(B.21)}$$

$$\Delta Y = Y_v.v + Y_p.p + Y_r.r \quad \text{(B.22)}$$

$$\Delta Z = Z_u.\Delta u + Z_w.w + Z_{\dot{w}}.\dot{w} + Z_q.q \quad \text{(B.23)}$$

$$\Delta L = L_v.v + L_p.p + L_r.r \quad \text{(B.24)}$$

$$\Delta M = M_u.\Delta u + M_w.w + M_{\dot{w}}.\dot{w} + M_q.q \quad \text{(B.25)}$$

$$\Delta N = N_v.v + N_p.p + N_r.r \quad \text{(B.26)}$$

where,

$$X_u = \frac{\partial X}{\partial u}\ ; Y_v = \frac{\partial Y}{\partial v};\ etc.$$

Those are called *dimensional stability derivatives*, and appendix B.3 shows how they can be calculated.

The above equations considers the following assumptions:

1. All the derivatives of the symmetric forces and moments (longitudinal motion) with respect to the asymmetric motion variables (lateral motion) are neglected.
2. The derivatives with respect to rates of change of motion variables are negligible, except for $Z_{\dot{w}}$ and $M_{\dot{w}}$.
3. The derivative X_q is also negligibly small.
4. The density of the atmosphere is assumed not to vary with altitude.

- **LINEAR EQUATIONS OF MOTION – STATE-SPACE FORM**

Finally, when equations (B.21) to (B.26) are substituted into equations (B.1) to (B.12) with the small-perturbations assumptions, the time dependent equations can be written and divided into two uncoupled groups, termed longitudinal and lateral equations of motion. Those equations may be arranged in a state vector form as follows:

$$\{\dot{x}\} = \mathbf{A}.\{x\}$$

Where **A** is the dynamic matrix of the airplane. The state vectors for the longitudinal and lateral motions are, respectively:

$$\{x\} = [\Delta u \quad w \quad q \quad \Delta\Theta]^T$$

$$\{x\} = [v \quad p \quad r \quad \Phi]^T$$

The dynamic matrices for longitudinal and lateral motions are, respectively:

$$\boldsymbol{A_{long}} = \begin{bmatrix} \frac{X_u}{m} & \frac{X_w}{m} & 0 & -g.\cos(\Theta_0) \\ \frac{Z_u}{m - Z_{\dot{w}}} & \frac{Z_w}{m - Z_{\dot{w}}} & \frac{Z_q + m.u_0}{m - Z_{\dot{w}}} & \frac{-m.g.\sin(\Theta_0)}{m - Z_{\dot{w}}} \\ \frac{1}{I_y}\left[M_u + \frac{M_{\dot{w}}.Z_u}{(m - Z_{\dot{w}})}\right] & \frac{1}{I_y}\left[M_w + \frac{M_{\dot{w}}.Z_w}{(m - Z_{\dot{w}})}\right] & \frac{1}{I_y}\left[M_q + \frac{M_{\dot{w}}.(Z_q + m.u_0)}{(m - Z_{\dot{w}})}\right] & -\frac{M_{\dot{w}}.mg.\sin(\Theta_0)}{I_y.(m - Z_{\dot{w}})} \\ 0 & 0 & 1 & 0 \end{bmatrix}$$

$$\boldsymbol{A_{lat}} = \begin{bmatrix} \frac{Y_v}{m} & \frac{Y_p}{m} & \left(\frac{Y_r}{m} - u_0\right) & g.\cos(\Theta_0) \\ \left(\frac{L_v}{I'_x} + I'_{xz}.N_v\right) & \left(\frac{L_p}{I'_x} + I'_{xz}.N_p\right) & \left(\frac{L_r}{I'_x} + I'_{xz}.N_r\right) & 0 \\ \left(I'_{xz}L_v + \frac{N_v}{I'_z}\right) & \left(I'_{xz}L_p + \frac{N_p}{I'_z}\right) & \left(I'_{xz}L_r + \frac{N_r}{I'_z}\right) & 0 \\ 0 & 1 & \tan(\Theta_0) & 0 \end{bmatrix}$$

where,

$$I'_x = (I_x I_z - I_{xz}^2)/I_z$$
$$I'_z = (I_x I_z - I_{xz}^2)/I_x$$
$$I'_{xz} = I_{xz}/(I_x I_z - I_{xz}^2)$$

The advantage of using the linearized equations of motion in the state-space form is that the homogeneous solution for the system of first-order differential equations is resumed to an eigenvalue problem, which can be easily solved with a digital computer software (e.g. MATLAB®). See appendix C for more details on the eigenvalue problem.

B.3 STABILITY DERIVATIVES

The following tables shows how the dimensional stability derivatives can be evaluated. Each entry in the tables represents the derivative of the column heading with respect to the row variable, similar to what is done by (Etkin & Reid, 1996). The numerical values of the designed aircraft are also shown.

Longitudinal Derivatives

Table B.2: Longitudinal dimensional derivatives.

	$\boldsymbol{X}$ $[\boldsymbol{N}]$	$\boldsymbol{Z}$ $[\boldsymbol{N}]$	$\boldsymbol{M}$ $[\boldsymbol{N}]$
$\boldsymbol{u}$ $[\boldsymbol{m/s}]$	$\rho u_0 S_w C_{W_0} \sin(\Theta_0) + \frac{1}{2}\rho u_0 S_w C_{x_u}$	$-\rho u_0 S_w C_{W_0} \cos(\Theta_0) + \frac{1}{2}\rho u_0 S_w C_{z_u}$	$\frac{1}{2}\rho u_0 \bar{c}_w S_w C_{m_u}$
$\boldsymbol{w}$ $[\boldsymbol{m/s}]$	$\frac{1}{2}\rho u_0 S_w C_{x_\alpha}$	$\frac{1}{2}\rho u_0 S_w C_{z_\alpha}$	$\frac{1}{2}\rho u_0 \bar{c}_w S_w C_{m_\alpha}$
$\boldsymbol{q}[\boldsymbol{rad/s}]$	$\frac{1}{4}\rho u_0 \bar{c}_w S_w C_{x_q}$	$\frac{1}{4}\rho u_0 \bar{c}_w S_w C_{z_q}$	$\frac{1}{4}\rho u_0 \bar{c}_w^2 S_w C_{m_q}$
$\dot{\mathbf{w}}$ $[\mathbf{m/s^2}]$	$\frac{1}{4}\rho \bar{c}_w S_w C_{x_{\dot\alpha}}$	$\frac{1}{4}\rho \bar{c}_w S_w C_{z_{\dot\alpha}}$	$\frac{1}{4}\rho \bar{c}_w^2 S_w C_{m_{\dot\alpha}}$

where, C_{W_0} is the aircraft nondimensional weight:

$$C_{W_0} = \frac{m.g}{\frac{1}{2}\rho V_\infty^2 S_w}$$

The other coefficients are the nondimensional derivatives. They are the partial derivative of a nondimensional coefficient (column heading) with respect to a nondimensional quantity (row).

Table B.3: Longitudinal nondimensional derivatives.

	C_x	C_z	C_m
$\hat{u} = \frac{u}{u_0}$	C_{x_u}	C_{z_u}	C_{m_u}
$\alpha = \frac{w}{u_0}$	C_{x_α}	C_{z_α}	C_{m_α}
$\hat{q} = \frac{q}{\left(\frac{2u_0}{\bar{c}_w}\right)}$	C_{x_q}	C_{z_q}	C_{m_q}
$\hat{\dot{\alpha}} = \frac{\dot{\alpha}}{\left(\frac{2u_0}{\bar{c}_w}\right)}$	$C_{x_{\dot{\alpha}}}$	$C_{z_{\dot{\alpha}}}$	$C_{m_{\dot{\alpha}}}$

The equations for each nondimensional stability derivatives will not be presented, because not all of them have an analytical formulation. When it was the case, the derivative was evaluated with help of Digital DATCOM software (see (USAF, 1978) and (Mc Donnel Douglas Astronautics Company, 1979)).

Table B.4 and Table B.5 presents the dimensional and nondimensional derivatives for the aircraft designed during this work, at cruise speed (97.8 m/s) and 36576 meters of altitude (12000ft).

Table B.4: Longitudinal dimensional derivatives at 36576 m (12000 ft) and V_∞ =97.8 m/s.

	X $[N]$	Z $[N]$	M $[N.m]$
u $[m/s]$	-49.43	-429.74	0
w $[m/s]$	100.38	-4242.80	-1413.3
$q[rad/s]$	0	-4173.80	-12813
$\dot{w}$ $[m/s^2]$	0	-13.05	-59.44

Table B.5: Longitudinal nondimensional derivatives at 36576 m (12000 ft) and V_∞ =97.8 m/s.

	C_x	C_z	C_m
$\hat{u} = \frac{u}{u_0}$	-0.077	-0.032	0
$\alpha = \frac{w}{u_0}$	0.157	-6.636	-1.70
$\hat{q} = \frac{q}{\left(\frac{2u_0}{\bar{c}_w}\right)}$	0	-10.04	-23.70
$\hat{\dot{\alpha}} = \frac{\dot{\alpha}}{\left(\frac{2u_0}{\bar{c}_w}\right)}$	0	-3.069	-10.75

Lateral Derivatives

Table B.6: Lateral dimensional derivatives.

	$Y\ [N]$	$L\ [N.m]$	$N\ [N.m]$
$v\ [m/s]$	$\frac{1}{2}\rho u_0 S_w C_{y_\beta}$	$\frac{1}{2}\rho u_0 b_w S_w C_{\ell_\beta}$	$\frac{1}{2}\rho u_0 b_w S_w C_{n_\beta}$
$p\ [rad/s]$	$\frac{1}{4}\rho u_0 b_w S_w C_{y_p}$	$\frac{1}{4}\rho u_0 b_w^2 S_w C_{\ell_p}$	$\frac{1}{4}\rho u_0 b_w^2 S_w C_{n_p}$
$r\ [rad/s]$	$\frac{1}{4}\rho u_0 b_w S_w C_{y_r}$	$\frac{1}{4}\rho u_0 b_w^2 S_w C_{\ell_r}$	$\frac{1}{4}\rho u_0 b_w^2 S_w C_{n_r}$

Table B.7 presents the nondimensional derivatives, which are the partial derivatives of the nondimensional coefficients with respect to a nondimensional quantity:

Table B.7: Lateral nondimensional derivatives.

	C_y	C_ℓ	C_n
$\beta = \frac{v}{u_0}$	C_{y_β}	C_{ℓ_β}	C_{n_β}
$\hat{p} = \frac{p}{\left(\frac{2u_0}{b_w}\right)}$	C_{y_p}	C_{ℓ_p}	C_{n_p}
$\hat{r} = \frac{r}{\left(\frac{2u_0}{b_w}\right)}$	C_{y_r}	C_{ℓ_r}	C_{n_r}

Table B.8 and Table B.9 presents the dimensional and nondimensional derivatives for the aircraft designed during this work, at cruise speed (97.8 m/s) and 36576 meters of altitude (12000ft).

Table B.8: Lateral dimensional derivatives at 36576 m (12000 ft) and V∞ =97.8 m/s.

	$Y\ [N]$	$L\ [N.m]$	$N\ [N.m]$
$v\ [m/s]$	-475.02	-404.26	272.76
$p\ [rad/s]$	-107.12	-28518.00	-1287.00
$r\ [rad/s]$	0	5731.10	-5870.40

Table B.9: Lateral nondimensional derivatives at 36576 m (12000 ft) and V∞ =97.8 m/s.

	C_y	C_ℓ	C_n
$\beta = \frac{v}{u_0}$	-0.743	-0.051	0.034
$\hat{p} = \frac{p}{\left(\frac{2u_0}{b_w}\right)}$	-0.027	-0.579	-0.026
$\hat{r} = \frac{r}{\left(\frac{2u_0}{b_w}\right)}$	0	0.116	-0.119

APPENDIX C – THE EIGENVALUE PROBLEM

The present appendix has the objective to briefly introduce the eigenvalue problem and show how it is related with the linearized equations of motion. More detailed explanation can be found on (Etkin & Reid, 1996), (Nelson, 1998) or (Roskam, 2001).

The linearized equation of motion is written in the following form:

$$\{\dot{x}\} = \mathbf{A}.\{x\} \tag{C.1}$$

Since no control inputs are considered here, equation (C.1) is a set of homogeneous first-order linear differential equations. This set of equations can be solved by assuming a solution of the form:

$$\{x\} = \{x\}_{t=0}.e^{\lambda.t} \tag{C.2}$$

where $\{x\}_{t=0}$ is the initial condition of the state vector. Substituting equation (C.2) into (C.1) yields:

$$\mathbf{A}.\{x\} = \lambda.\{x\} \tag{C.3}$$

which is a typical eigenvalue problem. The nontrivial solution should be found from:

$$\det(\lambda.\mathbf{I} - \mathbf{A}) = 0 \tag{C.4}$$

The roots of equation (C.4) are called characteristic roots or eigenvalues. For a n^{th} order system, usually there will be n eigenvalues.

In a dynamic system, the k-th eigenvalue can have the following form:

$$\lambda_k = n_k \pm i\omega_{d_k}$$

or,
$$\lambda_k = -\xi_k.\omega_{n_k} \pm i\omega_k\sqrt{1-\xi_k^2} \tag{C.5}$$

Where ξ_k is the damping ratio of the k-th eigenvalue, ω_{n_k} is the natural frequency, ω_d is the damped frequency.

From equations (C.1) and (C.5), in a resumed way, one can infer that:

1. If λ has real positive value, the system will be unstable;
2. If λ has real negative value, the system will be stable;
3. If λ has a nonzero imaginary component, the system will have an oscillatory behavior.

The eigenvalue provides important information about the system's behavior over time. Some of them are summarized in Table C.1:

Table C.1: Numerical parameters obtained from the eigenvalues.

Property			Description
ω_n	$=$	$(n^2 + \omega_d^2)^{1/2}$	Natural frequency
ξ_n	$=$	$-n/\omega_n$	Damping ratio
T	$=$	$\frac{2\pi}{\omega_d}$	Period of oscillation
$t_{double}\ or\ t_{half}$	$=$	$\frac{.693}{\lvert n \rvert}$	Time to half the mode amplitude, if it is stable. Time to double the mode amplitude, if it is unstable.
$N_{double}\ or\ N_{half}$	$=$	$.110\frac{\omega_d}{\lvert n \rvert}$	Time to half the mode amplitude, if it is stable. Time to double the mode amplitude, if it is unstable.

The physical meaning of the eigenvalues on a dynamic system is that they are commonly known as “dynamic modes”. The system total behavior is composed by a linear combination of all dynamic modes. For instance, the longitudinal motion of a fixed wing aircraft is composed by two dynamic modes. They are two damped oscillations, one of long period and lightly damped (phugoid), the other of short period and heavily damped (short-period). In Figure C.1 they can be easily visualized, where the short period mode is the one that quickly dies out before one second and the phugoid mode is the oscillation seen over the time. This different behavior are a directly manifestation of the eigenvalues on the aircraft behavior.

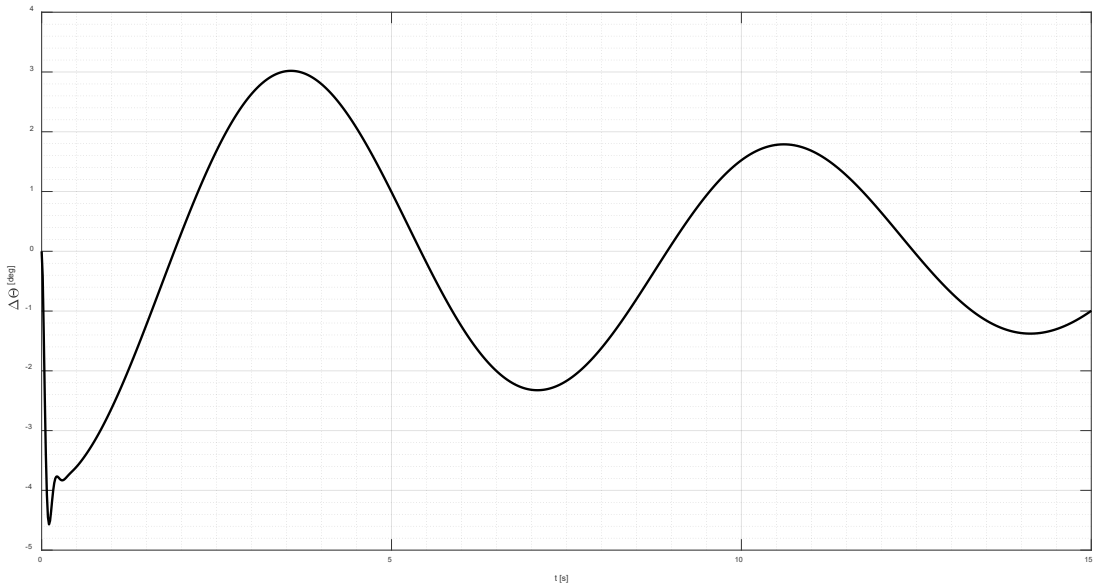

Figure C.1: Typical response of a fixed wing aircraft. Path angle over the time, for an initial condition of $\alpha = 5°$.

APPENDIX D – AIRCRAFT AERODYNAMIC CHARACTERISTICS

This appendix is dedicated to provide more data with respect to the aerodynamic behavior of the designed aircraft. All data presented is for a flight at 36576 meters altitude (12000 ft) and V∞ =97.8 m/s. Furthermore, for these analyses, the following configurations were considered:

Table D.1: Weight characteristics considered for analysis.

	Forward CG	Medium CG	Aft CG
h [% of $\bar{c}_w$]	21.67%	31.12%	40.58%
W [N]	19492	20020	23338

When not specified, the medium position is considered.

Drag polar at trim condition

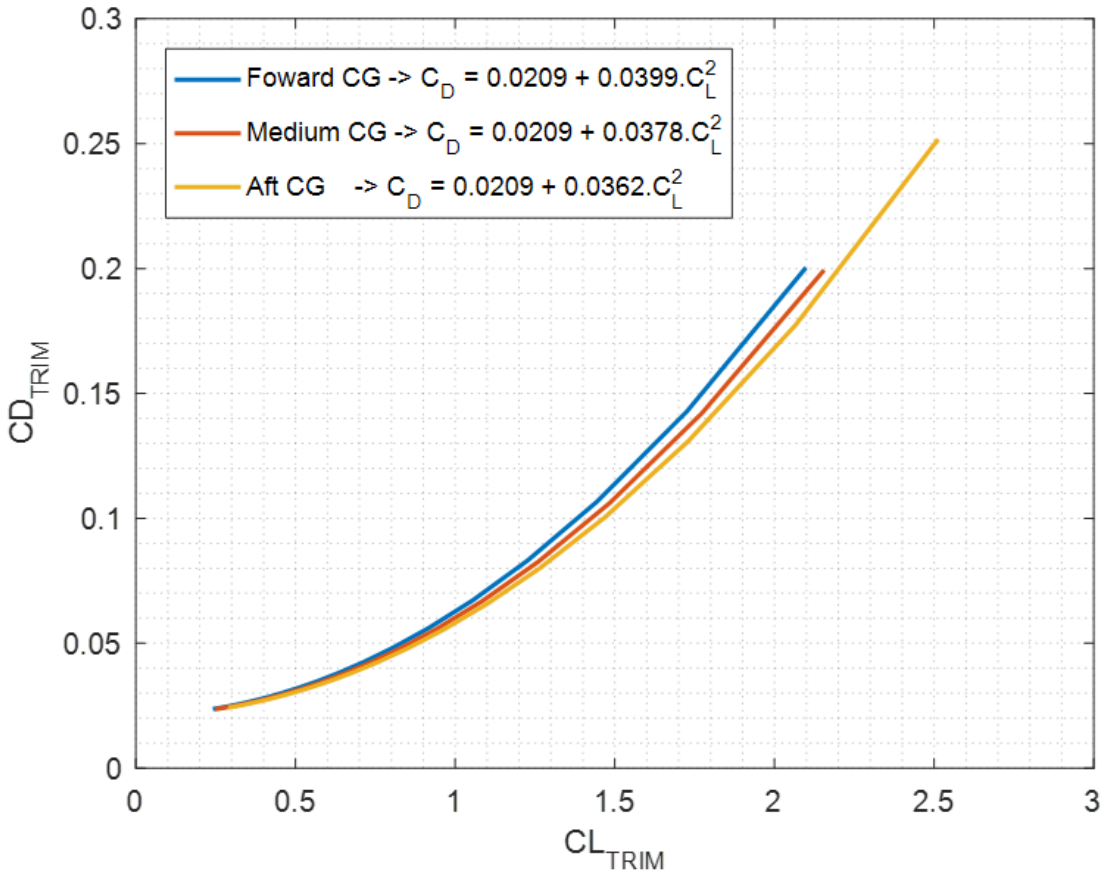

Figure D.1: Influence of the center of gravity on lift and drag coefficients for trim condition.

Pitching moment coefficient

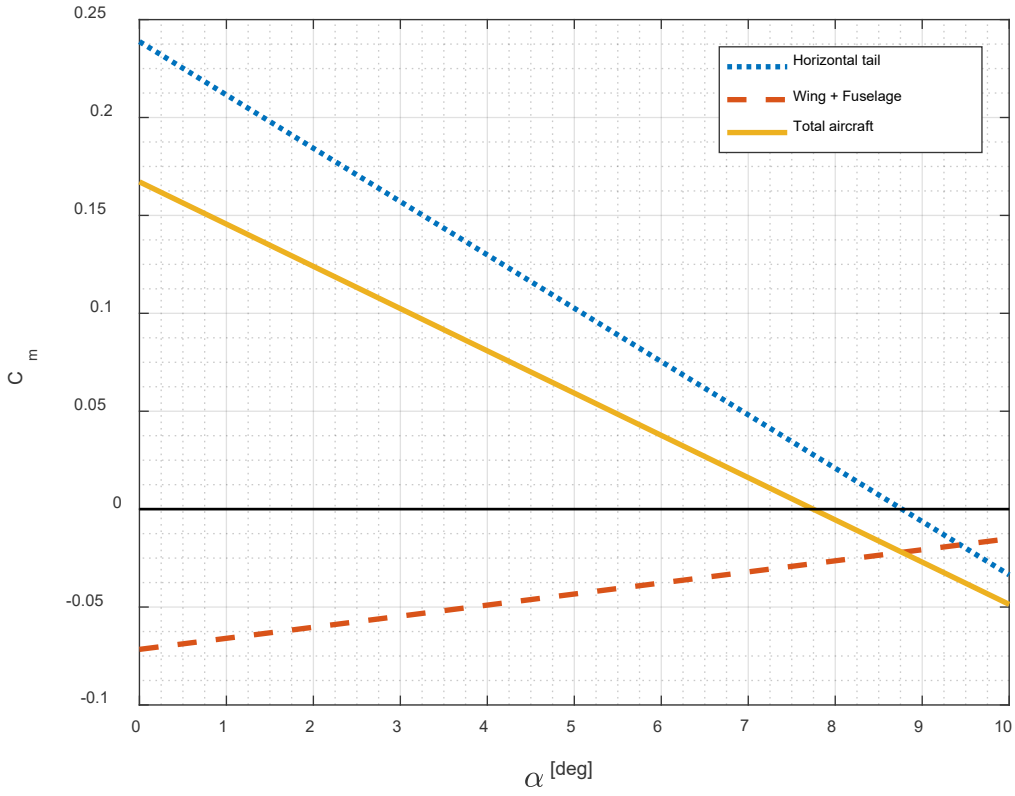

Figure D.2: Pitching moment contributions for the total aircraft configuration.

Trim condition

Table D.2 shows the trim configuration of the aircraft at stall and cruise velocities. At stall velocity it is considered sea level altitude and flap configuration, which increases the stall angle.

Table D.2: Trim configuration for different CG positions for V_{stall} and V_{cruise}.

		Forward CG (h = 21.67%)	Medium CG (h = 31.12%)	Aft CG (h = 40.58%)
V_{stall} $31.38\ m/s$	α_{trim}	18.7º	18.7º	21.3º
	$\delta_{e_{trim}}$	-17.2º	-9.4º	-2.2º
	$C_{L_{trim}}$	2.0985	2.1553	2.5125
	$C_{D_{trim}}$	0.2004	0.1994	0.2518
V_{cruise} $97.6\ m/s$	α_{trim}	1.0º	1.0º	1.3º
	$\delta_{e_{trim}}$	4.9º	5.8º	6.6º
	$C_{L_{trim}}$	0.2410	0.2475	0.2885
	$C_{D_{trim}}$	0.0236	0.0235	0.0242

Longitudinal modes at the complex plane

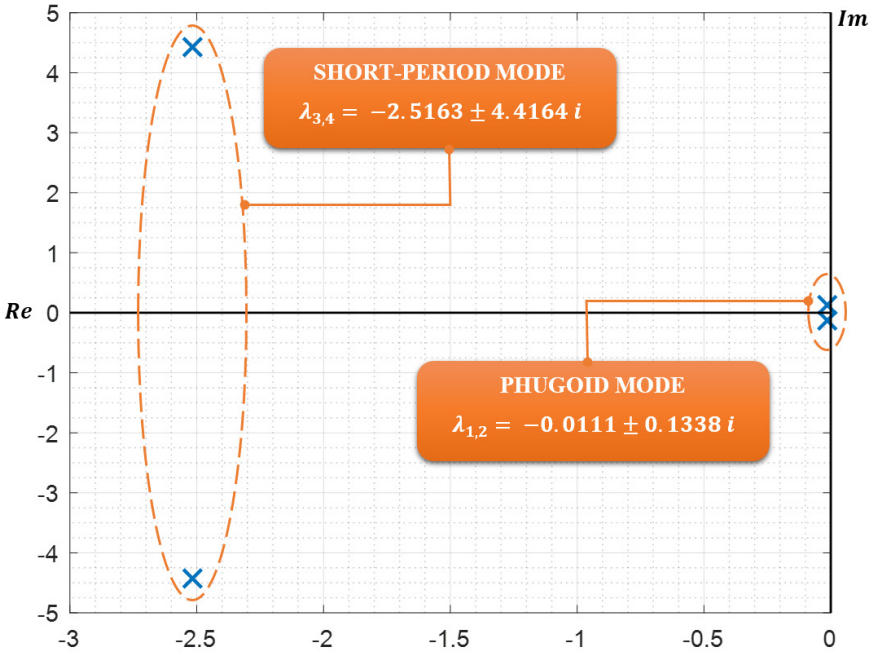

Figure D.3: Longitudinal modes.

Lateral modes at the complex plane

Because of the great difference in order of magnitude, the Re axis is plotted in log-scale for better visualization.

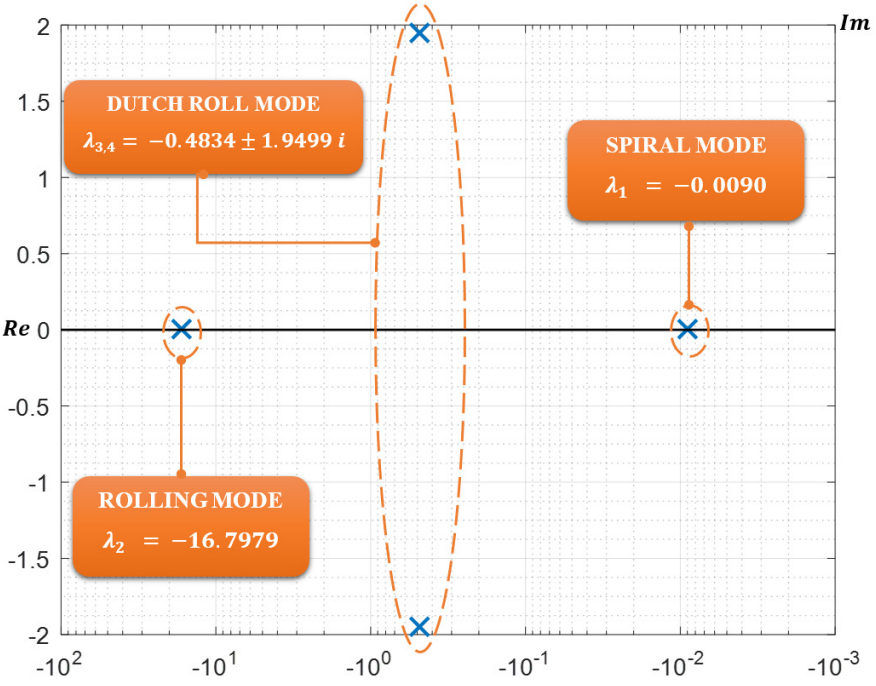

Figure D.4: Lateral modes.

Longitudinal dynamic response for 5º AoA initial condition

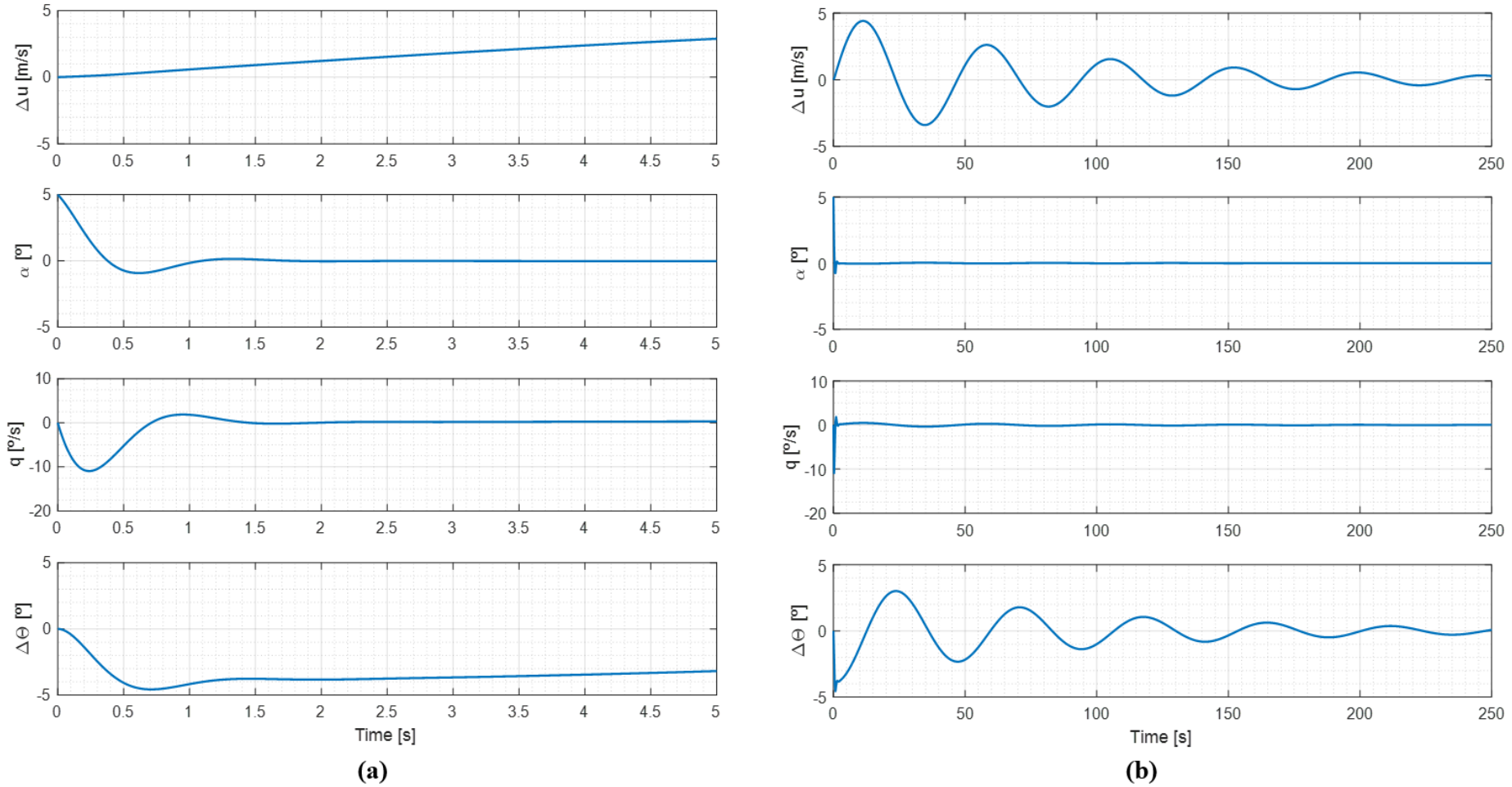

Figure D.5: Response to an angle of attack perturbation (α=5°). (a) Time-span of 5 seconds highlights the short-period mode behavior; (b) Time-span of 250 seconds highlights the phugoid mode.

Lateral dynamic response for 5º sideslip angle initial condition

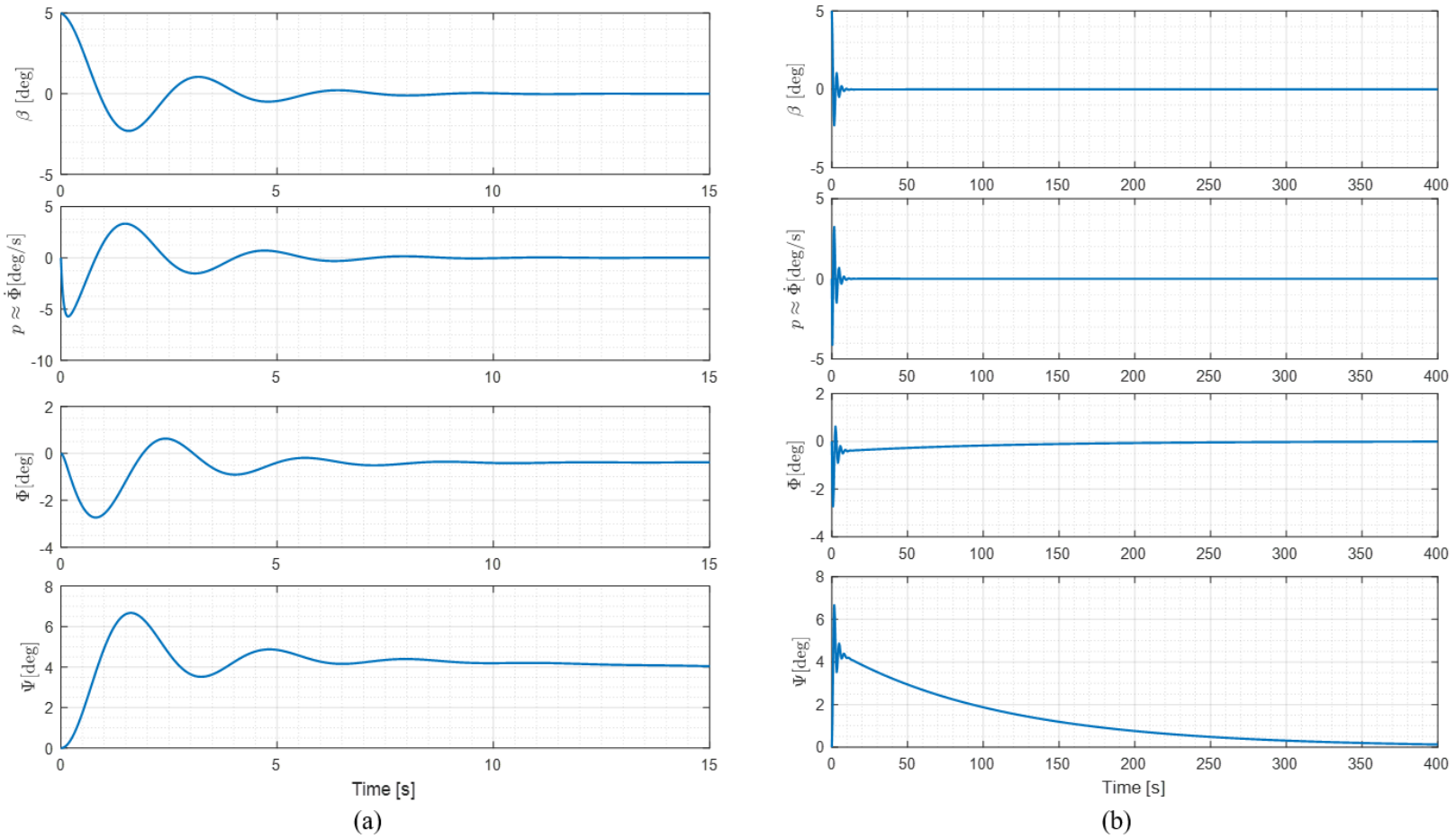

Figure D.6: Response to a sideslip angle perturbation (β=5°). (a) Time-span of 15 seconds highlights the dependence between roll and yaw movements; (b) Time-span of 400 seconds highlights the spiral mode, the last mode to die out.